ANL-7518

ANL-7518
ANL-7518
ANL-7518
ANL-7518
ANL-7518
ANL-7518
ANL-7518
ANL-7518
ANL-7518
ANL-7518
ANL-7518
ANL-7518
ANL-7518
ANL-7518
ANL-7518
ANL-7518
ANL-7518
ANL-7518

The facilities of Argonne National Laboratory are owned by the United States Government. Under the terms of a contract (W-31-109-Eng-38) between the U. S. Atomic Energy Commission, Argonne Universities Association and The University of Chicago, the University employs the staff and operates the Laboratory in accordance with policies and programs formulated, approved and reviewed by the Association.

MEMBERS OF ARGONNE UNIVERSITIES ASSOCIATION

The University of Arizona
Carnegie-Mellon University
Case Western Reserve University
The University of Chicago
University of Cincinnati
Illinois Institute of Technology
University of Illinois
Indiana University
Iowa State University
The University of Iowa
Kansas State University
The University of Kansas
Loyola University
Marquette University
Michigan State University
The University of Michigan
University of Minnesota
University of Missouri
Northwestern University
University of Notre Dame
The Ohio State University
Ohio University
The Pennsylvania State University
Purdue University
Saint Louis University
Southern Illinois University
University of Texas
Washington University
Wayne State University
The University of Wisconsin

LEGAL NOTICE

This report was prepared as an account of Government sponsored work. Neither the United States, nor the Commission, nor any person acting on behalf of the Commission:

A. Makes any warranty or representation, expressed or implied, with respect to the accuracy, completeness, or usefulness of the information contained in this report, or that the use of any information, apparatus, method, or process disclosed in this report may not infringe privately owned rights; or

B. Assumes any liabilities with respect to the use of, or for damages resulting from the use of any information, apparatus, method, or process disclosed in this report.

As used in the above, "person acting on behalf of the Commission" includes any employee or contractor of the Commission, or employee of such contractor, to the extent that such employee or contractor of the Commission, or employee of such contractor prepares, disseminates, or provides access to, any information pursuant to his employment or contract with the Commission, or his employment with such contractor.

Printed in the United States of America
Available from
Clearinghouse for Federal Scientific and Technical Information
National Bureau of Standards, U. S. Department of Commerce
Springfield, Virginia 22151
Price: Printed Copy $3.00; Microfiche $0.65

ANL-7518
Reactor Technology

ARGONNE NATIONAL LABORATORY
9700 South Cass Avenue
Argonne, Illinois 60439

REACTOR DEVELOPMENT PROGRAM PROGRESS REPORT

November 1968

Robert B. Duffield, Laboratory Director
Stephen Lawroski, Associate Laboratory Director

Division	Director
Chemical Engineering	R. C. Vogel
EBR-II Project	M. Levenson
Metallurgy	M. V. Nevitt
Reactor Engineering	L. J. Koch
Reactor Physics	R. Avery

Report coordinated by
L. B. Fosdick and A. Glassner

Issued December 27, 1968

FOREWORD

The Reactor Development Program Progress Report, issued monthly, is intended to be a means of reporting those items of significant technical progress which have occurred in both the specific reactor projects and the general engineering research and development programs. The report is organized in accordance with budget activities in a way which, it is hoped, gives the clearest, most logical overall view of progress. Since the intent is to report only items of significant progress, not all activities are reported each month. In order to issue this report as soon as possible after the end of the month editorial work must necessarily be limited. Also, since this is an informal progress report, the results and data presented should be understood to be preliminary and subject to change unless otherwise stated.

The issuance of these reports is not intended to constitute publication in any sense of the word. Final results either will be submitted for publication in regular professional journals or will be published in the form of ANL topical reports.

The last six reports issued in this series are:

May 1968	ANL-7457
June 1968	ANL-7460
July 1968	ANL-7478
August 1968	ANL-7487
September 1968	ANL-7500
October 1968	ANL-7513

REACTOR DEVELOPMENT PROGRAM

Highlights of Project Activities for November 1968

EBR-II

The reactor was operated for 774 MWd during November and had accumulated 21,478 MWd of operation by the end of the month. All runs were made at 50 MWt except for a 1-hr run at approximately 76 kW for irradiating an experimental subassembly containing dosimetry materials. Four other experimental subassemblies containing dosimetry or flux-monitoring materials were irradiated for 418 MWd at 50 MWt. Because of the short life of some of the isotopes produced during irradiation, the four subassemblies were removed from the reactor, washed, and dismantled--and their capsules containing short-lived isotopes removed, packaged, and made available to the experimenter--within 27 hr (21 hr less than the maximum time allowed by the experimenter).

Thirty-seven encapsulated Mark-II fuel elements that had been irradiated to a burnup of 1.9-2.3 a/o in EBR-II appeared to be in satisfactory condition when checked by neutron radiography. Five Mark-IA encapsulated fuel elements with a maximum burnup of 2.5 a/o were neutron radiographed and found to be in satisfactory condition.

ZPR-3

The program with Assembly 54, which was an iron-reflected version of the depleted uranium-reflected Assembly 53, has been completed and analysis carried out on the measurements made with these assemblies. These measurements have included central reactivity worths, reaction-rate traverses, and pulsed neutron measurement of prompt-neutron die-away curves. The program with Assembly 55, a plutonium-fueled zoned core with $k_\infty = 1$ in central zone, has also been completed. After null-reactivity measurements were made, the Assembly 55 configuration was used to measure the capture-to-fission ratio in ^{239}Pu by foil irradiation methods.

ZPPR

Reactor control and nuclear instrumentation systems have been checked, and are in operational status. Several prooftest reactor runs have been made to familiarize reactor operators and supervisors with the reactor control system.

Design drawings for the Doppler rod have been completed, and rod-timing circuits for the poison safety rods have been tested.

ZPR-6 and -9

Efforts have been directed toward the completion of exterior work in the conversion of the fast critical facilities ZPR-6 and -9 to plutonium-fueled operation. Estimated completion of all construction to date is 93.5%.

TABLE OF CONTENTS

	Page
I. LIQUID METAL FAST BREEDER REACTORS--CIVILIAN	1
A. Fuel Development--LMFBR	1
1. Oxide	1
2. Carbide	6
B. Physics Development--LMFBR	7
1. Theoretical Reactor Physics	7
2. Experimental Reactor Physics	12
3. ZPR-3 Operations and Analysis	21
4. ZPPR Operations and Analysis	25
5. ZPR Materials	28
C. Component Development--LMFBR	30
1. Sodium Technology Development	30
2. Reactor Mechanism and Instrumentation	32
3. Fuel Handling, Vessels, and Internals--Core Component Test Loop	33
D. Systems and Plant--LMFBR	34
1. 1000-MWe Plant	34
E. EBR-II	36
1. Research and Development	36
a. Reactor Experimental Support--Reactor Analysis and Testing	36
b. Nuclear Analysis Methods Development	39
c. Fuel Performance Studies--Mark I Series	41
d. Mark II Driver Fuel Element Development	43
e. Equipment--Fuel Related	44
f. New Subassemblies Design and Experimental Support	45
g. Instrumented Subassembly	47
h. Process Chemistry	48
i. Experimental Irradiation and Testing	50
j. FCF Process Analysis and Testing	54
k. FCF Equipment Improvement	54
l. Superheater and EM Pump Study and Test	54
m. Feasibility Study of Fuel Failure Detection--Chemical and Mechanical Methods	56
n. Materials-Coolant Compatibility	56
o. Study of Operation with Failed Fuel	57

TABLE OF CONTENTS

	Page
p. Driver Fuel Transient Performance Studies--TREAT Experiments	59
q. Systems Engineering	59
r. Leak Detection and Location--Xenon Method	64
2. Operations	66
PUBLICATIONS	75
II. OTHER FAST REACTORS--CIVILIAN--OTHER FAST BREEDER REACTORS	79
A. Fuel Development	79
1. Corrosion of Fuel Jacket Alloys	79
III. GENERAL REACTOR TECHNOLOGY	81
A. Applied and Reactor Physics Development	81
1. Theoretical Reactor Physics--Research and Development	81
2. Nuclear Data--Research and Development	81
B. Reactor Fuels and Materials Development	84
1. Fuels and Cladding	84
2. Coolants, Moderators, and Control Materials--Fundamentals of Corrosion in Liquid Metals	90
3. Radiation Damage on Structural Materials--Research and Development--In-Reactor Creep Studies	91
4. Techniques of Fabrication and Testing--Research and Development	92
C. Engineering Development	97
1. Heat Transfer and Fluid Flow	97
2. Engineering Mechanics	99
D. Chemistry and Chemical Separations	103
1. Aqueous and Volatility Processes--Research and Development--Fluoride Volatility Process	103
2. Closed Cycle Processes--Research and Development--Compact Pyrochemical Processes	111
3. General Chemistry and Chemical Engineering--Research and Development	113
PUBLICATIONS	116

TABLE OF CONTENTS

	Page
IV. NUCLEAR SAFETY	119
A. Reactor Kinetics--Other Reactor Kinetics--Research and Development	119
1. Reactor Control and Stability	119
2. Coolant Dynamics	120
3. Fuel Meltdown Studies with TREAT	121
4. Materials Behavior and Energy Transfer	123
5. Fast Reactor Safety Test Facility Study	125
B. TREAT Operations	126
1. Reactor Operations	126
2. Development of Automatic Power Level Control System	126
C. Chemical Reaction--Research and Development--Chemical and Associated Energy Problems (Thermal)	126
1. Analysis of Excursion Accidents	126
PUBLICATIONS	130

I. LIQUID METAL FAST BREEDER REACTORS--CIVILIAN

A. Fuel Development--LMFBR

1. Oxide

a. Fuel Studies

(i) Fuel Element Performance (L. A. Neimark, F. L. Brown, and R. Natesh)

Last Reported: ANL-7513, pp. 1-2 (Oct 1968).

Significant differences in postirradiation structures are observed in vibratorily compacted fuel elements when the linear power rating is increased from 17 to 21 kW/ft while initial fuel density and other fuel variables remain unchanged. This effect is illustrated in Fig. I.A.1, which

SOV-6
17 kW/ft, 83% Dense

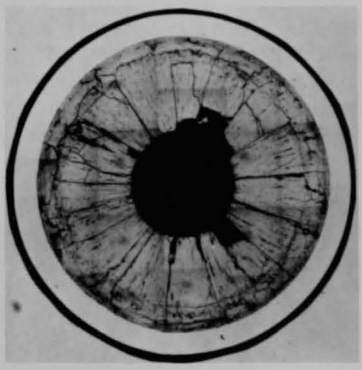

SOV-3
21 kW/ft, 83% Dense

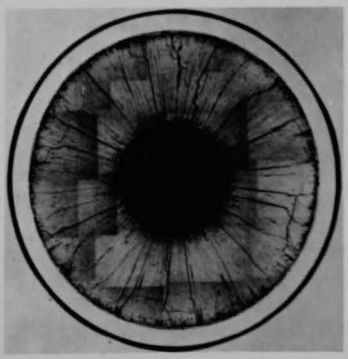

HOV-15
21 kW/ft, 80% Dense

Fig. I.A.1

Midplane Sections of Elements SOV-6, SOV-3, and HOV-15, Showing Effects of Power Rating and Fuel Density on Fuel Restructuring

includes metallographic sections through the midplanes of Element SOV-3 (21 kW/ft, 83% dense) from EBR-II Subassembly XO11, and Element SOV-6 (17 kW/ft, 83% dense) from Subassembly XO09 (see Progress Report for February 1967, ANL-7308, pp. 28-30). The increase in power rating enlarged the central void, enlarged the diameter of columnar-grain growth, increased fuel sintering at the periphery, and increased the radius at which a gray phase containing solid fission products was deposited. (This gray phase has been identified in other specimens as containing barium, strontium, and cerium.*) At 21 kW/ft the fuel at the fuel-cladding interface at the midplane was completely sintered and, at operating temperature, was in intimate contact with the cladding.

Comparable changes in restructuring effects appear to result when the initial density of the compacted fuel is reduced while the linear power rating remains constant, as illustrated in Fig. I.A.1 by comparing SOV-3 with HOV-15 (21 kW/ft, 80% dense).

Intergranular penetration of the Type 304 stainless steel cladding by a white-appearing phase (to a depth of 3 mils) was found in Element SOV-3 (see Fig. I.A.2). Attempts are now being made by electron-microprobe examination to identify the grain-boundary and cladding-surface constituents in SOV-3. Previously, cesium penetration into stainless steel cladding was found in an element operated at 17 kW/ft (see Progress Report for November 1967, ANL-7399, pp. 121-123).

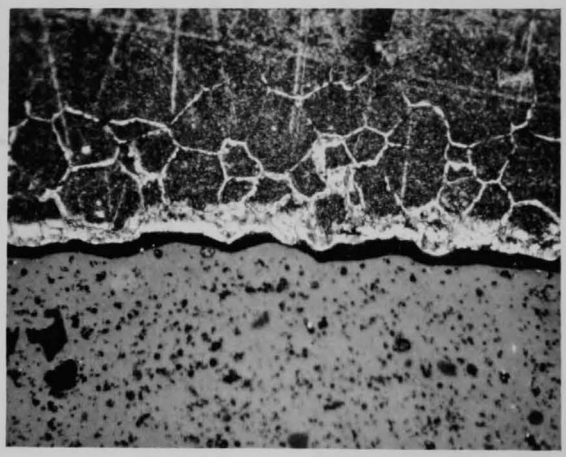

Fig. I.A.2. Intergranular Penetration of Type 304 Stainless Steel Cladding in Element SOV-3

*O'Boyle, D. R., Brown, F. L., and Sanecki, J. E., Solid Fission Product Behavior in Uranium-Plutonium Oxide Fuel Irradiated in a Fast Neutron Flux, to be published in J. Nucl. Mater.

Postirradiation examinations of Elements SOV-3, SOV-7, HOV-15, and TVOV-1, operated at linear power ratings between 19.6 and 21.4 kW/ft, indicate central fuel melting probably occurred. The evidence of melting consists of the following:

(1) Neutron radiographs showed that central voids in these elements were tapered below the midplane of the element, in contrast to straight central cavities in elements irradiated at only 17 kW/ft.

(2) The tapered areas contained a number of constrictions in the central void that appear to be the result of surface tension effects during the molten phase. These constrictions remained as the fuel solidified.

(3) Metallographic sections showed a large columnar-grain region adjacent to the central void in the tapered regions, and beta-gamma autoradiographs showed these grains to be essentially free of fission-product activity. These large columnar grains could result from relocation of molten fuel from hotter regions and subsequent solidification in the cooler regions below the midplane, as suggested by the presence of large columnar grains below the midplane and the absence of large columnar grains in regions around the midplane where the temperature was undoubtedly higher (as evidenced by more extensive sintering and grain growth).

(4) Center-of-gravity determinations showed changes from preirradiation locations of from 1/32 to 1/8 in., which indicates a downward movement of fuel.

Although these observations suggest fuel slumping, a number of questions remain unanswered; when fuel movement occurred is one question of particular importance.

Initial measurements of the diameters of Elements TVOV-1, HOV-15, SOV-3, and SOV-7 indicated a substantially larger maximum diameter change for Element TVOV-1 with V-20 w/o Ti cladding than for the other elements, which were clad with Hastelloy-X or Type 304 stainless steel (see Progress Report for September 1968, ANL-7500, Table I.A.2, p. 2). Remeasurements of the diameters and a closer evaluation of the data now indicate maximum diameter increases, during irradiation, of 1.8 mils (0.6%) for TVOV-1, 1.2 mils (0.4%) for both SOV-3 and SOV-7, and 0.8 mil (0.3%) for HOV-15. These new values appear to minimize the apparent anomaly that existed in earlier observations.

Fission-gas release from Element SOV-7 was 61% of the calculated amount generated. The release from Element HOV-15 was 82% of the calculated amount (since this element failed during exposure, the release was approximated from the amount of gas recovered from the capsule plenum). The lower density, higher fuel temperatures, and greater restructuring in HOV-15 (see Fig. I.A.1) are the likely causes of the higher release.

(ii) Compatibility between Uranium-Plutonium Oxide and Cladding Alloys (T. W. Latimer)

Last Reported: ANL-7513, pp. 3-4 (Oct 1968).

The results of microhardness measurements show that six vanadium alloys were hardened after contact with $(U_{0.8}Pu_{0.2})O_{1.97}$ for 1000 hr at 800°C in out-of-reactor diffusion couples. In two of these alloys, V-20 w/o Ti and V-15 w/o Cr-5 w/o Ti, a hardened zone was visible after polishing. Hardness profiles of these zones were reported in Fig. I.A.2, p.3, ANL-7513. Chemical analyses of disks of material containing the 14.0-mil hardened zone of V-20 w/o Ti and the 21.7-mil hardened zone of V-15 w/o Cr-5 w/o Ti have shown that these zones contain an average of 4.3 w/o and 2.3 w/o oxygen, respectively. Oxygen contents of V-20 w/o and V-15 w/o Cr-5 w/o Ti within 10 mils of these hardened zones were equal to the as-received values for the alloys, 0.083 w/o and 0.091 w/o, respectively.

(iii) Fuel Element Modeling (T. R. Bump)

Last Reported: ANL-7487, pp. 46-50 (Aug 1968).

A report on the SWELL-2 fuel-element-lifetime code has been drafted and is being reviewed. SWELL-2 uses an arbitrary pressure-reduction factor to estimate the pressure on the inner surface of the cladding that results from the pressure of the fission gas that is retained in the fuel. To introduce the elastoplastic properties of the fuel, it is planned that the next version of the code, SWELL-3, will determine the pressure on the cladding inner surface as indicated in Fig. I.A.3.

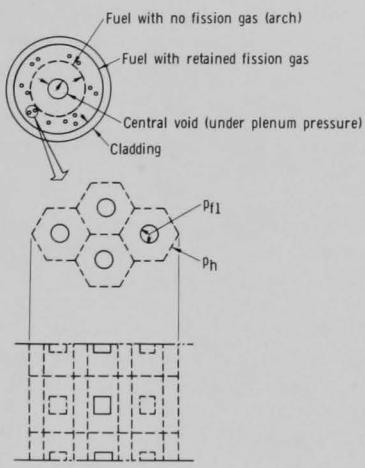

Fig. I.A.3. SWELL-3 Model for Fission Gas Retained in Fuel Pores

The pores that contain the fission gas retained in the fuel will be considered to be distributed transversely in a triangular lattice so that each pore is at the center of a hollow, right hexagonal prism. The pressure inside each prism is p_{fl}, the average pressure of the retained fission gas, and the pressure outside each prism is p_h, the "hydrostatic pressure." The pressure on the inner surface of the cladding and the "arch" outer surface is also equal to p_h. At each step of the calculations, a value of p_h is assumed, and corresponding strains of the prisms, cladding, and arch are calculated. If the strains are not compatible, the

assumed value of p_h is changed appropriately until compatibility is achieved (that is, an iterative approach is used). It is also planned to include the steady-state effects of fuel melting on the cladding strain in SWELL-3.

To aid in the interpretation and use of in-pile creep measurements with fuel-element materials, another computer code is being developed. This code employs an incremental generalized-plane-strain analysis to predict primary and secondary creep deformations in a hollow, finite circular cylinder loaded by axial tension or compression, internal and external pressure, and subjected to a radial temperature gradient. It is also planned to use this code to predict the dimensional cladding changes that might occur from the time a fuel element is last at power to the time its postirradiation dimensions are actually measured. We suspect that cladding strain might decrease significantly during that interval; if so, that decrease must be taken into account when comparing predicted dimensional changes (as from the SWELL code) with measured changes.

A third code being developed uses the same generalized-plane-strain approach as above to analyze two concentric cylinders with different creeprates; it assumes perfect slip at the interface. One possible application of this code is as a crude model for fuel-element behavior; in this case, the internal pressure would be specified as a function of time.

A search is being made for fuel-swelling theories that might be superior to those used in existing fuel-element-behavior codes. As part of this search, the work of N. C. Small* has been studied. His theory may be roughly characterized as a continuum model based on generalized steady-state creep equations modified to include a phenomenological treatment of sintering. To obtain local (microscopic) swelling rates, his theory considers both fission gas and fabricated pores. The difficulty in applying the results comes in defining the interaction between the macroscopic state of stress in a given fuel geometry and the stress state experienced by the two pore structures of the microscopic model. A rational description, as yet unavailable, of such an interaction is needed if the model is to yield a position-dependent swelling rate applicable to the known behavior patterns of oxide fuel.

The work of Agranovich et al.,** has also been studied. Their theory is based on a Boltzmann-like equation describing the transport, growth, and coalescence of fission-gas bubbles coupled with kinetics equations describing gas diffusion into the bubbles from an assumed supersaturated state within the fuel matrix. As a result of the strong emphasis on modeling the basic physical processes involved in the motion of fission-gas bubbles, the resultant swelling theory suffers from overcomplexity as well as severe attendant numerical and analytical difficulties. However, because it is based on more fundamental concepts than the usual engineering approaches, the basic philosophy of Agranovich et al. apparently offers a greater

*WAPD-TM-421 (Feb 1965); WAPD-TM-498 (July 1965); WAPD-TM-649 (Sept 1967); WAPD-TM-755 (Jan 1968).

**Third UN Int. Conf. on Peaceful Uses of At. Eng., A/CONF. 28/P/338a.

potential for success in the long run than does most other current work. Apparently, the framework of their approach so far has forced Agranovich et al. to neglect either macroscopic pore motion or growth. We plan to examine the possibility of including both aspects so as to obtain a more realistic swelling model.

We are preparing to study the possible deleterious effects of mild transients with EBR-II fuel elements at relatively high burnup. For the study, we will use the fuel-element deformation module of the SAS-1A code. We expect that this exercise will add to the understanding of the behavior of the fuel elements and also will suggest possible ways to modify the code, which is intended for oxide fuel elements under fast transients, so that it also can apply to slow transients.

2. Carbide

a. Fabrication and Evaluation

(i) Fuel Element Performance (L. A. Neimark and T. W. Latimer)

Last Reported: ANL-7513, pp. 4-5 (Oct 1968).

Three mixed-carbide fuel elements are being examined following irradiation in EBR-II Subassembly XG05 to an estimated maximum burnup of 7.2 a/o. Elements SMV-2 and HMV-5 contained vibratorily compacted, physically mixed powders of UC-20 w/o PuC, and were clad in Type 304 stainless steel and Hastelloy-X, respectively. Element NMV-11 contained vibratorily compacted hyperstoichiometric $(U_{0.8}Pu_{0.2})C$ (average carbon content = 5.11 w/o) and was clad in Nb-1 w/o Zr. The design and operating parameters of these elements were reported previously (see ANL-7513, Table I.A.1, p. 4).

All elements have been removed from their capsules. Element SMV-2 was intact, and fission-gas sampling has been completed; results of chemical analyses of the gas have not been received. The maximum diametral increase of SMV-2 was 2.1 mils or 0.73%, and the average diametral increase over the fueled section was 1.6 mils or 0.54%. Element HMV-5 was also intact, but fission-gas analysis is being delayed until modifications can be made in the sampling apparatus. The maximum diametral increase of HMV-5 was 5.1 mils or 1.7%. In this element the greatest diametral increase occurred in the upper fuel region. The average diametral increase over the fueled section was 2.5 mils or 0.85%. At the fluence level to which these elements were exposed ($\sim 5 \times 10^{22}$ nvt), a large proportion of the measured increases in diameter is probably the result of cladding swelling. Element NMV-11 had to be forcibly removed from its capsule. Visual examination of the cladding revealed several cracks parallel to the axis of the element; this cracking was observed over the entire length of the element. Evidence of this failure was previously reported in ANL-7513: neutron radiographs indicated a crack in the cladding, and fission gas was detected in the plenum of the capsule.

B. Physics Development--LMFBR

1. Theoretical Reactor Physics

a. General Fast Reactor Physics

(i) Multigroup Methods (H. H. Hummel)

Last Reported: ANL-7478, pp. 2-5 (July 1968).

(a) A New Definition of the Microscopic Multigroup Transport Cross Sections.* Most computer codes currently in use for the production of sets of multigroup cross sections for fast reactor analysis collapse the macroscopic multigroup transport cross sections according to the following equations:

$$\bar{\Sigma}_{tr_I} = \bar{\phi}_I \Big/ \int_I \frac{1}{\Sigma_{tr}(E)} \phi(E)\, dE \tag{1}$$

and

$$\bar{\phi}_I = \int_I \phi(E)\, dE. \tag{2}$$

A method for collapsing the microscopic transport cross sections, on the other hand, has not been clearly established. Three definitions that have received particular attention are

$$\bar{\sigma}^m_{tr_I} = \bar{\phi}_I \Big/ \int_I \frac{1}{\sigma^m_{tr}(E)} \phi(E)\, dE, \qquad \text{(Definition A)}^{**,\dagger} \tag{3}$$

$$\bar{\sigma}^m_{tr_I} = \frac{1}{\bar{\phi}_I} \int_I \sigma^m_{tr}(E)\phi(E)\, dE, \qquad \text{(Definition B)}^{\dagger,\dagger\dagger} \tag{4}$$

---

*Travelli, A., A New Definition of the Microscopic Multigroup Transport Cross Sections, Trans. Am. Nucl. Soc. 11(2), 532-533 (1968).

**Yiftah, S., Okrent, D., and Moldauer, P. A., Fast Reactor Cross Sections, Pergamon Press (1960), p. 102; Kerr, W. M. M., Parker, K., and Williams, D. V. J., The Calculation of Group Averaged Neutron Cross Sections: Galaxy 3 Facilities Available in S2 (Fortran) language for the IBM-7030 (Stretch) Computer, AWRE-O-97/64 (1965).

† Reactor Physics Constants, ANL-5800, Second Edition (1963), p. 557.

†† Zweifel, P. F., Ball, G. L., Group Cross Sections for Fast Reactors, Proc. Seminar of Physics of Fast and Intermediate Reactors, Paper SM-18/65, Vienna (1962).

and

$$\bar{\sigma}^{m}_{tr_I} = \frac{1}{\bar{\phi}_I} \int_I \sigma^{m}_{tr}(E) \left[\frac{\bar{\Sigma}_{tr_I}}{\Sigma_{tr}(E)} \right] \phi(E)\, dE, \qquad \text{(Definition C)*} \tag{5}$$

where the superscript m refers to the isotope under consideration.

Definitions A and B derive their justification from the analogy with the definitions, respectively, of the macroscopic multigroup transport and total cross sections. They suffer from the basic flaw of not adding up to the macroscopic transport cross sections when multiplied by the corresponding isotopic concentrations; Zweifel and Ball** showed that the macroscopic cross sections are consistently under- and overestimated when they are obtained from microscopic cross sections obtained, respectively, from Definitions A and B. Definition C was introduced recently by Toppel and Rago, who applied it in the MC^2 code, and, independently, by Ferziger and Zweifel. It can be derived directly by current weighting procedures, and it has the great advantage over Definitions A and B of adding up to the correct macroscopic transport cross sections.

The main requirement that is desired of the microscopic transport cross sections is that they add up to the macroscopic cross sections not only for the standard composition for which the ultrafine flux is calculated, but also for other compositions not too different from it. Thus, on considering M isotopes, if N^m is the concentration of the mth isotope in a general composition, and N_0^m is the concentration of the same isotope in the standard composition, the microscopic transport cross sections should satisfy the relation

$$\sum_{m=1}^{M} \bar{\sigma}^{m}_{tr_I} N^m \approx \bar{\Sigma}_{tr_I}\left[N^{(1)}, N^{(2)}, \ldots, N^M\right]. \tag{6}$$

By expanding Eq. (6) in a first-order Taylor series of the isotopic concentrations around the standard composition, one obtains the following equations, which should be satisfied by the microscopic transport cross sections:

$$\sum_{m=1}^{M} \bar{\sigma}^{m}_{tr_I} N_0^m = \bar{\Sigma}_{tr_I}\left[N_0^{(1)}, N_0^{(2)}, \ldots, N_0^M\right]; \tag{7}$$

---

* Toppel, B. J., Rago, A. L., and O'Shea, D. M., MC^2, A Code to Calculate Multigroup Cross Sections, ANL-7318 (1967); Ferziger, J. H., and Zweifel, P. F., The Theory of Neutron Slowing Down in Nuclear Reactors, M.I.T. Press (1966), p. 239.

** Ibid., see previous page.

$$\bar{\sigma}^{m}_{tr_I} = \frac{\partial \bar{\Sigma}_{tr_I}}{\partial N^m}\left[N_0^{(1)}, N_0^{(2)}, \ldots, N_0^{M}\right]; \qquad m = 1, 2, \ldots, M. \tag{8}$$

Of the three definitions mentioned above, only Definition C satisfies Eq. (7). No other equation is satisfied by any of the definitions. However, if the relative change of the transport collision density due to a small composition change is assumed not to depend on energy over the Ith group, it is possible to derive a definition of $\bar{\sigma}^{m}_{tr_I}$ that satisfies identically both Eq. (7) and (8).

From Eq. (8), and by differentiating Eq. (1) with respect to N^m, one obtains

$$\bar{\sigma}^{m}_{tr_I} = \frac{1}{\bar{\phi}_I}\int_I \left\{\sigma^{m}_{tr}(E)\left[\frac{\bar{\Sigma}_{tr_I}}{\Sigma_{tr}(E)}\right]^2 + \left[\frac{1}{\phi(E)}\frac{\partial\phi(E)}{\partial N^m}\right]\left[\bar{\Sigma}_{tr_I} - \frac{\Sigma^2_{tr_I}}{\Sigma_{tr}(E)}\right]\right\}\phi(E)\,dE, \tag{9}$$

whereas the assumed hypothesis yields

$$\frac{1}{\left[\Sigma_{tr}(E)\phi(E)\right]}\frac{\left[\partial\Sigma_{tr}(E)\phi(E)\right]}{\partial N^m} = C^m_I. \tag{10}$$

Therefore

$$\frac{1}{\phi(E)}\frac{\partial\phi(E)}{\partial N^m} + \frac{\sigma^{m}_{tr}(E)}{\Sigma_{tr}(E)} = C^m_I, \tag{11}$$

where C^m_I is an arbitrary constant for every isotope m and group I.

The expression for

$$\left[\frac{1}{\partial(E)}\frac{\partial\phi(E)}{\partial N^m}\right]$$

as obtained from Eq. (11) may be substituted into Eq. (9). All terms containing the arbitrary constant C^m_I cancel each other, and the following new definition for the microscopic multigroup transport cross section results:

$$\bar{\sigma}^{m}_{tr_I} = \frac{1}{\bar{\phi}_I}\int_I \sigma^{m}_{tr}(E)\left\{2\left[\frac{\bar{\Sigma}_{tr_I}}{\Sigma_{tr}(E)}\right]^2 - \left[\frac{\bar{\Sigma}_{tr_I}}{\Sigma_{tr}(E)}\right]\right\}\phi(E)\,dE. \qquad \text{(Definition D)} \tag{12}$$

It is possible to verify directly that Definition D satisfies identically both Eq. (8) (from which it was derived) and Eq. (7). It also satisfies the basic requirement of yielding identical results when collapsing, over the same energy groups, ultrafine cross sections or cross sections that have already been collapsed over an intermediate group structure.

If the assumption concerning the transport collision density expressed by Eq. (10) is made for the neutron current or for the neutron flux, the same procedure leads to two new definitions which are found to be equal, respectively, to Definition C and to the average of Definitions C and D. These assumptions, however, are physically unsatisfactory and yield less accurate results.

A test of the various definitions was performed in which the ELMOE-calculated* sodium transport cross sections for ZPR-3 Assembly 48** were collapsed from 603 groups to the 20 intermediate groups of the Argonne Set 224.† Table I.B.1 shows the composition of the reactor under consideration. Table I.B.2 summarizes the results of the test. Columns A, B, C, and D correspond to the homonymous definitions and are to be compared with the values given in the last column [see Eq. (8)]. Definition D satisfies Eq. (8) with consistently greater accuracy than any of the other definitions. The mean square deviation over lethargy provides an overall measure of the accuracy of a given approximation; on its basis, it appears from the test that Definition D is approximately 8 times more accurate than C, 20 times more accurate than B, and 4 times more accurate than A. Also the sodium-void effect for uniform removal is calculated more accurately in diffusion perturbation theory by means of the new definition. Similar results were obtained also from other tests concerning other standard reactor compositions.

TABLE I.B.1. Core Composition of ZPR-3 Assembly No. 48

Isotope	Concentration (atoms/cm^3 x 10^{-24})	Isotope	Concentration (atoms/cm^3 x 10^{-24})
^{239}Pu	0.001644	Na	0.006230
^{240}Pu	0.000106	Fe	0.009899
^{241}Pu	0.000010	Cr	0.002658
^{235}U	0.000016	Ni	0.001308
^{238}U	0.007406	Mo	0.000206
C	0.020765	Al	0.000110

*Rago, A. L., and Hummel, H. H., ELMOE: An IBM-704 Program Treating Elastic Scattering Resonances in Fast Reactors, ANL-6805 (1964).

**Broomfield, A. M., Anderson, P. I., Davey, W. G., Gasidlo, J. M., Hess, A. L., Keeney, W. P., and Long, J. K., ZPR-3 Assembly-48: Studies of a Dilute Plutonium-Fueled Assembly, ANL-7320 (1966), pp. 205-215.

† O'Shea, D. M., Hummel, H. H., Loewenstein, W. B., and Okrent, D., Twenty-Six-Group Cross Sections, Trans. Am. Nucl. Soc. 7, 242 (1964).

TABLE I.B.2. Comparison of Various Definitions of the Sodium Transport Cross Section in Assembly 48

Group Number	Lower Energy (eV)	$\bar{\sigma}_{tr}^{Na}$ (b) A	B	C	D	$\frac{\partial \bar{\Sigma}_{tr}}{\partial N^{Na}}$ (EXACT)
2[a]	2.222×10^6	1.687	1.721	1.720	1.728	1.723
3	1.342×10^6	1.634	1.667	1.662	1.658	1.657
4	8.244×10^5	2.715	2.786	2.770	2.751	2.756
5	4.976×10^5	4.043	4.448	4.408	4.340	4.340
6	3.003×10^5	3.202	3.306	3.289	3.272	3.264
7	1.844×10^5	3.481	3.857	3.763	3.657	3.664
8	1.094×10^5	3.204	3.205	3.206	3.278	3.300
9	6.721×10^4	3.415	3.437	3.440	3.537	3.583
10	4.056×10^4	4.409	5.254	4.982	4.654	4.606
11	2.491×10^4	3.891	3.895	3.885	4.290	4.481
12	1.503×10^4	4.110	4.112	4.102	4.182	4.191
13	9.077×10^3	4.998	5.052	5.050	5.050	5.053
14	4.293×10^3	8.332	9.002	9.040	9.242	9.234
15	2.591×10^3	31.716	64.211	43.084	30.357	31.288
16	2.031×10^3	8.211	9.718	9.413	8.940	8.691
17	1.225×10^3	3.813	3.921	3.920	3.917	3.917
18	9.608×10^2	3.035	3.036	3.036	3.036	3.037
19	5.799×10^2	3.016	3.016	3.016	3.017	3.022
20	2.743×10^2	3.017	3.017	3.017	3.017	3.023
21	1.016×10^2	3.019	3.019	3.019	3.019	3.021
Mean Square Deviation over Lethargy, barns		0.047	0.235	0.091	0.012	-
Sodium-void Effect,[b] % δk		-3.97	-4.21	-4.15	-4.11	-4.09[c]

[a]The upper energy of Group 2 is 3.684 MeV.
[b]Diffusion-theory perturbation calculations for a bare sphere.
[c]From a calculation using 605 groups.

The new definition is now being included in a new version of the MC^2 code. Its use in this connection and in connection with other codes for the preparation of multigroup cross-section sets will make it possible to produce more significant data at practically no additional computational expenditure.

b. Fast Critical Experiments--Theoretical Support
(F. W. Thalgott, R. B. Nicholson, and R. G. Palmer)

Last Reported: ANL-7500, pp. 11-13 (Sept 1968).

The CALHET* (calculation of the heterogeneity effect) code has been received from Atomics International. It has been modified to run with the CDC-1604 and to accept standard XLIBIT cross-section sets. It is now operational.

*Report No. AI-67-91.

2. Experimental Reactor Physics

a. Fast Critical Experiments--Experimental Support (Idaho)

(i) Neutron Spectrometry (W. G. Davey)

Last Reported: ANL-7513, p. 6 (Oct 1968).

Proton-recoil spectrum measurements were made in ZPR-3 Assembly 55 over the energy range from 230 eV to 1.5 MeV. Preliminary studies indicated that the data between 230 eV and 10 keV were distorted as a result of a count-rate-sensitive amplifier in the discrimination electronics system. A modification of the amplifier was made and the measurement was repeated. The data are being analyzed.

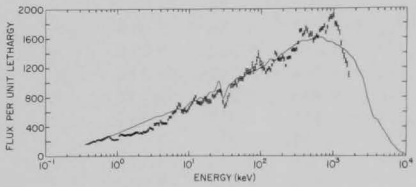

Fig. I.B.1. Comparison of Measurement of Proton-recoil Spectrum with MC^2 Calculation for ZPR-3 Assembly 53

The data from the neutron-spectrum measurement of Assembly 53 have been compared with a MC^2 calculation with the results shown in Fig. I.B.1. The output of the MC^2 code was smoothed through a Gaussian window corresponding to the resolution of the counter and was normalized to the data over the energy range from 1 keV to 1 MeV. Relatively large discrepancies between the calculation and the experiment are present above 600 keV and between 1 and 6 keV. The reasons for these discrepancies are unclear and are being studied.

(ii) On-Line Computer Applications (W. G. Davey)

Last Reported: ANL-7500, pp. 13-14 (Sept 1968).

A program has been written for the CDC-1604 to provide a plot showing the face of each half of ZPPR with the drawer master number printed in each location of the matrix. This diagram is provided for front and back drawers for each half. The program also provides the number of kilograms of plutonium constituted by each drawer type, and the total for each half. Thus, the reactor loading is displayed for easy visual inspection (as well as ready for a report) and the fissile mass computed for the loading.

A program for the CDC-1604, which finds material combinations to provide a desired power reactor composition in ZPPR, has been modified for application at ZPR-3. The additional reactor materials

available at ZPR-3 were added. Modifications that substantially reduced computer time were made to both versions of the code (ZPPR and ZPR-3).

Work is continuing on determining the location and identification of plutonium fuel at ZPR-3. Procedures for recording fuel movement have been modified so that as little extra work as possible will be required for record keeping. The form for recording fuel inventory has been modified for ease in use at both reactor locations.

(iii) Integral Studies of Cross Sections (W. G. Davey)

Last Reported: ANL-7500, p. 14 (Sept 1968).

Work continued in behalf of the national Cross Section Evaluation Working Group (CSEWG) on the testing of the microscopic cross sections in ENDF/B with integral fast-reactor experiments. A review of all of the past critical assemblies in the facilities ZPR-3, -6, -9, ZEBRA, VERA, and other reactors was undertaken to arrive at a selection of "benchmark" cases for the integral testing of ENDF/B and its correlated multigroup-cross-section preparation codes. A tentative choice of eight fast assemblies covering a broad range of composition and characteristic spectra is under closer study. In the selection, the relative quality and accuracy of the experimental data have been considered. It has been found that many results have large uncertainties, particularly the central reactivity measurements, which are subject to sample-size effects.

b. Fast Critical Experiments--Experimental Support (Illinois)

(i) On-line Computer Applications (R. Gold)

Last Reported: ANL-7487, pp. 7-10 (Aug 1968).

(a) Noise Studies of a Digital Reactor Control System. The polarity-correlation algorithm previously developed for fast reactor noise analysis* has been used to study the dynamic characteristics of a computerized reactor control system.** For these tests, the control system was applied to one of the control rods on the Argonne Thermal Source Reactor.

The algorithm was set up to calculate the autocorrelation function of the motion of the control rod. During any one control interval, the control system commands the rod to withdraw (increasing reactivity), insert, or remain stationary. Thus, the sequence

*Cohn, C. E., "Fast-reactor Noise Analysis by Polarity Cross Correlation," in Reactor Physics Division Annual Report, July 1, 1966 to June 30, 1967, ANL-7310, pp. 415-423.

**Cohn, C. E., "Experiments in the Computer Control of Critical Assemblies," Ibid., pp. 408-410.

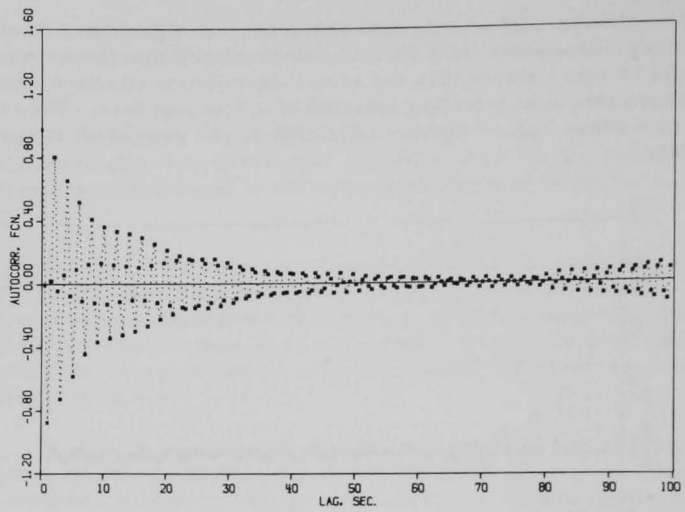

Fig. I.B.4. Autocorrelation Function of Rod-control Signal with 0.5-sec Sampling Interval and Actual Control Algorithm

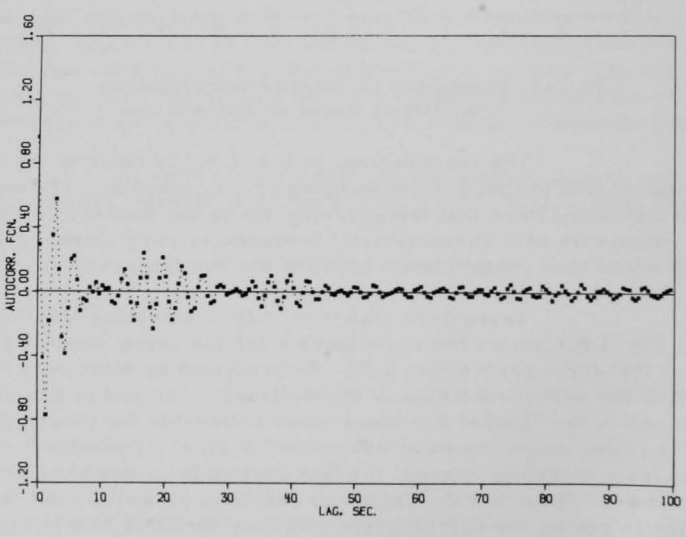

Fig. I.B.5. Autocorrelation Function of Rod-control Signal with 0.5-sec Sampling Interval and Zero-order Hold

(b) Programs for Noise Analysis of EBR-II. A series of computer programs has been written to perform noise analysis as an aid in the study of EBR-II dynamics. The programs calculate autocorrelation and cross-correlation functions from data records acquired by the Navcor data-acquisition system connected to the IBM-1620 computer. These programs operate on the CDC-1604 computer, with some ancillary codes operating on the 1620. Provision is also made for the interpretation of the correlograms in terms of system parameters.

The dynamic properties of a random-noise waveform can be described in the time and frequency domains, respectively by the correlation function and the power spectrum, which constitute a transform pair. It has been customary to look upon the power spectrum as the primary quantity and to consider the correlation function only as an intermediate step in the calculation. However, it can be quite advantageous to dispense with the power spectrum and treat the correlation function as the primary quantity. By so doing, problems of aliasing and spectral windows are eliminated. Moreover, the correlogram can be readily interpreted in terms of the dynamic properties of a system.

For computational efficiency, these programs calculate correlation functions by use of the Fast Fourier Transformation (FFT). Here, each time series to be correlated is extended in length by an amount equal to or greater than the maximum lag at which the correlation function is wanted. The added-on part is set equal to zero and the modified time series is transformed. The transform of the lagged time series is multiplied by the complex conjugate of the transform of the unlagged time series. The inverse transform of the product series yields the correlation function. Each member of the result must be divided by the number of points in the original time series minus the lag of the particular member in order to obtain an unbiased estimate. For autocorrelation, only one time series is transformed. The inverse transform of the square modulus of the result yields the autocorrelation function.

In these programs, an input time series of 1000 sampling intervals is extended to 2048 sampling intervals as described above. (A time-series length which is a power of two is optimal for the FFT.) The series is transformed, and the result is saved. If there are more data, the next thousand points are treated in the same way and its transform added to the previous transforms. This continues until all data have been processed. The resulting sum of transforms is multiplied as described above and inverse-transformed to yield the average correlation function for all the data. This is output to a maximum lag of 999 sampling intervals.

The Navcor-1620 digitizing system writes data on tape in BCD in blocks of four-digit numbers. The high-order digit of each number carries a word mark. If the number is negative, the low-order digit

carries a minus sign. To the 1604, the codes for these flagged digits appear as the logical sum of the codes for the digit and the code for a minus sign (except for zero, which appears as a minus sign alone). Thus the codes for the flagged digits one through nine appear as the codes for the letters J through R, respectively.

The program reads a block of numbers from the tape into an integer array. One word from that array, containing two numbers, is separated into characters, the characters being stored in a separate two-dimensional array.

The first character of each number is compared to entries in a table containing the above-mentioned flagged-digit codes. If a match is found, the corresponding unflagged code from another table is substituted. If no match is found, then that character is invalid. It is replaced by the code for zero, and a diagnostic message is printed. If the fourth character in either number is outside the numeric range, the sign for that datum is set negative and the character is treated as for the first character. If the second or third character is outside the numeric range, the code for zero is substituted and a diagnostic message is printed.

The translated digits of one number are reassembled into a word and are converted to a floating-point number less than unity.

The programs are written in FORTRAN-63.

(1) Calculation of Autocorrelation Functions--Program AUTOCORR. AUTOCORR reads a single time series from the tape and calculates its autocorrelation function. It reads a specified number of blocks from the tape, and reads a specified whole number of thousands of points from each block.

The output from the program consists, first, of the amplitude distribution. A printout of the correlogram is then presented, along with a punched deck. A typical running time was $9\frac{1}{2}$ min on two blocks of 8000 points each.

(2) Calculation of Cross-correlation Functions--Program CROSSCOR. CROSSCOR calculates the cross-correlation function between two time series digitized concurrently. It assumes that a number of time series have been sampled sequentially in a cycle, and that each time series has been sampled a whole number of thousands of times, up to a total of 9000 points or less in any one block.

The output for each cross correlation consists of two printouts and decks as described above. The first gives the correlogram

with the first time series lagged; the second gives the correlogram with the second time series lagged. Correct interpretation of the results must take into account the 150-μsec delay between successive samplings in a given sampling cycle.

(3) Correlogram Interpretation--Program CORRFIT. CORRFIT fits a correlogram with a function consisting of a sum of exponentials and exponential cosines. The nonlinear least-squares fit is performed by the variable metric minimization algorithm. This program requires subprograms FCN, VMM, and MATMPY.

(4) Ancillary Programs for the IBM-1620. Two programs have been written for plotting of results with the 1620. One plots the autocorrelation function, while the other plots the two-sided cross-correlation function with the second time series lagged. These programs require as input the punched decks described above.

c. Planning and Evaluation of FFTF Critical Assembly Experiments (D. Meneghetti)

Last Reported: ANL-7513, pp. 7-9 (Oct 1968).

The first assembly of the resumed Phase-B Fast Flux Test Facility Critical Program is to be a cylindrical critical having a core height of 36 in. and having 12-in.-thick axial and radial reflectors. The nominal compositions of core and reflector corresponding to construction of the assembly in the ZPPR facility are given in Table I.B.3.

TABLE I.B.3. Composition of Assembly I in ZPPR (atoms/cm^3) x 10^{-24}

Nuclide	Core	Axial Reflector	Radial Reflector
O	0.01442066	-	-
Na	0.00860629	0.013358	0.006495
Fe	0.01215677	0.008418	0.007163
Cr	0.00259267	0.002394	0.002048
Ni	0.00129094	0.019264	0.046215
Mn	0.00022017	-	-
Mo	0.00032997	-	-
^{235}U	0.00001334	-	-
^{238}U	0.00597782	-	-
^{239}Pu	0.00128254	-	-
^{240}Pu	0.00017469	-	-
^{241}Pu	0.00002376	-	-
C	0.00110393	-	-

The critical mass for this assembly has been estimated by use of a calculational analysis combined with previous comparisons of calculated and experimental values for ZPR-3 Assembly 51. The fissile mass, i.e., the mass of $^{239}Pu + ^{241}Pu + ^{235}U$, is estimated as 367 kg. The corresponding total plutonium mass is 411 kg, which corresponds to a core volume of about 699 liters.

As the atomic densities for ZPR-3 for a corresponding system having identical drawer-loading patterns are larger than for ZPPR because of the inherently smaller void fraction of the facility, estimates of critical size have also been made for construction in ZPR-3; the atomic densities in Table I.B.3 are then to be increased by the factor 1.0406. The resulting estimated fissile mass is 335 kg. The corresponding total plutonium mass is 375 kg, and the corresponding core volume 613 liters.

(i) Calculated Estimate of Worths of Coupled-core-drawer Safety Rods in ZPR-3. Since calculational estimates of the critical mass for Assembly I of the resumed Phase-B FFTF critical program indicated that criticality may be achieved within the total plutonium limit of 430 kg, the worths of coupled drawers as safety rods were also estimated.

The core-loading pattern for this assembly consists of a two-drawer cell pattern in which one drawer is normally more heavily loaded than the other. Estimates were based upon calculations together with previous results of calculational and experimental comparisons of rod worths in ZPR-3 Assembly 51. The rod worths have been estimated for the cases of paired coupling of the heavy and lightly loaded drawers and of paired coupling of two heavily loaded drawers. The calculations indicate that for four coupled-pairs, located about 20.5 cm radially in each half of the facility, withdrawn 10 in., the total worths would be about -1.3% $\Delta k/k$ and -1.7% $\Delta k/k$, respectively, for the heavy-light and for the heavy-heavy coupled-drawer cases.

(ii) A Method for Approximating Solutions of Axially Split Cylindrical Cores. In previous Monthly Reports (see ANL-7427, -7438, -7445, and -7487), a method was described for approximating solutions of axially split cylindrical cores. In ANL-7513, pp. 8-9, the method was used to calculate the k_{eff} of the split-cylinder critical assembly, 52E.

The latter calculation included an improvement in the algorithm for $B^2_{yj} = \frac{-1}{r\phi_j} \frac{\partial \phi_j}{\partial r}$ near r = 0. This results in changes to the last two lines of Table I.B.1 in ANL-7487, p. 12 (Aug 1968). The results are in much better confirmation of the two-dimensional simulation method than was indicated previously.

These revisions, together with additional information designed to show better the dependence of the simulation accuracy on the number of mesh intervals in the one-dimensional MACH computations, are shown in Table I.B.4.

TABLE I.B.4. Comparisons in One- and Two-dimensional Calculations

Diffusion Program	k_{eff} for Reflected Cylinder	k_{eff} for Slab Simulation	Number of Mesh Intervals
MACH 1D	1.0000	1.0009	30
MACH 1D	1.0000	0.9999	38
MACH 1D	1.0000	0.9999	148
CANDID 2D	1.0098	1.0097	14 x 13
CANDID 2D	1.0084	1.0083	19 x 23

3. ZPR-3 Operations and Analysis (W. G. Davey and R. L. McVean)

Last Reported: ANL-7513, pp. 9-15 (Oct 1968).

a. Basic Studies of Plutonium Systems. Data taken in Assembly 54 have been reduced, and subsequent to realignment of the center tube of the ZPR-3 matrix, Assembly 55 has been installed and brought to criticality. Assembly 55 is a zoned core with $k_\infty = 1$ in the central zone and is basically a plutonium-fueled version of an experiment performed with ZPR-9, during April 1968, with a ^{235}U-fueled core.

(i) Assembly 54. The experiments performed with Assembly 54 were duplicates of some of the experiments performed with Assembly 53, the object being to obtain a direct comparison between the same measurements in iron- and depleted uranium-reflected cores. One such experiment was the measurement of central reactivity worths of various materials. Table I.B.5 lists the values measured in Assemblies 53 and 54 along with their ratios. As expected, the worths in the smaller core (54) are slightly higher, the only exceptions being the smaller of the two depleted uranium samples. On the basis of comparison with data from previous assemblies in the physics series, it is believed that the Assembly 53 value is too high. Complete descriptions of the samples are given in ANL-7513.

TABLE I.B.5. Central Reactivity Measurements in Assemblies 53 and 54

Sample Material	Sample Size	Reactivity Worth (Ih/kg) Assembly 53	Assembly 54	Ratio 54/53
Pu[a]	0.010-in.-thick annulus	+655.7 ± 2.3	739.2 ± 4.7	1.127 ± 0.008
	0.007-in.-thick annulus	+650.1 ± 4.1	706.1 ± 8.2	1.086 ± 0.014
U (93.1 w/o ^{235}U)	0.0034-in.-thick annulus	+497.2 ± 4.1	535.9 ± 9.7	1.077 ± 0.021
	0.0014-in.-thick annulus	+481.2 ± 9.7	525 ± 17	1.091 ± 0.042
U (0.21 w/o ^{235}U)	0.200-in.-dia cylinder	-60.67 ± 0.59	-65.43 ± 0.98	1.078 ± 0.019
	0.100-in.-dia cylinder	-75.9 ± 1.7	-72.8 ± 2.7	0.959 ± 0.041
B[b]	0.200-in.-dia cylinder	$-(2.102 \pm 0.020) \times 10^4$	-	-
	0.100-in.-dia cylinder	$-(2.557 \pm 0.022) \times 10^4$	$-(2.676 \pm 0.009) \times 10^4$	1.046 ± 0.009
	0.060-in.-dia cylinder	$-(2.911 \pm 0.013) \times 10^4$	$-(3.173 \pm 0.022) \times 10^4$	1.089 ± 0.009

[a]98.62 w/o Pu; 1.22 w/o Al; 95.05 w/o ^{239}Pu; 4.5 w/o ^{240}Pu; 0.45 w/o ^{241}Pu.
[b]92.8 w/o B; 92.1 w/o ^{10}B.

As for Assembly 53, reaction-rate traverses for ^{239}Pu, ^{235}U, ^{238}U, and ^{10}B were made in the radial direction. The traverse data, normalized to unity at the center of the core, are shown in Figs. I.B.6 through I.B.9 for ^{239}Pu, ^{235}U, ^{238}U, and ^{10}B, respectively.

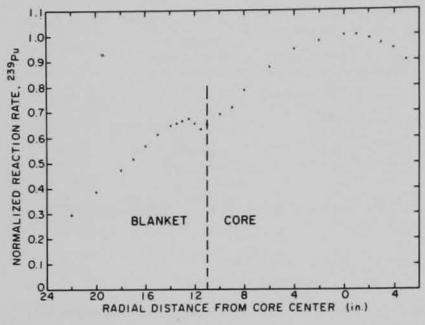

Fig. I.B.6. Normalized Radial Reaction-rate Traverses for ^{239}Pu in Assembly 54

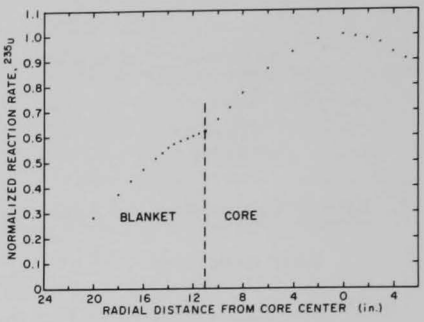

Fig. I.B.7. Normalized Radial Reaction-rate Traverses for ^{235}U in Assembly 54

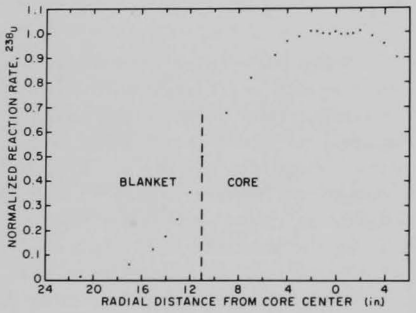

Fig. I.B.8. Normalized Radial Reaction-rate Traverses for ^{238}U in Assembly 54

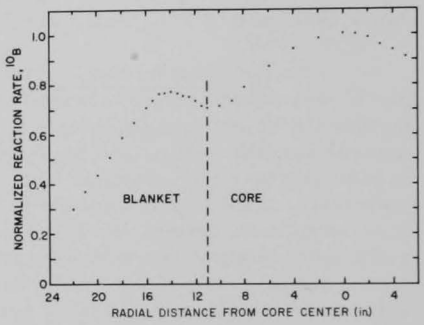

Fig. I.B.9. Normalized Radial Reaction-rate Traverses for ^{10}B in Assembly 54

Pulsed neutron measurements have been performed with Assembly 53 and the iron-reflected version of Assembly 54. The reactor was pulsed with a Texas Nuclear Model 9405 neutron generator utilizing the 14-MeV neutrons from the (d,t) reaction. Prompt-neutron die-away curves were measured at several subcritical states varying from -300 to -1224 Ih.

The data were analyzed by a least-squares fit of the decay constant versus the amount of subcriticality. The results were $\beta/\ell = (0.481 \pm 0.014) \times 10^4$ for Assembly 53 and $(0.303 \pm 0.009) \times 10^4$ for Assembly 54.

Comparisons with MACH 1 calculations showed that the calculations produced values for β/ℓ which were 8 to 20% higher than provided experimentally, a result consistent with previous findings of other laboratories.

(ii) Assembly 55. Assembly 55 is a zoned core in which the composition of the central zone is adjusted so that $k_\infty = 1$. This configuration was designed for the specific purpose of measuring the capture-to-fission ratio (α) in ^{239}Pu. In the central zone, where $k_\infty = 1$, a neutron balance involves measurement of reaction rates only since the net leakage is zero.

Prior to actual loading of Assembly 55, the center hole of the ZPR-3 matrix was realigned. This was necessary because the reactivity measurements in the central zone are performed by oscillating a long drawer through both halves of the reactor. The tubes in the movable half were shimmed to correct the misalignment, and checks made with all of the inert materials of Assembly 55 in the matrix indicated that the problem had been eliminated.

The approach-to-critical was interrupted at about 90% of the eventual critical mass and with 4 of 10 rods out to allow for measurements with the proton-recoil spectrometer. Preliminary analysis of the spectrometer data indicated some difficulties with higher count rates, so that the measurements were repeated with essentially the same fraction of the critical mass loaded but all 10 control and safety rods withdrawn.

After initial criticality had been achieved, the control and safety rods were calibrated. Total safety-rod worth was 1.54% $\Delta k/k$ with rods spiked by adding fuel from neighboring drawers. In addition to the increase in fuel loading, some of the rods were loaded with most of the fuel at the front or along the inner edge to increase their worths further.

The reactor configuration, after the completion of the null-reactivity experiment, described below, is shown in Figs. I.B.10 and I.B.11. The core half-height is 18 in. and the axial reflector consists of 6 in. of stainless steel followed by 6 in. of depleted uranium. There is no axial driver. Total plutonium mass is 419.9 kg, safely under the limit of 430 kg. The mass of fissionable material in the core is:

$^{239}Pu + {}^{241}Pu$	385.3 kg
^{235}U	28.0 kg
Total Fissile Material	413.3 kg

Because of the 430-kg limit for total plutonium, it was necessary to add some ^{235}U-fueled drawers at the outside of the driver in order to achieve criticality. The locations of these drawers are indicated in Figs. I.B.10 and I.B.11.

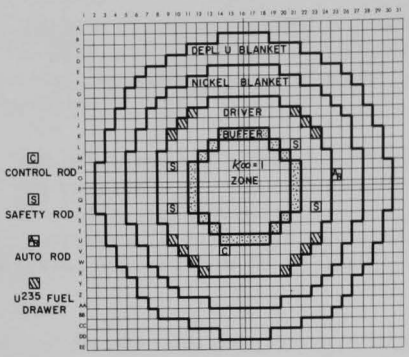

Fig. I.B.10. Reference Core for Half 1 of Assembly 55

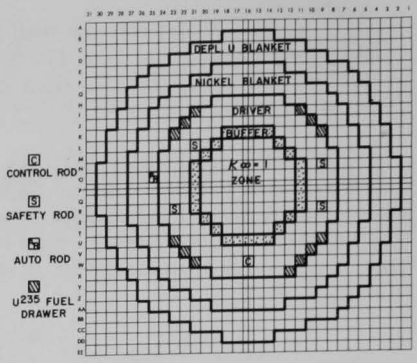

Fig. I.B.11. Reference Core for Half 2 of Assembly 55

Adjustment of the central zone to a composition closely approximating $k_\infty = 1$ was then begun. The reactivity worths of samples of various materials were measured in the center of the zone by oscillating 2-in. cubical sample containers into and out of the center of the core, using the drawer shown in Fig. I.B.12. At the "in" position, the samples are at core center, and the remainder of the drawer is filled with plates typical of the surrounding core. At the "out" position, the samples are completely out of the core. An automatic sample changer is used to exchange samples during a run.

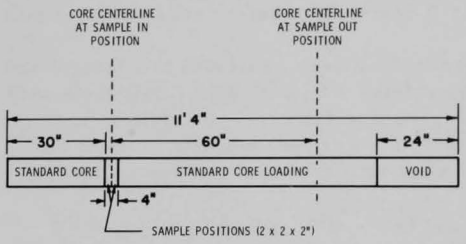

Fig. I.B.12. Schematic Diagram of the Long Drawer Used in the Null Reactivity Measurements with ZPR-3 Assembly 55

The measurement of the $k_\infty = 1$ zone involved oscillating a 2 x 2 x 2-in. sample of typical core material. If the composition were truly that of an infinite critical reactor, removal of a small portion of the material would have a zero or "null" reactivity effect. In Assembly 55, the initial test indicated a positive worth for the sample. As a result, composition "shimming" was done in a 6-in. cube at core center by adding 0.005 or 0.015 in. of depleted uranium foil to the drawers adjacent to special, thin-graphite plates. Subsequent reactivity measurements indicated that the shimmed sample had a net worth of +0.014 Ih. This was assumed to be "null" since previous estimates indicated that an error in the null composition of ±0.05 Ih or less would be negligible in comparison with other sources of error in the experiment. After the null composition had been confirmed, the entire central zone was adjusted to that composition

of rod-motion commands forms a ternary (three-valued) time series, whose members have values of +1, -1, or 0, respectively.

For these tests, the reactor was in equilibrium at a steady power of $2\frac{1}{2}$ W. The fluctuations observed were excited by inherent neutronic noise and detection noise. Each test was run for about 20 min with a fixed deadband equal to the estimated standard deviation of one flux reading.

To obtain the necessary data, the computer program doing the control was made to punch a character onto paper tape, indicating the rod-motion command given during each sampling interval. Following the run, the data on the tape were processed. When read back into the computer, each character on the tape was translated to the appropriate data value in memory.

To make the algorithm handle the ternary series, it was necessary only to provide for the compilation of a no-operation instruction to correspond to a zero datum. For autocorrelation, of course, only one string of instructions is compiled and that acts upon its own originating time series. The resulting code would read 1000 data points from the tape, and calculate the autocorrelation function for every value of lage from zero through 200 sampling intervals. Then the code read another thousand points from the tape and calculated the autocorrelation function for these, repeating the process until the end of the run. (If the last segment read did not contain a full thousand points, that segment was discarded.) The autocorrelation functions from each calculation were averaged to give the final results. These were plotted by the computer up to a selected maximum lag.

The correlogram for the normal control setup with a 0.1-sec sampling interval is shown in Fig. I.B.2. This system has been

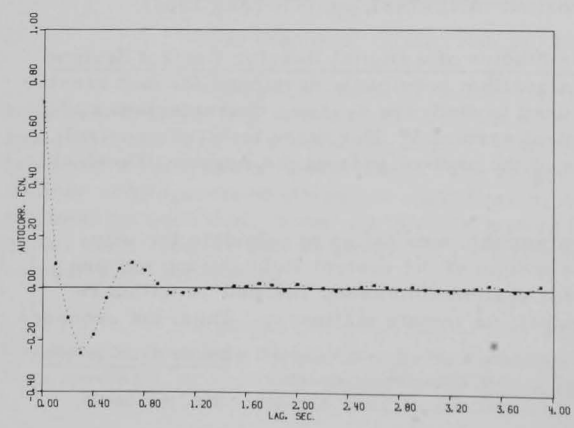

Fig. I.B.2

Autocorrelation Function of Rod-control Signal with 0.1-sec Sampling Interval and Actual Control Algorithm

analyzed by Marciniak,* who compared the control algorithm actually used with a simple zero-order hold. Marciniak predicted that the zero-order hold should be more stable than the actual algorithm in all cases, except for a thermal reactor with sampling interval of 0.1 sec or less. The result for the zero-order hold is shown in Fig. I.B.3. As predicted, it is more underdamped.

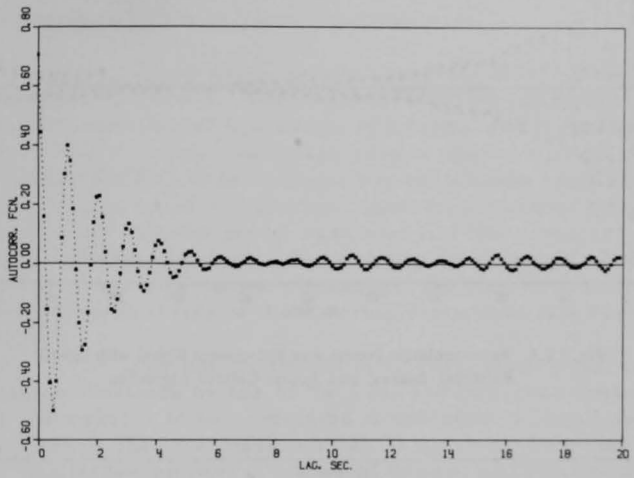

Fig. I.B.3. Autocorrelation Function of Rod-control Signal with 0.1-sec Sampling Interval and Zero-order Hold

The correlogram in Fig. I.B.3 is close to the familiar exponential-cosine shape, but the damping is not monotonic. To explain that, one may conjecture that the correlogram is the sum of two exponential-cosine components with characteristic frequencies very close together. The resultant would then contain beats between the two frequencies.

Tests were also run with a sampling interval of 0.5 sec. Fig. I.B.4 shows the correlogram for the actual control algorithm, Fig. I.B.5 that for a zero-order hold. As predicted by Marciniak, the response of the zero-order hold is more strongly damped at this sampling interval. Also, the "beats" are much more noticeable for these cases. Neither is satisfactory for an actual control system. Therefore, the upper limit of usable sampling interval for this system is somewhere between 0.1 and 0.5 sec. Note that the degree of damping, as well as the "beats," are easier to see on the correlogram than they would be in a power-spectrum plot.

*Marciniak, T. J., "Study of a Linearized Sampled-Data Control Algorithm for Zero-Power Reactor," in Reactor Physics Division Annual Report, July 1, 1966 to June 30, 1967, ANL-7310, pp. 410-415.

by replacement of a 1/8-in.-thick column of graphite plates with 1/16-in.-thick depleted uranium and graphite plates in the proper ratio.

Once a satisfactory null-reactivity measurement had been achieved, two identical sets of foils were irradiated on different days, to determine the various reaction rates in the central zone. At the same time, corresponding sets of foils were irradiated in the thermal column of AFSR to provide thermal calibration data. Central reactivity worths of various materials, including a fuel plate with high ^{240}Pu content, were also measured, but the final results are not yet available.

Additional experiments to be performed include radiochemical analysis of a Pu-Al fuel plate and substitution of high-^{240}Pu fuel plates into the central zone to determine the effect of ^{240}Pu content on the value of α.

b. Heterogeneity. The investigation of fission-product gamma rays by the use of lithium-drifted detectors continued, with data accumulation from ^{238}U and ^{235}U foil traverses in ZPR-3 Assemblies 53 and 54, and ^{238}U and ^{239}Pu foil counting for Assembly 55. Most of the data analysis for the ^{238}U traverse has been completed, but some minor changes in the analysis code appear to be needed before a more accurate determination of ^{238}U capture can be made.

Investigation of the ^{238}U fission-product ratio of mass 132 to mass 97 seems to indicate a yield change with varying spectrum across the cell, but more analysis will be necessary before more definite conclusions can be drawn.

One thermal exposure of ^{235}U in AFSR has been made to compare fission-product-yield data with well-established values. About 110 spectra have been taken so far, and more will follow. Counting will continue for at least three months to obtain good data for 65-day ^{95}Zr and 40-day ^{103}Ru.

4. ZPPR Operations and Analysis (W. G. Davey and P. I. Amundson)

Last Reported: ANL-7513, pp. 25-27 (Oct 1968).

a. Basic Studies of Large Plutonium Systems Program. The preloading program for ZPPR Core I has been stopped due to potential programmatic changes involving both in-cell and core-blanket material alterations.

This program will be resumed as soon as the requirements for core and blanket-drawer design as well as core and blanket dimensions are clarified in sufficient detail to allow system planning to proceed.

b. Doppler Effect

(i) Design. Design drawings for the Doppler rod have been completed. A thermal baffle is being added to the existing oven.

(ii) Equipment. The ion pump and vacuum valves have been functionally tested and are leak-tight.

Controllers have been ordered for the heaters required by the new design.

c. Reactor Equipment Development

(i) Experimental Equipment

(a) Rod-timing circuits for the poison safety rods have been successfully tested.

(b) Minor mechanical problems, discovered as a result of coupling the radial perturbation sample changer, drive mechanism, and system controller, are being handled on a priority basis due to increased emphasis on these measurements early in the anticipated Core-I program.

(ii) Automation of Data Acquisition

(a) Data-collection System. Construction of the ANL-designed portion of the Data Collection System is complete and testing is in progress. Installation and testing of data link cables to the cell has been completed. Installation and testing of that part of the system which is located in the cell has been completed. Early delivery of purchased items is anticipated.

The ANL-designed portion of the system includes two digital display units, one display plus control unit, two in-cell multiplexers, one digital clock, and two buffer scaler registers.

(b) Counting Room. Interfacing of the Incremental Magnetic Tape Unit with the SEL-810A computer is in progress.

d. Heterogeneity. Approximately 75% of the equipment necessary for the automated gamma-spectrometry system for the ZPPR counting room has been received and tested. The equipment received consists of three Ge(Li) detectors, three amplifiers, one sample changer, one SEL-810 computer, one magnetic-tape system, and a digital I/O unit for the computer. Interface work is presently underway. An A/DC has been received on loan which will allow accelerated final interface design.

The three Ge(Li) detectors have characteristics which will allow work in particular regions of interest with greater detail than if they were all equivalent. The major features of each detector are tabulated below.

Detector A--Number L-394

5-sided drift--trapezoidal

System Resolution FWHM

@ 1332 keV (^{60}Co)--3.3 keV
@ 81 keV (^{133}Ba)--2.0 keV

Efficiency (relative to NaI)

@ 1332 keV--4.1%

Maximum efficiency at ~80 keV

Window cut-off at ~40 keV.

Detector C--Number L-370

5-sided drift--trapezoidal

Systems Resolution FWHM

@ 1332 keV--3.5 keV
@ 81 keV--1,8 keV

Efficiency at 1332 keV--3.6%

Maximum efficiency at ~80 keV

Window cut-off at ~40 keV.

Detector E--Number L-414

Circular drift--true coaxial

System Resolution FWHM

@ 1332 keV--$<$3.25 keV
@ 81 keV--2.1 keV

Efficiency at 1332 keV--3.7%

Maximum efficiency at ~70 keV

Window cut-off--$<$25 keV.

The single analyzer and three analyzer programs for the SEL-810 computer are nearly complete. The remaining required code is the magnetic-tape data-output section which will be formulated as the I/O routines are evaluated and checked out on the computer.

e. Preparations for Operation

(i) Reactor Control and Nuclear Instrumentation. The reactor Control and Nuclear Instrumentation Systems have been checked and are considered in an operational status.

Work on the system centers on "prooftest" runs with no fuel in the matrix. These runs are also used for operating familiarity training for reactor supervisors and operators.

5. ZPR Materials

a. Development of Fabrication Techniques (J. E. Ayer)

Last Reported: ANL-7478, pp. 34-35 (July 1968).

(i) Stacked-foil Elements. A group of 56 elements were fabricated for the Reactor Physics Division to measure the capture-to-fission ratio (^{239}Pu alpha) in ZPR-3. Included in this group were: 2 plate elements, 2 instrument traverse elements (ITE), 4 coin elements, and 48 foil elements. The fuel used in these elements was Pu-1.2 w/o Al. The dimensions of each element type is given in Table I.B.6.

TABLE I.B.6. Dimensions of Fabricated Fuel Elements

Element Type	Cladding	Nominal Dimensions (in.)							
		Length		Width		Diameter		Thickness	
		Fuel	Cladding	Fuel	Cladding	Fuel	Cladding	Fuel	Cladding
Plate	304 SS	1.924	2.000	1.766	1.945	-	-	0.085	0.125
ITE	304 SS	1.924	2.000	1.765	1.949	-	-	0.085	0.125
Coin	304 SS	-	-	-	-	0.478	0.518	0.041	0.125
Foil	1100 Aluminum	-	-	-	-	0.375	0.500	0.0005	0.011

The fuel for all elements was obtained from previously fabricated stock. The plate, ITE, and coin fuels were recovered from four core plates of ZPR-3. Two of the recovered plates were cleaned, inspected, and rejacketed into plate elements. The other two plates were fabricated into ITE and coin elements by punching a 5/8-in.-dia hole in the centers of the plates and shearing through the holes parallel to the long side. The two halves were assembled into jackets. The coins were fabricated from the punched disks by hot rolling the material to a 0.041-in. thickness and machining to size.

The fuel for the foil elements was obtained from stock used for EBR-I breeding-gain specimens. Fuel of required thickness,

between 0.0004 and 0.0006 in., was obtained by cold rolling sheet stock to final dimension. A punch and die were used in a hand-operated press to punch out the disks.

The fuels were cleaned and weighed just before being loaded into jackets. The plate, ITE, and coin fuels were loaded into the jackets through funnels to prevent plutonium contamination of the exterior surfaces of the jackets. These elements were TIG closure welded with end plugs while the jackets were held in copper chills.

The foil elements were fabricated* by cold welding of two aluminum disks with a plutonium disk sandwiched between them. The aluminum was 5-mil foil that had been thoroughly cleaned and abraded. A combination welding and trimming die operated in a hydraulic press was used to fuse a 0.020-in.-wide band around the outer edge of the aluminum disks. This cold welding reduced their combined thickness by 70%. The outer edge was trimmed in the same die by a shear ring.

*Shuck, A. B., Hins, A. G., Burt, W. R., and Beatty, R. A., Breeding Gain Specimens for EBR-I Core IV, ANL-6659 (1963).

C. Component Development--LMFBR

1. Sodium Technology Development

a. Engineering Development

(i) Sampling Development (J. R. Humphreys)

Last Reported: ANL-7513, pp. 36-38 (Oct 1968).

(a) Nonradioactive-sodium Distillation Sampling. The impurity (oxygen) monitoring run continued with the Sodium Analytical Loop. Oxygen concentration in the sodium was changed during 23 days by adjusting the cold-trap temperature in increments from a high of 455°F to a low of 250°F and then upward to 601°F. Dip samples, taken after equilibrium was established at the temperature increments, were vacuum-distilled and the residues were analyzed for sodium by atomic absorption. Oxygen contents, calculated on the basis of the entire residue being in the form of Na_2O, were:

Cold-trap Temp (°C)	Oxygen by Analysis (ppm)	Cold-trap Temp (°C)	Oxygen by Analysis (ppm)
235	39, 33, 36, 35, 34	208	15
218	27, 24, 26, 24	215	26, 26, 26, 21
121	3	234	30, 35, 29
127	3	316*	60, 54, 60, 55

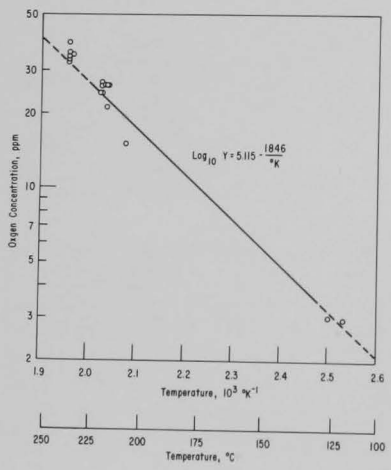

Fig. I.C.1. Oxygen-concentration Analyses vs Cold-trap Temperature in Sodium Analytical Loop

The values obtained are plotted in Fig. I.C.1 with the solubility curve reported previously (see Progress Report for June 1968, ANL-7460, p. 32). Oscillatory plugging-temperature data taken during this cold-trap temperature-cycling test are being analyzed.

(ii) Monitoring Development (S. B. Skladzien)

Last Reported: ANL-7513, p. 38 (Oct 1968).

(a) Oxygen Monitoring. The impurity concentrations in the Sodium Analytical Loop were varied by operating the cold trap at different temperatures. The response of the inline meters and the chemical analysis

*System is unsaturated with respect to oxygen at this temperature.

of sodium for oxygen at each cold-trap temperature are given in Table I.C.1 and are discussed below.

TABLE I.C.1. Meter Response to Impurity Changes

Time Cold Trap at Temperature (hr)	Cold-trap Temperature (°C)	Oxygen Meter (V)		Resistivity Meter (microhm) (corrected to 316°C)	Oxygen Concentration[a] (ppm)
		No. 202	No. 203		
4	218	1.127	1.113	312.12	27.3
23	219	1.127	1.115	312.11	24.3
28	218	1.128	1.116	312.10	26.5
119	218	1.129	1.116	312.07	24.0
Average	218	1.128	1.115	312.10	25.5
1[b]	129	1.131	1.119	311.88	10.0
4	121	1.141	1.126	311.70	2.9
27	133	1.144	1.129	311.57	3.2
30	127	1.143	1.129	311.64	2.6
Average	128	1.143	1.128	311.70	2.9
0[b]	214	1.132	1.119	311.82	14.9
20	218	1.130	1.118	312.06	26.5
24	217	1.130	1.118	312.06	25.6
92	212	1.131	1.117	312.03	26.3
96	215	1.132	1.119	312.03	21.6
Average	215	1.131	1.118	312.04	25.0
1[b]	234	1.130	1.115	312.10	30.5
24	233	1.129	1.115	312.13	35.0
27	233	1.129	1.115	312.13	29.1
Average	233	1.129	1.115	312.12	32.0
22	316	1.126	1.112	312.29	60.2
25	317	1.126	1.112	312.29	53.9
45	316	1.125	1.112	312.28	60.5
49	317	1.125	1.111	312.30	54.6
Average	317	1.126	1.112	312.29	57.3

[a]Dip samples, vacuum distilled, atomic absorption analysis.
[b]Not enough time to reach equilibrium; the corresponding data were not used in the average.

The two United Nuclear Corporation oxygen meters responded quantitatively to each change in the cold-trap temperature. A calibration line for each meter was obtained by plotting the cell voltage versus oxygen concentration. The equations of the lines obtained were

$$\text{Meter No. 202:} \quad E = 1.147 - 0.0053 \text{ Log } C;$$

$$\text{Meter No. 203:} \quad E = 1.134 - 0.0053 \text{ Log } C.$$

The last reported* calibration of the same meters gave

$$\text{Meter No. 202:} \quad E = 1.161 - 0.026 \text{ Log } C;$$

$$\text{Meter No. 203:} \quad E = 1.151 - 0.026 \text{ Log } C.$$

*ANL Reactor Development Program Progress Report, May 1968, ANL-7457, p. 38.

In the 7 months since that calibration, the sensitivity of both meters dropped considerably. However, the response over the duration of the test was in proportion to the oxygen concentration in sodium. Therefore, we conclude that these meters can be used to indicate relative oxygen changes in sodium, but frequent calibrations would be necessary if they are to be used to measure absolute concentrations of oxygen.

(b) Sodium Electrical-resistivity Monitoring. The dc absolute resistivity meter showed a change of approximately 0.6 microhm in the sodium resistance during the present cold-trap run. The response to changes of oxygen concentration (by cold-trap injections) was 0.0042%/ppm oxygen; the last previously reported* response was 0.0067%/ppm oxygen, which was obtained from a series of hydroxide injections into sodium. The difference might be explained by the presence or absence of other impurities, such as hydrogen.

2. Reactor Mechanism and Instrumentation

a. FFTF Instrumentation (R. A. Jaross)

(i) In-core Flowmeter Development (R. A. Jaross).

(a) Prototype Permanent-magnet Flowmeter Tests

Last Reported: ANL-7500, p. 37 (Sept 1968).

The overall length of the flowmeter is being reduced from $20\frac{1}{4}$ in. to 12 in.; part of the reduction is being accomplished by omitting space for thermocouples in the fluid-entry nose of the flowmeter. Preliminary pressure-drop calculations for the 12-in. flowmeter indicate a drop of less than 6 psi at a sodium velocity of 40 ft/sec.

The use of a cylindrical magnet instead of two curved magnets and soft-iron pole pieces is being investigated to increase the flux density in the air gap so as to increase output signal and flowmeter sensitivity. The cylindrical magnet would have longitudinal slots along its inner surface to accommodate the ceramic-insulated lead wires.

(b) Eddy-current Flowmeter Tests

Last Reported: ANL-7500, pp. 37-39 (Sept 1968).

Sample universal-type coils for the preliminary eddy-current flowmeter experimental verification tests have been wound successfully. The high-temperature coils are being wound with Secor Metals Corporation 0.015-in.-dia, nickel-coated silver magnet wire having

*ANL Reactor Development Program Progress Report, January 1968, ANL-7419, p. 28.

ceramic insulation. We had planned to procure the high-temperature coils from Atomics International, but their equipment is not suitable for winding coils of the universal type.

Coils have been made by Atomics International using nickel-plated silver wire insulated with fiberglass wet-wound by immersing the insulated wire in a phosphate-bonded ceramic slurry; however, the insulation thickness runs from approximately 4 to 9 mils, which is excessive and would greatly curtail the sensitivity of the flowmeter.

Our search for other suppliers of insulated nickel-clad silver magnet wire for 1200°F operation in the sizes required for future flowmeters has not been fruitful to date. Three suppliers of uninsulated nickel-clad silver magnet wire have been asked for quotations: (1) Sylvania Electric Products, Inc., Warren, Pennsylvania; (2) Physical Sciences Corporation, Arcadia, California; and (3) Cooner Company, Van Nuys, California. Industrial sources that can apply a suitable insulation to the bare magnet wire are being sought.

(ii) Failed-fuel Location Method (E. Sowa)

Last Reported: ANL-7513, pp. 40-41 (Oct 1968).

(a) Sodium Test Loop. Construction of the demonstration sodium loop has proceeded. The pump support assembly, tank return line, tank support brackets, the gas-detection chamber, the gas-circulation pumps, and the Conoseal connectors have been received. The connectors are being incorporated into the gas-disengagement section of the loop. Control panels, instrumentation, and circuitry are being assembled and installed.

Fund limitations have dictated the elimination of the gas-detection system from the surge tank; experiments will be started without the use of this auxiliary.

Calculations made during preparation of the state-of-the-art report show that a low separation rate of gas can be expected. Alternative procedures are being investigated to enhance the disengagement of the gas to the detection chamber.

3. Fuel Handling, Vessels, and Internals--Core Component Test Loop (CCTL) (R. A. Jaross)

Last Reported: ANL-7513, p. 41 (Oct 1968).

Modification, test, and reassembly of the pump were completed. The CCTL was operated at 400°F max and pump speed reached 200 rpm.

Cold-trap operation, face-seal oil leakage at low pump speed, and the facility smoke-detector alarm were checked.

Operation on a 24-hr/day basis has begun. As of November 20, the CCTL operated 346.2 hr; pump downtime was 3.8 hr total, of which 1.7 hr was for obtaining the first sodium sample for chemical analysis and 2.1 hr was for adjusting the sodium operating level in the CCTL expansion tank.

Oil leakage through the modified face seal averaged 2.2 cm^3/hr. Pressure-drop data at various test-assembly flow conditions are unchanged from data taken before the pump face-seal was modified.

The CCTL has been operated to keep sodium flow through the FFTF test assembly at the 400-gpm design value. As shown in Table I.C.2, the temperature of the sodium in the loop has been increased as the impurity-oxygen content (as indicated by the plugging temperature) has been reduced. To remove the oxygen from the sodium, the temperature of the NaK coolant entering the cold trap has been reduced.

TABLE I.C.2. Typical Plugging Data for CCTL

Date	Loop Temp (°F)	Inlet Temp of Cold-trap Coolant NaK (°F)	Plugging Temp (°F)
10/30/68	355	268	258
11/1	380	274	290
11/4	375	290	247
11/11	420	240	238
11/12	455	225	238
11/13	500	235	238
11/14	550	240	240
11/15	550	242	249
11/19	650	195	225
11/20	650	195	<215

D. Systems and Plant--LMFBR

1. 1000-MWe Plant

a. Contract Management, Technical Review, and Evaluation (L. W. Fromm)

Last Reported: ANL-7513, pp. 41-42 (Oct 1968).

The AEC-ANL International Conference on Sodium Technology and Large Fast Reactor Design was held at Argonne November 7-9, 1968. Some of the results of the 1000-MWe LMFBR Follow-on Studies were presented at the Conference.

The only impediment to publication of the Task-I reports is a settlement on patent clearance of the Atomics International study. An AEC-RDT decision on this is expected soon.

The quarterly report for the period of March 1 through June 30, 1968 has been published and distributed.

(i) Babcock & Wilcox Co. Subcontract. Work continues on Task IV, which is about 85% complete. All research and development program descriptions have been drafted, and calculations for the cost-benefit subtask have been completed. The draft of the Task-IV report is expected to be issued soon.

ANL is continuing to review the conceptual system design descriptions (CSDD). Seven draft CSDDs have been revised to reflect ANL comments.

(ii) Westinghouse Electric Corp. Subcontract. The report on the tradeoff study of the single-module versus four-module cores is being reviewed. Work continues on the Task-III parametric studies of both reference plants and on component designs for the final Task-II report. The architect-engineer selected the containment structure design and has developed a plot plan.

Most parts of the Task-IV report have been drafted, and coordination has begun.

A topical report of the Task-V safety studies is being prepared for reproduction.

(iii) General Electric Co. Subcontract. All engineering for the Task-II, -III, and -V reports has been completed. The Task-II report is being typed for reproduction. Report information for Tasks III and V is being reviewed. The Task-III report is about 90% drafted. Some areas of the Task-III report are being modified to fulfill the Task-III requirements.

For Task IV, research and development requirements are being identified, and information and programs are being developed to fulfill the requirements.

(iv) Combustion Engineering, Inc., Subcontract. The Task-IV work is about 95% complete. Except for the safety section, all drafts have been completed and final editing is in progress.

(v) Atomics International. The thermal-hydraulic analysis of the Task-III reference reactor is continuing. Summary details of the Task-III reactor and plant were described at the International Conference on Sodium Technology and Large Fast Reactor Design. Two papers presented at the ANS winter meeting in Washington, D.C., also described work performed for the 1000-MWe LMFBR Follow-on Study.

E. EBR-II

1. Research and Development

a. Reactor Experimental Support--Reactor Analysis and Testing (R. R. Smith)

Last Reported: ANL-7513, pp. 43-50 (Oct 1968).

(i) Nuclear Analysis and Safety

(a) Improved Flow Distribution in EBR-II (J. F. Koenig and F. D. McGinnis)

Further calculations were made in the study of flow required in each row of the reactor to equalize maximum temperatures of the inner surfaces of the driver-fuel cladding. (See ANL-7513 for details on methods and the conditions assumed for calculational purposes.)

A flow balance was made for conditions of reduced core pressure drop, equal maximum cladding temperature in each row, and a total core exit flowrate of 9000 gpm. For a core with a uranium blanket, the maximum cladding temperature was calculated to be 967°F. Similarly, the maximum cladding temperature for a stainless steel-reflected core was calculated to be 972°F. The temperature distributions in the fuel subassemblies and the required flowrates are shown in Table I.E.1. For comparison purposes, the calculated temperature distributions at 50 MWt for the present orificed core are also shown. For the reorificed core, the maximum cladding temperatures would be reduced approximately 35°F for the uranium-blanket core and 28°F for the stainless steel-reflected core at 50 MWt. At 62.5 MW, the maximum cladding temperatures would be reduced 44 and 35°F, respectively. The reactor configuration used for this study assumed that Row 5 was filled with experimental subassemblies so that the maximum temperature decrease occurred in fuel subassemblies in Rows 4 and 6 in the control-rod subassemblies. The core pressure losses would be about 32 and 33 psi for the uranium-blanket and stainless steel-reflected cores, respectively.

If the core pressure loss were maintained at its reference value of 41 psi, the total flow through the driver subassemblies would be less than that for the reduced-pressure-drop case. Therefore, the temperature decrease would be reduced. Table I.E.2 summarizes the reduced-pressure-drop and reference-pressure-drop results for a uranium-blanket and stainless steel-reflected core. In comparison to the reduced-pressure-drop case, the maximum clad temperature would increase 10°F (to 977°F) for the uranium-blanket core and 7°F (to 979°F) for the stainless steel-reflected core.

TABLE I.E.1. Subassembly Flowrates and Temperature Distributions at Reduced Core Pressure Drop and 50-MWt Power

Row	Flowrate (gpm)		Maximum Fuel-rod Temperatures (°F)					
			Present			This Study		
	Present	This Study	Inside of Cladding	Fuel (Avg)	Centerline	Inside of Cladding	Fuel (Avg)	Centerline
			Uranium Blanket					
1&2 FA[a]	138.0	122.6	941	1003	1054	967	1028	1078
3 FA	121.0	119.0	959	1018	1067	967	1026	1074
SR[b]	84.5	81.8	961	1019	1065	967	1025	1072
4 FA	92.6	109.2	1002	1057	1097	967	1022	1066
5 FA	77.0	92.4	1012	1060	1094	967	1017	1054
CR[c]	60.0	67.3	995	1044	1079	967	1015	1052
6 FA	66.5	76.5	1000	1040	1069	967	1008	1036
			Stainless Steel Reflector					
1&2 FA	151.0	125.8	927	992	1046	972	1034	1086
3 FA	133.0	122.3	945	1007	1058	972	1034	1083
SR	90.6	84.3	956	1017	1067	972	1033	1082
4 FA	97.6	112.9	998	1054	1098	972	1029	1075
5 FA	82.6	98.7	986	1037	1074	972	1022	1063
CR	64.3	70.9	996	1048	1086	972	1024	1064
6 FA	71.4	83.0	1000	1043	1074	972	1016	1046

[a]FA: Fuel Subassembly.
[b]SR: Safety Rod.
[c]CR: Control Rod.

TABLE I.E.2. Subassembly Flowrates for Reduced Pressure Drop and 40.8-psi-pressure-drop Core at 50-MWt Power

	Uranium-blanket Core		Stainless Steel-reflected Core	
	Core Pressure Drop (psi)		Core Pressure Drop (psi)	
	32	40.8	33	40.8
Maximum Temp inside Cladding (°F)	967	977	972	979
Subassembly Flowrate (gpm)				
Row:				
1&2 FA[a]	122.6	117.4	125.8	120.7
3 FA	119.0	114.0	122.3	118.1
3 SR[b]	81.8	77.5	84.3	81.8
4 FA	109.2	104.0	112.9	109.6
5 FA	92.4	88.8	98.7	95.9
5 CR[c]	67.3	64.3	70.9	68.7
6 FA	76.5	73.4	83.0	80.4

[a]FA: Fuel Subassembly.
[b]SR: Safety Rod
[c]CR: Control Rod.

The flow-distribution requirements for the uranium-blanket and stainless steel-reflector cores are different. The stainless steel-reflected core was chosen as a reference because it has a higher neutron flux in the core and higher power density in the outer rows, both of which are more desirable in a test reactor. The changes in the maximum clad temperature that would occur if the orificing for the stainless steel-reflector core was used in a uranium-blanket core are shown in Table I.E.3. The maximum difference in temperature of cladding in the various rows is about 14°F.

TABLE I.E.3. Subassembly Flowrates and Maximum Cladding Temperatures When Using Orificing for a Stainless Steel-reflected Core in a Uranium-blanket Core at 50-MWt Power and 40.8-psi Core Pressure Drop

		Uranium-blanket Core	
Row	Stainless Core Flowrate (gpm)	Flowrate (gpm)	Max Cladding Temp (°F)
1&2 FA[a]	120.7	115.7	979
3 FA	118.1	113.2	979
3 SR[b]	81.8	78.4	975
4 FA	109.6	105.1	974
5 FA	95.9	91.7	969
5 CR[c]	68.7	65.8	972
6 FA	80.4	77.1	965

[a]FA: Fuel Subassembly.
[b]SR: Safety Rod.
[c]CR: Control Rod.

(ii) Higher Power Operation

(a) Mark-II Fuel (R. A. Cushman)

The thermal and hydraulic safety analysis of the Mark-II experimental fuel subassemblies has been completed. The analysis complied with the criteria for irradiation of unencapsulated experiments in EBR-II. The fuel was assumed to have swollen to 75% of its original density because of irradiation effects, and the thermal conductivity was assumed to have been reduced correspondingly.

(b) Nickel Reflector (R. A. Cushman)

Calculations are being made to determine the rate of heat generation and the resultant temperature distribution in the proposed nickel reflector for Rows 7 and 8. Power productions of 7.2 kW for a 7-N-4 subassembly and of 3.6 kW for an 8-N-4 subassembly (those at the center of the flats of Rows 7 and 8, respectively) have been calculated for a reactor power level of 50 MWt. Coolant flowrates of 0.9 and 0.45 gpm have been specified for Rows 7 and 8, respectively. Detailed temperature distribution is being calculated, using the revised THTB program.

b. Nuclear Analysis Methods Development

Last Reported: ANL-7513, pp. 50-56 (Oct 1968).

(i) Oxide Driver Core. A conceptual design of an oxide core for EBR-II was developed as a starting point for exploratory neutronics and thermal-hydraulics calculations. The driver-fuel element is assumed to be a Type 316 stainless steel tube, of 0.220-in. OD with a 0.016-in. wall, containing UO_2-20 w/o PuO_2 at a smeared density of 85%. The plutonium is 80 a/o ^{239}Pu and 20 a/o ^{240}Pu; the uranium is enriched to about 50% in ^{235}U. The active length of the fuel column is 14.22 in. A driver subassembly is made up of 61 such elements, and the core extends to the first six rows. Of the total of 91 core subassemblies, eight are control-rod and two safety-rod subassemblies; each of these ten subassemblies is assumed to contain 37 fuel elements identical to those used in the driver subassemblies. The core contains 13 experimental subassemblies, nine of which are fueled approximately like a driver subassembly and four of which are subassemblies for structural experiments, and contain 50 v/o 316 stainless steel-50 v/o sodium. The axial reflector material is Type 316 stainless steel. In Rows 7 through 11, the reflector material is nickel; in Rows 12 through 15, depleted uranium metal is used.

The reactor is assumed to be at an average temperature of 820°F, with its expansion both radially and axially controlled by that of its Type 316 stainless steel structure. For added realism, fission products equivalent to 2% burnup are included. Homogenized atom densities are computed directly from the detailed geometries of the various subassemblies, thus further contributing to a realistic model.

The ^{235}U enrichment was estimated using self-consistent one-dimensional diffusion theory to simulate the two-dimensional core. Here, iteration was done on group-independent transverse bucklings in slab and radial geometry to a consistent core composition. The cross-section set 238 was used; it is the most nearly appropriate of currently available sets.

The ^{235}U enrichment was found to be 55.9%. The axial reflector saving was 14.00 cm and the radial saving 19.49 cm. The radial maximum-to-average source distribution in the core was 1.238, and the median energy for the core flux was 373 keV. The peak flux, normalized to 62.5 MW, was 3.6×10^{15}.

Immediate plans are to check the foregoing results by using group-dependent transverse bucklings in radial geometry. The homogenization assumption will be checked by a radial calculation with each row of subassemblies separately identified. A two-dimensional diffusion problem, using the DIF2D code, will also be performed to test one-dimensional approximations. A thermal-hydraulics analysis of the reference design will then be made with the EVALUATE code. This will furnish information on core pressure drop as well as maximum fuel and cladding temperatures that will serve as a basis for discussion leading to a second iteration on the design.

(ii) Monte Carlo Methods. Interpretation of integral data from critical experiments has been impeded by difficulties in treating heterogeneity effects. The slab lattices used in these experiments complicate the computation of effective group cross sections. Therefore, the AMC code has been modified to compute effective cross sections and temperature derivatives in slab lattices. This version of the code is expected to be useful in analyzing current critical experiments and also as a reference method to check approximate semianalytical methods as they are developed.

(iii) Seven-tube Cluster Absorber-follower Control Rod. The temperature at the center of the natural B_4C and the temperature differentials in the 7-tube-cluster absorber-follower control rod were recalculated by using updated heat-generation rates. At midcore and Reactor Row 5, the heat-generation rates are:

(a) for natural B_4C of 93% density: 20.1 W/cc [14.0 W/cc due to (n,α) reaction and 6.1 W/cc due to gamma heating];

(b) for stainless steel: 19.7 W/cc due to gamma heating.

Assuming a chopped-cosine heat-generation distribution, the center temperature of the B_4C is expected to be 980°F at the top of the core and 879°F at 4 in. above the center of the core. The detailed results are shown in Table I.E.4.

TABLE I.E.4. Heat-generation Rates and Temperatures of B_4C and Stainless Steel Capsule

Position of B_4C	Heat-generation Rates (W/cc)				Temperatures (°F)					
	B_4C[a]									
	(n,α) Reaction	X Ray	Total	Stainless Steel	Δt B_4C	Δt He Gap	Δt SS Cladding	Δt Na Film	t Na	t B_4C at Center
At Top of Core	9.1	3.8	12.9	12.3	12.0	25.6	4.3	2.3	936	980
At 4 in. above Centerline of Core	12.6	5.3	17.9	17.1	16.5	35.6	6.0	3.0	818	879
At Center of Core[b]	14.0	6.1	20.1	19.7						

[a]B_4C: Natural, 93% of theoretical density.
[b]Data shown for reference only.
Note: Melting point of B_4C is about 3700°F.

(iv) Oscillator-rod Subassembly--Mark II. Calculations were made to predict the center temperature of the B_4C in the Mark-II oscillator rod by using heat-generation rates at the midcore as follows:

(a) for B_4C of 87% density and 94% enrichment: 62.1 W/cc [(n,α) reaction and gamma-heating];

(b) for Al_2O_3: 5.4 W/cc;

(c) for stainless steel: 19.7 W/cc.

The calculated results for B_4C at the midcore and with a sodium flowrate of 5 gpm are as follows:

$$t_{B_4C} \text{ at center} = 865°F \qquad t_{Na} = 716°F$$
$$\Delta t_{B_4C} = 36°F \qquad \Delta t_{He\ gap} = 100°F$$
$$\Delta t_{cladding} = 11.7°F \qquad \Delta t_{Na\ film} = 7°F$$

c. Fuel Performance Studies--Mark I Series (C. M. Walter)

Last Reported: ANL-7500, pp. 56-57 (Sept 1968).

(i) Driver Fuel Operation at High Temperatures and Burnups. The original maximum burnup level of 1.2 a/o was set for Mark-IA driver fuel when only limited knowledge of fuel behavior was available. At that time the conservative approach of avoiding cladding contact by the swelling fuel was adopted. Accordingly, a considerable effort was made to obtain a low-swelling fuel (e.g., the specification of range of silicon content for U-Fs that is in force).

Recently a new approach has been developed based on the philosophy that the life of a fuel element is determined by the occurrence of cladding rupture or unacceptable cladding strain. The establishment of this philosophy requires an experimental program to determine cladding strain in encapsulated high-burnup Mark-IA elements. Table I.E.5 reviews the EBR-II irradiations included in the current program.

TABLE I.E.5. High-burnup Mark-IA Experiments

Capsule	Subassembly	Present Max Burnup (a/o)	Final Max Burnup (a/o)	Max Mean Cladding Temp (°F)	Max Temp at Fuel Center (°F)	Projected Irradiation Completion Date
BF-02	XO15	2.9	3.7	897	1025	April 1969
BF-03	XO15	2.9	3.7	897	1025	April 1969
BF-04	XO17	2.5	2.9	918	1061	Jan 1969
BF-05	XO17	2.5	2.5	918	1061	Oct 1968
BF-08	XO17	2.4	2.9	918	1061	Jan 1969
BF-09	XO17	2.5	2.5	918	1061	Oct 1968
BF-11	XO17	2.4	2.9	918	1061	Jan 1969

Five high-burnup (2.5 a/o maximum) Mark-IA encapsulated fuel elements, Capsules BF-04, BF-05, BF-08, BF-09, and BF-11, have been removed from Subassembly XO17, neutron radiographed, and pronounced sound (i.e., no cladding bulging or failure). Two, BF-05 and BF-09, have been de-encapsulated and measured for diameter increase (see Table I.E.6).

TABLE I.E.6. Increase in Diameter of Cladding (%) of Capsules BF-05 and BF-09

	Distance from Bottom End of Fuel (in.)							
Capsule	0.2	2.2	4.2	6.2	8.2	10.2	12.2	14.2
BF-05	0.58	0.73	0.77	0.79	0.80	0.63	0.45	0.32
BF-09	0.49	0.46	0.57	0.72	0.65	0.49	0.50	0.14

Maximum strains of about 0.6% were found for both elements (after about 0.15% was subtracted for stainless steel swelling). The uncertainty in these strain measurements is probably about ±0.1%. The BF-05 element will be used for TREAT experiments with high-burnup fuels; the BF-09 element is being destructively examined. The BF-04, BF-08, and BF-11 elements are being returned to EBR-II for further irradiation in a reconstituted XO17 subassembly.

The BEMOD* computer code has been developed to help model the behavior of metallic fuel elements with an emphasis on predicting cladding strain and fuel-element lifetime. This code is based on

*Jankus, V. Z., BEMOD: A Code for the Lifetime of Metallic Fuel Elements, ANL topical report to be published.

the physical properties of the fuel and cladding materials, and has no disposable parameters. Uncertainties exist, however, in the application of the property measurements, especially with respect to strength of the swelling fuel and creep of the cladding. For instance, recent experiments by Gilbert* suggest that radiation-enhanced creep may be important under conditions in the EBR-II.

In Fig. I.E.1, the maximum strain versus burnup, with and without a flux, as calculated by BEMOD is compared to experimentally determined values for BF-05 and BF-09. Flux-enhanced creep of the cladding is an appreciable factor in the calculation. One of the parameters, the strength of the fuel, was chosen so that the flux-enhanced curve would nearly coincide with the strain measurements of BF-09. Based on the fuel strength, the unenhanced data show a much lower strain at equivalent burnups. Higher-burnup elements and more refinements in the code will be required before the flux effect can be completely sorted out.

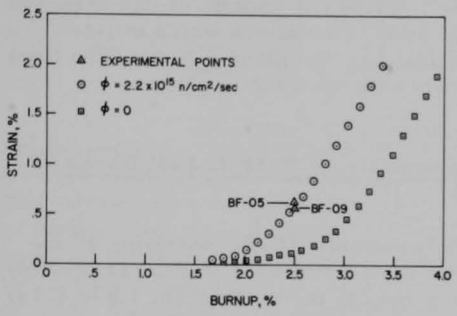

Fig. I.E.1. Comparison of Maximum Experimental Strain of Capsules BF-05 and BF-09, with Calculated Curves of Burnup vs Strain

The data plotted in Fig. I.E.1 predict that a maximum burnup of about 3.3 a/o can be obtained before cladding strains of 2% are reached. Table I.E.5 shows the planned irradiations that will go to and beyond this burnup. These irradiations should provide the data necessary to confirm or modify the existing calculation and to determine the design limit of Mark IA.

d. Mark II Driver Fuel Element Development

(i) Element Irradiation Tests

(a) Encapsulated Irradiations of Prototype Mark-II Elements in CP-5 (W. N. Beck)

Last Reported: ANL-7500, p. 57 (Sept 1968).

Capsule CP-59 contains three prototype Mark-II elements that are being irradiated at maximum cladding temperatures of 610°C and have accumulated a calculated burnup of 1.6 a/o. The thermocouples monitoring the central fuel temperature have failed, but the

*Gilbert, E. R., private communication, Oct 1968.

pressure sensor recording the plenum pressure of one of the elements (BF-04) continues to provide information on the release of fission gas from the fuel pin.

As previously reported, an initial sudden gas release occurred when the fuel volume had increased ~33%.* Calculations indicated that 36% of the fission gas was released to the plenum during this initial release. The percentage of gas release then gradually increased, signifying that the fuel volume was also increasing. This event took place between 0.47 and 0.80 a/o burnup, during which period the percent of gas released increased from 36 to 58%. Computer code calculations which utilize pressure-data input indicate that the fuel has elongated 0.20 in. The final dimension change will be measured when the element is neutron radiographed.

(b) Irradiation of Encapsulated Mark-II Fuel Elements (M. A. Pugacz)

Experimental Subassembly XO29, containing 37 encapsulated Mark-II fuel elements, has been dismantled at FCF for examination after accumulating maximum burnup in the range from 1.9 to 2.3 a/o. All fuel elements have been neutron radiographed at TREAT. Examination of the radiographs indicated that the fuel swelled to the inside diameter of the jacket. In no case was there evidence of breaching or failure of the cladding tube or any of the components making up the capsule.

At this burnup, all three restrainer designs were effective in inhibiting axial growth of the fuel. As observed in the neutron radiographs, the fuel pin grew axially up to the restrainer, regardless of its original location with respect to the top of the fuel element, and stopped. For example, if the restrainer was located 0.25 or even 0.75 in. above the top of the fuel, the fuel grew that distance and stopped.

Current plans call for removing three capsules for destructive examination. The three vacancies thus created will be filled by capsules already at Idaho, and the subassembly will be reinserted into the reactor to accumulate additional burnup.

e. Equipment--Fuel Related (E. Hutter)

(i) New Control Rod Subassemblies

Last Reported: ANL-7500, p. 58 (Sept 1968).

(a) Increased-worth Control Rod. Fabrication of the B_4C-cluster absorber-follower mockup was completed. The standard upper

*Beck, W. N., and Fousek, R. J., Fission Gas Release and Microstructural Changes in High Burnup U-Pu Fast Breeder Alloys, Trans. Am. Nucl. Soc. 9(2), 415 (1966).

shielding piece was removed from the IHE (increased holddown effect) control-rod test assembly and replaced with the B_4C-cluster mockup. Flowtests conducted with the new control-rod configuration indicated pressure drops greater than the required 38.8 psi at 61-gpm flow. As a first step to reduce the pressure drop, the lower shield piece of the control rod was redesigned and is now being fabricated. Additional flowtests will be conducted when fabrication is completed.

(ii) Engineering Consultation (O. S. Seim, J. A. Pardini, and T. E. Sullivan)

Last Reported: ANL-7500, pp. 58-59 (Sept 1968).

(a) IHE Dummy Control Rod. In accordance with the continuing policy to increase reactor safety and reliability, new dummy control rods (for reactor-kinetics experiments) will be fabricated utilizing the IHE (increased holddown effect) control-rod configuration. The IHE type of control rod, using an additional (intermediate) bushing below the upper bushing, provides a more positive downward seating force by decreasing the upward lifting force of the circulating coolant. This configuration will prevent the lifting force of coolant flow from raising the control rods during refueling, even when both primary-system sodium pumps are inadvertently operated at maximum flow.

The new IHE dummy control rod will utilize 19 stainless steel elements and will incorporate aluminum-bronze bushings. Assembly and detailed drawings for fabricating the rod have been completed.

(b) Tools for Inserting and Removing Safety-rod Thimbles. The new tools for inserting and removing safety-rod thimbles have been fabricated, tested, and shipped to Idaho. The tools proved satisfactory in removing one safety-rod thimble from the reactor and inserting another.

f. New Subassemblies Design and Experimental Support (E. Hutter)

(i) Irradiation Subassemblies (O. S. Seim, H. Halle, T. R. Bump, and B. M. Hoglund)

Last Reported: ANL-7513, pp. 57-64 (Oct 1968).

(a) Mark B. Drawings of the reinforced grid and modified capsule tips for the Mark B-7A have been completed and approval has been given to begin fabrication. A large number of new drawings was involved in this effort because the Mark B-7 is used in each reactor region (core and inner and outer blankets). New drawings were made of modifications of existing hardware, which will allow that hardware to be used until the new items can be procured.

The modifications were prompted by problems that developed during reassembly of long-term irradiation capsules. These capsules had swelled and distorted during irradiation, thereby reducing the initial design clearances. Because of the reduced clearances, more force was required to insert the 7-capsule bundle into the hexagonal tube. In some cases, the force was great enough to deform the grid members.

The new grid design has a square X-section bar and a thicker web section to provide greater rigidity. The capsule tips were changed to accept a thicker "T" bar and to provide a greater cross section of metal through the slotted portion.

(b) Mark E

(1) Mark E-37. The screen-type debris collector of the Mark E-37 was given a hydraulic flowtest in the Plexiglas test section of the unpressurized water loop. Debris from a fuel-pin meltdown, simulated with small particles of tin-bismuth alloy, was released from a container below the 40 x 40 mesh screen during conditions of full coolant flow.

Test results indicated that all particles larger than 0.020 in. in diameter were caught and that the container was not damaged. As the debris was being caught, coolant flow through the collector was not reduced by any measurable amount because the debris tended to accumulate mainly in the solid (nonperforated) top end of the collector.

Further flowtests are planned for the entire Mark E-37 subassembly to determine the characteristics of flow versus pressure drop. These tests will also determine the finest mesh size that can be used for the collector.

(2) Mark E-61. The design of the Mark-E-61 subassembly was modified to increase the length of the upper and lower shield pieces, and to reduce the radiation dose rate on the reactor cover and grid structure. The grid support, lower collector, and middle hexagonal tube also were completely redesigned to simplify disassembly. Drawings of the modified subassembly have been distributed for internal review and comment.

(c) Mark H. Fabrication of eight sets of hardware is continuing. Completion has been rescheduled for the first week in December.

g. Instrumented Subassembly (E. Hutter)

Last Reported: ANL-7513, pp. 65-67 (Oct 1968).

(i) Research and Development (A. Smaardyk and H. H. Hooker)

(a) Drywell Liner Tube. Tests have been conducted to verify the calculated capability of the drywell liner tube to withstand external pressure. A 6-ft length of drywell tube was sealed within a pressure vessel so that external pressure could be applied to the liner while measuring the change in the internal minor diameter. The liner exhibited completely elastic behavior to at least 80 psi; maximum deflection was 0.016 in. at this pressure. Because actual operating pressures in the instrumented subassembly will be only 10-15 psi, testing beyond 80 psi was considered unnecessary.

A limiting external pressure of 60 psi had been calculated for a tube with a finite initial ellipticity. This pressure proves to be conservative because the tests indicate that yielding does not occur at 80 psi.

(b) Prototype Fuel Pin Thermocouples (T. P. Mulcahey)

The 0.062-in. tantalum tubing (sheath material) was found to have some defects penetrating through as much as 16% of the wall thickness; a penetration of less than 10% is desired. The tubing is being eddy-current tested to determine if any sections meet the 10% criterion. The entire order, consisting of 250 ft of tubing, will be checked until 20 usable pieces, each $17\frac{1}{2}$-in. long, are found.

Delivery of the additional thoria insulators required if more than nine thermocouples are to be built has been delayed. A new delivery date is being established.

Further testing has shown that copper brazing is acceptable for joining the tantalum sheath to the Type 304 stainless steel adapter. The copper braze will be used in constructing the fuel-pin thermocouples.

Three hermetic seals heated to 1100°F for 30 min were found to be leak tight at room temperature. The seals will now be tested under 200-psi internal pressure at temperatures up to 1100°F.

A seal-cleaning procedure developed by Central Shops permits joining of the Kovar tubes to the hermetic seals by electron-beam welding. A strong, leak-tight weld is formed when the seals are precleaned

with nitric acid. Kovar tubes are being welded to 20 hermetic seals that are to be used for the final thermocouples. Twenty alumina insulators (for use in the hermetic seals) and 14 adapters are being machined.

The fixture for welding the 0.010-in.-dia W-3% Re/W-25% Re wires to the 0.020-in.-dia 308L/Alumel wires has been completed. The fixture for brazing the 308L and Alumel wires into the hermetic seals is being constructed.

h. Process Chemistry (D. W. Cissel)

Last Reported: ANL-7500, pp. 62-65 (Sept 1968).

(i) Sodium Coolant Quality Monitoring and Control (W. H. Olson, C. C. Miles, E. R. Ebersole, and G. O. Haroldsen)

(a) Primary Sodium

(1) Radionuclides. The results of analysis for radionuclides in primary sodium are listed in Table I.E.7.

TABLE I.E.7. Radionuclides in Primary Sodium

Sample Date	Results Corrected to	^{137}Cs (10^{-2} μCi/g)	^{131}I (10^{-4} μCi/g)
10/18/68	10/18/68		5.40
10/22/68	10/22/68	1.58	3.61
11/3/68	11/3/68		5.86

(b) Secondary Sodium

(1) Trace Metals. A sample of secondary sodium taken October 24, 1968, was analyzed for trace metal impurities by atomic absorption. Results are listed in Table I.E.8.

TABLE I.E.8. Trace Metal Impurities in Secondary Sodium

Metal	Concentration (ppm)	Metal	Concentration (ppm)
Al	<1.0	Cu	<0.2
Bi	<0.5	Fe	<0.6
Cd	<0.05	Mn	<0.1
Co	<0.2	Pb	0.7
Cr	<0.1	Sn	<2.4
		Zn	<0.1

A vacuum-distillation method of concentrating impurities is being tried for use with spark-source mass-spectrometric analysis. In this method, a sodium sample of 12-15 g is taken in a tantalum crucible. The sodium is vacuum distilled from the crucible by induction heating, and the residue is taken up by aqua regia for analysis. Several experiments have been made to determine which elements might be lost in the distillation process. All the analytical work for these investigations was performed by atomic absorption. Table I.E.9 shows the elements investigated and their recoveries after distillation.

TABLE I.E.9. Recovery of Metals in Residue from Sodium Distillation

	Experiment I		Experiment II		Experiment III	
Metal[a]	Micrograms Added	Percent Recovered	Micrograms Added	Percent Recovered	Micrograms Added	Percent Recovered
Al	60	100	60	100		
Bi	108	95	108	94		
Cr	20	100	20	99		
Co	40	97	40	99		
Cu	40	101	40	99		
Pb	20	84	120	88	120	100
Mg	20	96	20	99		
Mn	8	100	8	100		
Mo	58	101	58	100		
Ni	40	103	40	97		
Cd	10	74	10	4	10	0
Ca	11	33	54	57	54	106
Sn	209	86	104	24	209	100
Zn	10	52	10	50	10	1.5

[a]All elements added as chlorides.

In two experiments, cadmium, calcium, lead, tin, and zinc were apparently lost to some extent in distillation when spiked into the sodium with the other nine elements listed. However, when these elements were used together in the third experiment, only cadmium and zinc were lost. Further investigation showed that the losses were spurious for the calcium, tin, and lead. Silica interference caused the atomic-absorption method to give low results.

An exploratory run has been made of the determination of trace metals in secondary sodium by using vacuum distillation followed by spark-source mass spectrometry. The results of the run are shown in Table I.E.10.

TABLE I.E.10. Spark-source Mass-spectrometric Analysis of Vacuum-distillation Residue from EBR-II Secondary Sodium

Element	Concentration in Sodium[a] (ppm)	Concentration Measured by Atomic Absorption (ppm)	Element	Concentration in Sodium[a] (ppm)	Concentration Measured by Atomic Absorption (ppm)
Ag	0.1		K	0.04	
Al	0.006		Mg	0.3	0.4
B	0.02		Mn	0.05	<0.04
Bi	0.04	<0.2	Ni	0.3	0.1
Ca	3		Pb	0.4	1.0
Cd	0.09	<0.05	Si	1	
Co	0.005	<0.1	Sn	0.04	<4.0
Cr	0.9	0.05	V	0.02	
Cu	0.03	<0.1	Zn	0.04	
Fe	3	<1			

[a]10-g sample.

i. Experimental Irradiation and Testing (H. Lawroski)

Last Reported: ANL-7513, pp. 71-75 (Oct 1968).

(i) Experimental Irradiations (R. Neidner)

(a) Status of Experiments in EBR-II. The status of the experimental irradiation subassemblies in EBR-II as of November 30 is shown in Table I.E.11.

Subassembly XO21A was discharged at the end of Run 31. Capsule PNL-7-23 will be removed from the subassembly, having accumulated its exposure goal of about 0.4×10^{22} nvt. A replacement capsule will be installed, and the subassembly, redesignated XO21B, will be recharged during the loading for Run 33.

To provide space for Subassemblies XO45 through XO49 for the special dosimetry tests in the reactor, Subassemblies XO18, XO19, XO25, and XO41 were removed from the grid for the 413-MWd Run 31F.

Subassembly XO39, containing capsules from an earlier subassembly (XO11) and some new capsules, was removed from the grid for Runs 31B, 31C, and 31D because of reactor operation at reduced power (30 MW). The five mixed-oxide capsules from PNL in Subassembly XO39 were believed to be sensitive to reduced-power operation, and the objective of these capsules might have been compromised if they had been left in the reactor. The subassembly was returned to the grid at the start of Run 31E.

TABLE I.E.11. Status of EBR-II Experimental Irradiations

Subassembly (Position)	Date Charged	Capsule Content and Number of Capsules ( )		Experimenter	Accumulated Exposure (MWd) 11/25/68	Estimated Goal Exposure (MWd)	Approx Accumulated Burnup (fuels--a/o) (nonfuels--nvt x 10^{-22})
XG03 (7D1)	7/16/65	UO_2-20 w/o PuO_2	(2)	GE	18,203	23,300	4.7
		Stainless Dummies	(17)				
XG04 (7B1)	7/16/65	UO_2-20 w/o PuO_2	(2)	GE	18,203	45,000	4.7
		Stainless Dummies	(17)				
XA08 (4F2)	12/13/65	UC-20 w/o PuC	(8)	ANL	14,597	20,700	9.0
		Structural	(9)	ANL			5.4
		Structural	(2)	GE			5.4
X010 (7F3)	3/24/66	UO_2-20 w/o PuO_2	(4)	GE	15,134	20,400	5.6
		Structural	(11)	ANL			3.0
		Structural	(4)	PNL			3.0
X012 (4B2)	8/10/66	UO_2-20 w/o PuO_2	(19)	NUMEC	10,973	21,400	6.6
X015 (4A2)	11/15/66	UO_2-20 w/o PuO_2	(11)	NUMEC	9,318	11,500	5.6
		UO_2-20 w/o PuO_2	(2)	GE			5.2
		UC-20 w/o PuC	(4)	ANL			5.7
		U-Fs (Mk-1A)	(2)	ANL			2.9
X018 (2B1)	12/6/66	Structural	(3)	GE	9,349	22,900	3.8
		Structural	(1)	PNL			3.8
		Structural	(2)	ANL			3.8
		Structural and Heavy-metal Fission-yield Sample	(1)	ANL			3.8
X019 (6D2)	1/13/67	UO_2-20 w/o PuO_2	(7)	GE	7,977	13,000	2.9
		UC-20 w/o PuC	(3)	UNC			3.4
		Structural	(8)	PNL			2.2
		Graphite	(1)	PNL			2.2
X020 (6B5)	1/13/67	UO_2-PuO_2	(9)	GE	8,390	13,000	3.0
		UC-20 w/o PuC	(3)	UNC			3.6
		Structural	(4)	PNL			2.3
		Structural	(2)	ANL			2.3
		Graphite	(1)	PNL			2.3
X021A (2D1)	2/25/67	Structural	(6)	PNL	8,964	23,200	3.7
		Structural	(1)	PNL	1,228		0.5
X025 (4E2)	10/10/67	Structural	(19)	GE	7,061	7,700	2.6
X027 (4B3)	11/21/67	UO_2-25 w/o PuO_2	(18)	GE	5,489	7,700	3.3
		Structural	(1)	PNL			2.0
X032 (6E5)	11/22/67	UO_2-25 w/o PuO_2	(19)	PNL	5,792	11,900	2.5
X033 (5E2)	12/22/67	UC-20 w/o PuC	(19)	UNC	4,860	10,900	2.6
X034 (2F1)	4/13/68	Structural	(7)	ORNL	5,018	14,800	2.1
X035 (7B4)	4/13/68	Structural	(7)	ORNL	4,604	44,800	0.9
X036 (7E1)	7/25/68	UO_2-25 w/o PuO_2	(19)	GE	2,887	33,300	0.8
X038 (7C5)	5/7/68	Structural	(7)	INC	4,092	17,700	0.8
X039 (3C2)	8/15/68	UO_2-25 w/o PuO_2	(5)	PNL	1,431	3,000	0.6
		UC-20 w/o PuC	(1)	LASL			0.9
		Structural	(4)	GE			0.6
		UO_2-20 w/o PuO_2	(1)	ANL			0.9 + 3.7[a] = 4.6
		UO_2-20 w/o PuO_2	(7)	GE			0.9 + 3.7[a] = 4.6
		Structural	(1)	GE			0.6 + 4.7[a] = 5.3
X040 (5B2)	8/14/68	UO_2-20 w/o PuO_2	(19)	ANL	2,177	7,000	1.1
		UO_2-25 w/o PuO_2	(16)	GE			1.1
X041 (7A3)	7/24/68	Structural	(7)	PNL	2,553	16,700	0.5
X042 (7D5)	7/24/68	Boron Carbide	(4)	PNL	2,966	27,800	0.6
		Tantalum	(3)	PNL			
X044 (7A1)	9/28/68	Oxide Insulator	(1)	LASL	1,228	8,100	0.2
X045 (2B1)	11/4/68	Dosimetry	(2)	PNL/ANL	~0	~0	0
X046 (2B1)	11/6/68	Dosimetry	(2)	PNL/ANL	413	500	0.02
X047 (4E2)	11/6/68	Dosimetry	(1)	PNL/ANL	413	500	0.01
X048 (6D2)	11/6/68	Dosimetry	(1)	PNL/ANL	413	500	0.01
X049 (7A3)	11/6/68	Dosimetry	(1)	PNL/ANL	413	500	0.01

[a]Previous exposure from another subassembly.

(b) Status of Irradiation Experiment Proposals Given Approval in Principle. The status of all irradiation experiments that have been given approval in principle but have not been loaded into the reactor is summarized in Table I.E.12.

TABLE I.E.12. Status of Experiments with Approval in Principle

Sponsor	Material of Test	No. of Capsules	Suggested Reactor Row[a]	Date of AIP	Estimated Delivery
ANL	Oxide fuel, Group O-3	19	3	9/22/67	1/69
	Carbide fuel, Group C-5	19	2	9/22/67	Indefinite
	Mark-II fuel (unencap)	455	Core	9/22/67	2/69
	Mark-II fuel (encap)[b]	25	4	6/3/67	6/68[c]
	Metal fuel, M-4	19	3	2/13/68	Indefinite
	Structural, Group S-9	19	4	9/22/67	1/69
	Magnetic materials	7	7	6/8/67	1/69
	Instrumented subassembly	1	5	5/9/68	2/69
BMI	Nitride fuels	4	5	8/28/68	12/68
GE	Oxide fuels, Group 7	4	4	9/2/66	2/68[c]
	Oxide fuels, Group 5	19	4	1/20/67	12/68
	Oxide fuels (unencap), Group 9A	37	4	1/20/67	11/68
	Oxide fuels (unencap), Group 9B	37	6	5/9/68	2/69
	Oxide fuels (unencap), Group 9C	37	5	5/9/68	12/68
	Oxide fuels (unencap), Group 9D	37	7	5/9/68	1/69
INC	Structural	14	7	8/28/68	1/69
LASL	Carbide fuels	6	3	2/27/67	1/69
NRL	Structural materials	7	7	9/6/67	2/69
ORNL	Oxide insulators	7	8	9/21/67	2/69
	Sol-gel oxide fuel	5	4	5/9/68	11/68
PNL	Oxide fuel (unencap), PNL-3	37	3	9/21/67	9/68[c]
	Oxide fuel (unencap), PNL-4	37	4	9/21/67	1/69
	Oxide fuel (unencap), PNL-5	37	3	9/21/67	12/68
	Graphite materials	7	7	7/31/67	Indefinite
	Thermocouple materials	5	4	7/31/67	1/69
		2	4	7/31/67	2/68[c]
UNC	Carbide fuel (UNC 88)	1	4	12/9/65	10/66[c]
	Carbide fuel (UNC 129-147)	19	7	6/6/67	1/69
	Carbide fuel (UNC 185-190)	6	3	1/20/67	6/68[c]
	Carbide fuel (UNC 191-209)	19	3	8/28/68	4/69
W	Carbide fuel (+ V-alloy)	4[d]	4	8/28/68	12/68
	Carbide fuel (+ V-alloy)	12	e	8/28/68	Indefinite

[a]Based on fission rates at a reactor power of 50 MWt.
[b]Replacements for capsules of same type whose irradiation is nearing completion (e.g., Subassembly X029).
[c]Date received.
[d]Two capsules delivered. Expected delivery of others as indicated.
[e]Space-available basis.

(c) New Experimental Subassembly Design. Two preliminary designs have been submitted for a subassembly for irradiating fuel capsules at capsule surface temperatures of up to 1200°F. Special effluent-mixing devices are incorporated in the upper subassembly plenum to mix cold bypass flow with the hot experimental-channel flows and thus maintain the subassembly exit temperature within the specified limits. After review of these preliminary designs, one of the two designs will be developed.

An EBR-II plant-modification proposal for the Mark-H-37 experimental subassembly has been submitted for acceptance and subsequent approval. The Mark H-37 is very similar to the recently approved Mark F-37, the principal difference being the size of the wire-wrap spacer and of the grid spacings. Both subassemblies are designed to receive 0.250-in.-dia fuel elements. The pitch-to-diameter ratios of Types F and H are 1.25 and 1.16, respectively.

(ii) Handling and Examination

(a) Irradiated Subassemblies XO45 through XO49. Subassemblies XO45 through XO49 contained special dosimetry capsules whose primary purpose was to characterize the EBR-II neutron flux. One subassembly, XO45, was irradiated at close to zero power (approximately 76 kW) and the others at 50 MW. The special capsules contained a large variety of dosimeter foils and wires, ranging upwards from short-half-life copper (12.9 hr). Special handling and coordination of all phases of the tests were executed to the satisfaction of the prime experimenter, Pacific Northwest Laboratory (PNL), and the counting of the short-half-life foils was accomplished within the desired time.

(b) Testing of Procedures for Removing Sodium from Subassemblies; Cyclical Testing of Stressed Capsules. Disassembly of Subassembly X900, containing pressurized capsules, was completed in the Air Cell. Depressurization and metallography of the samples have not been started.

j. FCF Process Analysis and Testing (M. J. Feldman)

Last Reported: ANL-7487, p. 57 (Aug 1968).

(i) Test and Analytical Methods (M. J. Feldman, J. P. Bacca, E. R. Ebersole, and V. G. Eschen)

As part of the program to develop the capability for remote re-encapsulation, developmental work was started on pressure-vacuum sodium loading and on capsule-welding techniques. Several successful welds were performed on prototype capsules. The sodium-loading equipment has been set up and is ready for testing.

k. FCF Equipment Improvement (M. J. Feldman)

Last Reported: ANL-7513, pp. 75-76 (Oct 1968).

(i) Process Equipment (N. R. Grant and J. P. Bacca)

The spare injection-casting furnace installed in the Argon Cell is being used for routine operations.

(ii) Auxiliary Equipment (W. L. Sales and K. H. Kinkade)

General specifications and drawings are being prepared for a spare crane trolley to be used in the Air or Argon Cell while repairs or overhauls are being made to an existing trolley. The new trolley will be of modular design so that each of its parts can be handled by the electromechanical manipulator with a 750-lb max capacity. The trolley will be remotely assembled in the Air or Argon Cell as needed.

l. Superheater and EM Pump Study and Test (R. A. Jaross)

(i) Superheater Vibration Study (G. S. Rosenberg)

Last Reported: ANL-7500, p. 71 (Sept 1968).

To gain insight into how a heat-exchanger tube impacting with a baffle plate affects the vibrational characteristics and response of that tube, a force-excited beam clamped at both ends and with stops at the midpoint was considered. Single-mode approximations were employed to obtain an equation for an equivalent system consisting of a force-excited vibration of a unit mass on a bilinear spring. An approximate solution based on the assumption that the response is sinusoidal at the forced frequency was obtained by balancing the inertia force and applied force against the spring force at their maximum values. For a given force amplitude and frequency, the amplitude of motion can be graphically or analytically computed.

The forcing function associated with periodic vortex shedding can be represented as

$$F = F_0 \cos \omega_v t,$$

where $F_0 = C_k \rho \bar{u}^2 d/2$, $\omega_v = 2\pi N_s \bar{u}/d$, C_k is the lift coefficient, ρ is fluid density, $\bar{u}$ is mean crossflow velocity, d is tube diameter, and N_s is the Strouhal number. With this forcing function and $C_k = 1$, $N_s = 0.2$, the curves given in Fig. I.E.2 have been constructed for the geometry and material properties of the EBR-II superheater tubes. The nondimensional variables ξ^*, u^* and δ^* are defined as $\xi^* = 1.59\, \xi/\delta$, $u^* = \bar{u} N_s / f_t d$,

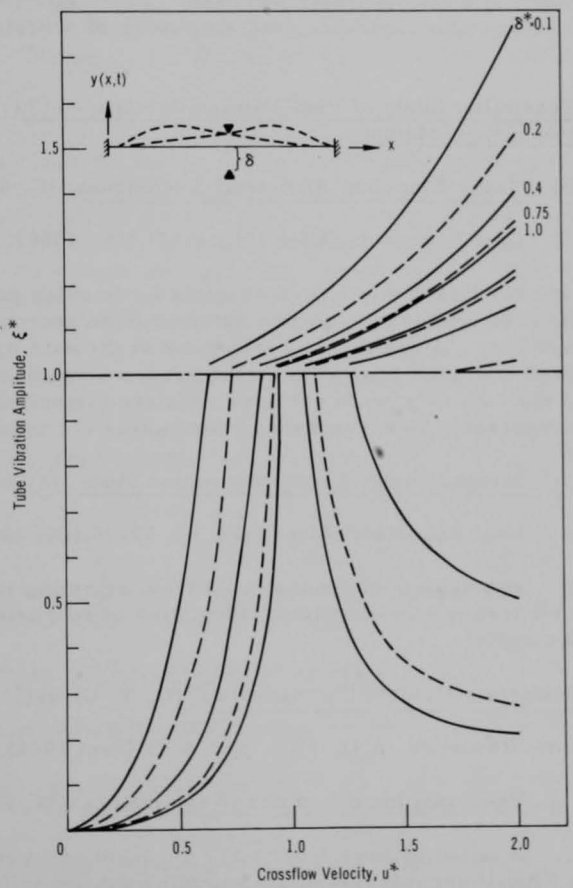

Fig. I.E.2. Tube Vibration Amplitude as a Function of Crossflow Velocity for Various Tube-baffle Clearances

and $\delta^* = \delta/d$, where δ is the tube-baffle clearance, f_t is the fundamental natural frequency of the tube, and ξ is related to the tube displacement through the equation

$$y(x,t) = \begin{cases} \dfrac{\phi(x)\delta}{1.59}\,\xi^* \cos \omega_v t, & \xi^* \le 1 \\[2ex] \left[\dfrac{\phi(x) - (\xi^* - 1)\,\phi(2x)}{1.59}\right] \delta \cos \omega_v t, & \xi^* > 1,\ 0 \le x \le \ell/2, \end{cases}$$

where y is the tube displacement and $\phi(x)$ is the mode shape associated with the free vibration of a clamped-clamped beam. For a given mean crossflow velocity and baffle-tube clearance, the amplitude of vibration can be determined.

m. Feasibility Study of Fuel Failure Detection--Chemical and Mechanical Methods

(i) Trace Elements Analytical Techniques (C. E. Crouthamel)

Last Reported: ANL-7513, p. 77 (Oct 1968).

Work is continuing on adapting a computer program to the analysis of the complex gamma spectra obtained from neutron activation of separated impurities. A preliminary treatment of the data with the computer program showed that additional work on the program was needed and that the library of the data on gamma energies required further expansion. The modifications necessary to correct these difficulties are underway.

(ii) Sodium Loop--Tag Confirmation Study (F. A. Cafasso)

Last Reported: ANL-7513, pp. 77-78 (Oct 1968).

Fabrication of the loop cold trap, sampling reservoir, and reservoir vapor trap is now complete; fabrication of supports for the loop piping is 80% complete.

n. Materials-Coolant Compatibility (D. W. Cissel)

Last Reported: ANL-7500, pp. 74-76 (Sept 1968).

(i) Problems Identified due to Operations (W. E. Ruther)

A failed bellows from a 1/2-in. (nominal) valve (designated SN 17) in the EBR-II secondary-sodium sampling system is being examined. The bellows is made of Type 347 stainless steel and had been in service for

about 4 yr at an operating temperature of 580°F. The valve had been cycled about 100 times during the bellows lifetime.

Two small leaks were found in the innermost portions of two adjacent bellows convolutions. Although indications of mechanical damage (dents, nicks, etc.) were evident on the outermost parts of the nearby convolutions, there was no indication that mechanical damage from any external source had contributed to the actual leaks.

Microscopic examination near the two detected holes revealed intergranular attack, which may have been a result of carburization during sodium exposure. A specimen exhibiting such attack is currently in the electron microprobe for evaluation, and chemical analyses are being made for total carbon in the bellows adjacent to the defected area.

A section of the bellows containing one of the known failures was metallographically mounted so that the polishing plane would be normal to the expected leak direction. The first polishing exposed the sodium entrance to the failure. The failure entrance on the sodium side was a branched crack about 0.8 mm long by 0.06 mm wide at the widest point. The specimen was then reground, exposing a similar area 30-50 μm deeper in the metal. The crack at this cross section was no longer continuous, but appeared as smaller individual pores. The total cross-sectional area of the failure was much less at this depth than on the sodium-exposed surface. The failure will be followed through the thickness of the bellows (100-150 μm) by successive regrinding and repolishing steps.

These observations, particularly the wide branching nature of the entrance crack, suggest that interaction of the bellows with the sodium (or its impurities) may have contributed to the failure. A transverse section of the bellows wall clearly shows the initiation of intergranular penetration. Although the attack is much more pronounced on the sodium side (depth of ~5-10 μm), it is also present on the air side of the bellows. The examination also indicates that the metal has not been sensitized and that a normal amount of inclusions is present.

o. Study of Operation with Failed Fuel (R. R. Smith)

Last Reported: ANL-7478, pp. 69-71 (July 1968).

(i) Bare-pin Experiments. The responses of all fission-product monitors have been tested and calibrated through the deliberate insertion of two unclad Mark-IA U-5 Fs fuel pins in the EBR-II core. The tests, also investigated the effects of gas leakage into the reactor building. Although a considerable amount of analytical work remains to be done, the results of radiometric analyses of ^{133}Xe and ^{135}Xe activities in the cover gas may be cited at this time.

Pertinent events prior to and during the tests are given in Table I.E.13.

TABLE I.E.13. Time-Power History for Bare-pin Tests

Date (1968)	Time	Event
Oct 12	1822	Reactor critical, 50 kW
	2030	Reactor at 30 MW
Oct 13	2200	Started power decrease
	2215	Reactor critical, 50 kW
Oct 14	2300	Reactor at 30 MW
Oct 18	1020	Started power decrease
	1127	Reactor critical, 50 kW
Oct 19	1545	Reactor critical, 50 kW
	1956	Reactor at 30 MW
Oct 22	1331	Started power decrease
	1430	Reactor critical, 50 kW
Oct 26	0640	Power at 30 MW
Oct 28	2220	Power increased to 50 MW
Nov 3	1800	Started power decrease
	1934	Reactor critical, 50 kW
Nov 5	1740	Reactor critical, 50 kW
	2103	Power at 50 MW
Nov 14	0400	Started power decrease
	0411	Reactor critical, 50 kW
Nov 15	1005	Reactor critical, 50 kW (beginning of bare-pin tests)
	1155	Power at 10 MW
	1228	Power at 20 MW
	1300	Power at 30 MW
	1450	Power at 40 MW
	1530	Power at 50 MW
Nov 17	1803	Started power decrease
	1953	Reactor critical, 50 kW (end of tests)

The results of radiometric analyses for ^{133}Xe and ^{135}Xe in the cover gas are plotted in Fig. I.E.3. Upon the application of corrections for residual background, radioactive buildup, etc., the data shown will be used to estimate the signal-to-noise ratios for the ^{133}Xe and ^{135}Xe index species. Such ratios will then be compared with the signal-to-noise ratios for the FGM, FERD, and RCGM monitoring systems.

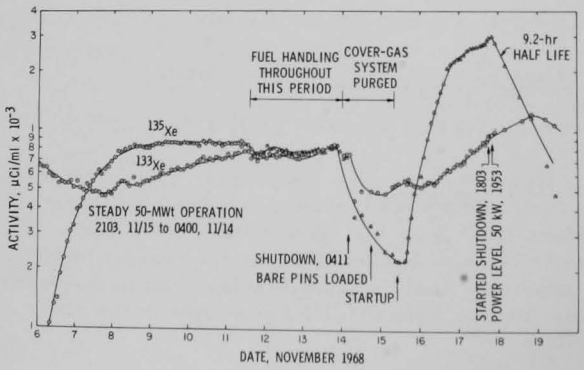

Fig. I.E.3

Cover-gas Activities before and during Bare-pin Experiment

Primary-coolant samples were taken before and after the bare-pin tests. These will be analyzed for ^{137}Cs, ^{131}I, and uranium. From the analyses conducted for ^{131}I, it may be possible to conclude whether or not a suspect leaker involves the release of bond sodium or fission-product gases.

p. Driver Fuel Transient Performance Studies--TREAT Experiments

(i) Mark IA Fuel TREAT Experiments

Last Reported: ANL-7500, p. 76 (Sept 1968).

The Mark-I photographic test capsules are being modified for the next two test series with two "high-swelling" pins, one pin irradiated to 1.2 a/o burnup and the other to 2.5 a/o burnup.

The stresses resulting from expansion of irradiated fuel have been analyzed. The calculations were based on a fuel compressibility derived indirectly from fuel-swelling data. The results show that the stresses in an EBR-II Mark-IA fuel pin resulting from radial or axial expansion to the containment limits of the fuel pose no serious threat to the integrity of the fuel.

q. Systems Engineering (B. C. Cerutti)

(i) Surveillance, Evaluation, and Studies of Systems

Last Reported: ANL-7513, pp. 78-79 (Oct 1968).

(a) Primary Coolant Flow Monitors (R. O. Haroldsen)

Of the 61 automatic trip circuits that are active during power operation, 17 assure proper cooling of the reactor. Five of the 17 circuits monitor flow in the high-pressure, low-pressure, and outlet plenums of the reactor. Two more monitor the rate of change of flow. The remaining 10 circuits monitor various secondary parameters of the two primary pumps, including clutch cooling, supply power, and motor temperatures. Many of the spurious scrams throughout the history of EBR-II operation have originated from this complex of trip circuits.

One of several activities to reduce the number of spurious scrams is a plant-change proposal for simplifying the scram circuitry. (Such simplification, of course, must not compromise the safety of the reactor.) The first phase of this effort is directed toward simplification of the flow monitors. A draft has been completed of an engineering submittal

for simplifying the flow-monitoring system. This draft includes documentation of system behavior for justifying a significant reduction in the number of trip circuits without compromising reactor safety. The submittal proposes to eliminate all but 5 of the 17 monitors. Three of these monitors (for Pumps 1 and 2, high-pressure flow, and the total flow) would be employed in a two-out-of-three logic circuit. The two remaining low-pressure flow monitors would be employed as independent circuits.

(b) Main Core Gripper of Fuel-handling System (J. B. Waldo)

On the basis of recommendations from LMIC and several packing suppliers, three types of Teflon-impregnated packings were ordered for the packing gland of the main core gripper. These packings will be tested in the spare packing gland available in storage before one is selected and tested in the gland of the core gripper.

(c) Replacement of Safety-rod Thimble (J. B. Waldo)

Special handling tools for removing the safety-rod thimble were received from ANL-Illinois. They were checked out in a grid mockup and appeared to operate satisfactorily. The removal tool was modified slightly to promote complete drainage of sodium from the thimble. The necessary fixtures and adapters for the IBC and the temporary coffin were fabricated. The safety-rod thimble was removed from the reactor and transferred to the FCF without difficulty. The new thimble was also installed without difficulty.

(d) Pump Rectifier of FERD System (K. J. Moriarty)

Operation of the rectifier at reduced capacity (reduced system flow) with mixed diodes (old and new) was found to be unsatisfactory primarily because of the excessive heating of the new diodes. At room temperatures and low capacity, the remaining old diodes performed satisfactorily. As the diode temperatures increased, the reverse-direction resistance decreased, permitting varying amounts of current to pass in the reverse direction; an oscilloscope trace indicated that as much as 60% of the reverse-direction wave form existed. Temperatures taken of the diode heat sink indicated that essentially all of the original diodes were damaged and leaking in the reverse direction at operating temperatures.

All original diodes were replaced with improved units: Motorola Model MR 1230. The operating characteristics of the new diodes are essentially identical to those of the original diodes, except for a higher allowable temperature rise: the MR 1230 is rated at 190°C; the original units were rated at 120°C.

A thermocouple was installed as part of each new diode and interconnected in a terminating point external to the rectifier, but accessible with the rectifier operating. The rectifier was restarted, and the diodes were aged in place. All diode temperatures were monitored during the aging process for evidence of diode breakdown or excessive heating. The rectifier capacity was increased in increments to 6000 Amp (100% flow), over a 72-hr period. Table I.E.14 shows typical diode temperatures at 100% flow.

TABLE I.E.14. Typical Temperatures of New Diodes in Rectifier of Pump in FERD System (°C at 100% flow)

	Diode Number					
Row No.	1	2	3	4	5	6
1	63	67	72	73[a]	73[a]	69
2	51	57	60[b]	58	57	55
3	53	59	62	61	59	57
4	53	61	66	65	62	60
5	54	61	63	65	63	62
6	56	63	63	69	68	63
7	54	60	64	63	63	61
8	52	57	62	66	62	58
9	50	56	58	59	59	57
10	48[c]	53	53	57	53	51

[a]Highest temperature recorded.
[b]Average temperature.
[c]Lowest temperature recorded.

From the data obtained, the most satisfactory method for monitoring diode condition appears to be temperature measurement. Excessive temperatures are an indication that there are failed or failing diodes in the circuit. Those diodes indicating low temperatures are the unsatisfactory units.

(e) Primary Sodium Coolant Pump (K. J. Moriarty)

During this reporting period, the pump controls failed once, resulting in a reactor scram. Immediately prior to the failure the reactor was subcritical by one control rod and the pumps were operating at 100% flow. An electrical-noise burst originating in the reactor building was considered to be the cause of the perturbation. All three source channels indicated a fast period and an increased counting rate. The pump controllers were manually reset and their recovery monitored. Both controllers responded normally.

(f) EBR-II Shutdown Cooler (H. W. Sine)

A test was conducted to determine the change in air flow up the stack of the No. 1 shutdown cooler due to the recently installed 24- by 90-in. louver in the hood over the stack. The velocity of air up the stack when the shutdown cooler was off (lower dampers closed) increased 80%, and the velocity of air up the stack when the shutdown cooler was on (lower dampers open) increased 20%.

During this test, it was noticed that some of the lower dampers of the shutdown cooler closed only about halfway. An inspection of the actuating linkage of these dampers revealed two places where slippage occurred. A new shaft with a welded-on blade is being made to eliminate this slippage. When this new shaft is installed and tested, additional steps will be taken, if required, to make the dampers operate as intended. Measurements of air flow will be repeated at this time.

(ii) Reactor and Primary System Improvements

Last Reported: ANL-7513, p. 79 (Oct 1968).

(a) Pressure-Temperature Instrument Thimble (R. O. Haroldsen)

The original EBR-II process instrumentation included two capillary-type pressure sensors and several temperature sensors in the outlet plenum of the reactor. Failure of one pressure sensor and successive failure of most of the temperature sensors has left the reactor without spare sensors for vital instrumentation. Replacement of these sensors is impractical.

Spare pressure and temperature instrumentation has been designed into a thimble which will penetrate to the reactor outlet plenum when installed in the auxiliary gripper hole, the only available access to this plenum. The location of this instrument probe (shown in Fig. I.E.4) is a compromise as regards to temperature measurement because the probe will be located away from the discharge from the plenum. The mixing in the plenum, however, is sufficient for the temperature sensors in the probe tip to give a representative plenum temperature.

Figure I.E.5 shows the instrument thimble as constructed. The thimble contains two pressure sensors which utilize NaK-filled capillary tubes. Eight Chromel-Alumel thermocouples are brazed from the inside of the thimble to thermocouple buttons. The thermocouple wires and capillary tubes follow a spiral groove on the surface of the shield plug to the top of the assembly.

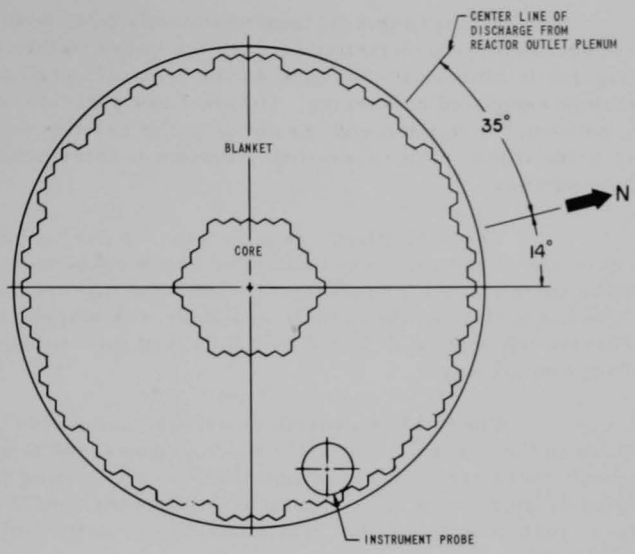

Fig. I.E.4. Location of Pressure-Temperature Instrument Thimble

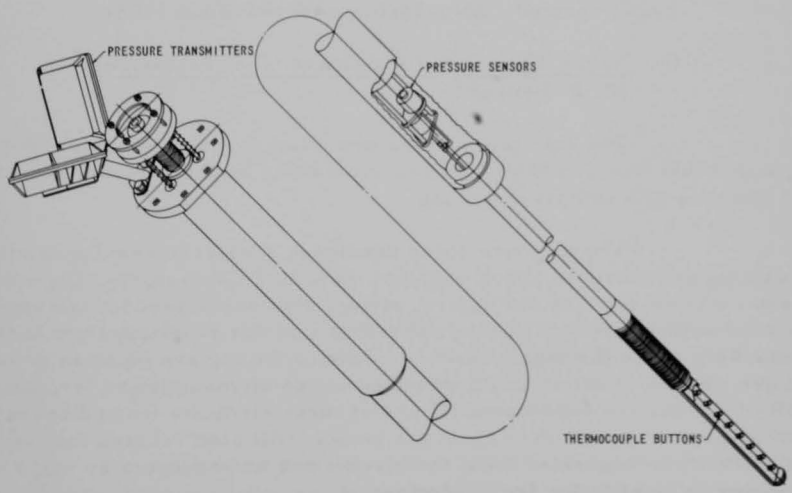

Fig. I.E.5. Assembly of Pressure-Temperature Instrument Thimble

A labyrinth seal located immediately above the thermocouple probe will seal the penetration through the cover of the reactor vessel. This construction is similar to that used on the control-rod driver. The entire assembly is supported on springs. Motion-limit switches will monitor any binding between the thimble and the cover of the reactor vessel while the cover is being lifted. The cover-lifting system is interlocked to these motion-limit switches.

The NaK-filled pressure sensors have a bellows assembly on each end of the capillary tube. For space reasons, the capillary tubes had to be installed prior to filling with NaK and making final connections. The top portion of the thimble assembly was shipped to the manufacturer (Barton Division of ITT) for installation of the capillary system prior to filling and sealing.

One thimble assembly has been completed and is ready for installation in the reactor. Parts for a complete second thimble are on hand. However, there are no plans at this time for completing its fabrication. Delaying fabrication of the second unit will permit consideration of more advanced instrumentation that may be available by the time a new system is required.

r. Leak Detection and Location--Xenon Method (R. E. Rice)

Last Reported: ANL-7460, pp. 43-44 (June 1968).

(i) Xenon Tagging for Identification of Failed Fuel (P. B. Henault)

The feasibility of the xenon-tagging technique for identifying failed fuel was demonstrated experimentally by the release, recovery, and analysis of a sample xenon tag.

The tags now being developed consist of varying mixtures of natural and enriched xenon supplied by Mound Laboratory. The enriched xenon contains more of the lighter, stable, nonfission-product isotopes than does the natural xenon. The unique isotopic ratios resulting from these mixtures provide the tags. Small amounts of the tag are being injected into the gas plenum of unencapsulated mixed-oxide elements to be irradiated in EBR-II so that any subsequent failure of these elements that releases fission-product gas to the argon-gas blanket will also release the tag. The tag can then be separated from the blanket gas and analyzed by mass spectrometry to identify the failed element.

Calculations had indicated that the xenon technique would provide a feasible and efficient means for locating failed fuel. A test has

been made to verify this conclusion experimentally. The xenon was collected from samples containing 10 cu ft of the primary argon cover gas, using a cooled (-79°C) charcoal trap, both before and after the addition of a tag to the cover gas. The cold-trapped xenon was then analyzed for isotopic composition by mass spectrometry.

To establish background conditions, the xenon from 70 cu ft of primary argon was quantitatively cold trapped on activated charcoal at dry-ice temperature during a 2-hr trapping period. This was done immediately after reactor shutdown at the end of Run 30A, with equilibrium concentrations of ^{133}Xe and ^{135}Xe present in the cover gas as radioactive tracers. This background sample was analyzed and shown to contain approximately 40% natural xenon and 60% stable fission-product xenon.

During the reactor startup for Run 31A (Oct. 1, 1968), with the primary pumps at 100% flow, 0.7 ml (STP) of xenon tag was added to the primary argon cover gas (~7 x 10^6 ml, STP). The xenon from 10 cu ft of cover gas was then cold trapped, as described above, 24 and 48 hr after addition of the tag and analyzed by mass spectrometry. The data from the test are tabulated in Table I.E.15.

TABLE I.E.15. Results of Xenon-tagging Experimental Test

Xenon Isotope	Natural Abundance (a/o)	Concentration in Background Sample Including Fission Gas (a/o)	Concentration in Tag (a/o)	Concentration in Tag plus Background	
				After 24 hr (a/o)	After 48 hr (a/o)
124	0.10	-	5.58	5.31	5.40
126	0.09	-	1.92	1.83	1.89
127	-	0.2			
128	1.92	0.9	10.32	9.73	9.90
129	26.44	10.3	63.02	60.33	61.06
130	4.08	1.6	4.32	4.16	4.25
131	21.18	17.3	9.43	9.83	9.85
132	26.89	22.8	5.03	6.05	5.77
134	10.44	25.3	0.34	1.64	1.44
136	8.87	21.5	0.026	1.12	0.73
$^{129}Xe/^{124}Xe$			11.29	11.35	11.31

The ratio of ^{129}Xe to ^{124}Xe was examined to identify a specific tag. As shown in the table, the ratio of these isotopes in the original tag was 11.29 as compared to ratios of 11.35 and 11.31 in the samples of argon cover collected at 24 and 48 hr, respectively, after tag addition.

Based on these data, the background xenon in the cover gas prior to addition of the tag was calculated to be between 0.007 and 0.021 ml (STP) in 7 x 10^6 ml (STP) of argon, or between 1 and 3% of the volume of the added tag.

2. Operations

a. Reactor Plant (G. E. Deegan)

Last Reported: ANL-7513, pp. 79-82 (Oct 1968).

(i) Operations (J. R. Davis)

Run 31C, a 75-MWd run to search for the fission-product source, was completed on October 22. Analysis of the activity of the primary-tank blanket gas indicated that the fission-product source was still in the reactor.

Fuel loading for Run 31D returned the core to approximately the configuration of Run 31A. Run 31D consisted of 30-MW operation for the first 75 MWd and 50-MW operation for an additional 235 MWd. The blanket-gas activity at 50 MW stabilized at approximately the level that it had reached when the fission-product release was first observed in September during Run 30B.

During the loading for Run 31E, the controlled-flow subassembly, the two 91-pin, 70%-enriched subassemblies, and experimental Subassembly XO39 were returned to the core, and an experimental dosimetry subassembly was placed in Row 2 of the core. The reactor was operated for 1 hr at 50 kW, when the dosimetry subassembly was removed.

Four other experimental dosimetry subassemblies were irradiated at 50 MW for eight days in Run 31F. During this run, six control rods were checked as part of the search for the fission-product source. No significant change was observed in the activity of the primary-tank blanket gas with successive control rods in the fully down position for 50 MWd of operation.

Run 31G was a bare-pin experiment in which the reactor was operated at 50 MW for two days with a special control rod fully inserted in the core. This control rod contained standard fuel elements as well as two unclad fuel pins, each surrounded by stainless steel dummy pins. Activities in the blanket gas, reactor building, and primary sodium were monitored during this run; no significant contamination or radiation problems were encountered. The reactor instrumentation for detecting fission products responded satisfactorily.

Loading for Run 32A was temporarily interrupted to remove the safety-rod thimble in position 3-D-1. Following replacement of the thimble, fuel handling was resumed.

Final checkout of the primary purification system is in progress prior to filling the system with sodium.

The reactor operated for 774 MWd during November and had accumulated 21,478 MWd by the end of the month.

b. Fuel Cycle Facility (M. J. Feldman)

Last Reported: ANL-7513, pp. 82-90 (Oct 1968).

(i) Fuel Production

(a) Hot Line (N. R. Grant)

Table I.E.16 summarizes the production activities for November 1968.

The continuing program of obtaining samples for silicon analysis from all batches of fuel returned from the reactor has apparently resolved the problem of erratically high silicon values in the injection-casting batches. The analyses provide the information necessary for blending fuel from various batches to produce casting batches of a desired silicon concentration. Utilization of the recently installed replacement injection-casting furnace has also contributed to the restoration of normal processing rates for reprocessed fuel.

One of the electromechanical manipulators in the Air Cell is inoperable because of a failed shear pin in the carriage drive train. Repair is scheduled for December, when occupancy can be obtained of the shielded cell in the manipulator repair facility now being constructed on the roof of the Air Cell.

(b) Cold-line Production and Assembly (D. L. Mitchell)

Normal production is continuing in the cold line; however, efforts required for acceptance inspection of the vendor-produced fuel resulted in reducing the throughput for cold-line-produced fuel in the bonding and bond-testing area. The month's production data are summarized in Table I.E.17.

(ii) Inspection of Vendor Fuel (D. L. Mitchell)

Acceptance inspection of vendor-produced Mark-IA elements continued. Efforts are being continued to resolve the differences in eddy-current determinations of bond defects by the vendor (Aerojet-General Corporation) and by ANL. A number of elements have been stripped of their stainless steel jackets in attempts to obtain correlation between the voids that can be observed in the sodium of the stripped elements and the voids indicated by eddy-current traces.

TABLE I.E.16. Production Summary for FCF Hot Line

	November 1968	Total This Year
Subassemblies received		
Core, Control, Safety	13	122
Other	5[a]	69
Subassemblies dismantled for processing	10	102
Subassemblies dismantled for examination, etc.	7	29
Subassemblies fabricated	2	30
Subassemblies transferred to reactor	4	63
Subassemblies stored in L&O vault and interbuilding corridor	0	0
Subassemblies sent to ICPP for storage	0	5
Elements decanned		
From irradiated subassemblies	779	7115
Rejects	54	427
Other	0	188
Total decanned	833	7730

Melt Refining

	Irradiated Fuel	Recycle Material	New Fuel
Number of runs	4	5	0
Average pour yield, %	91.8	91.5	-
Total runs 1968 to date	51	28	4

Processing

	November 1968	Total This Year
Injection-casting runs	15	86
Elements processed		
Accepted	370	3240
Rejected	56	763
Elements welded	358	3079
Elements rewelded	0	4
Elements leak tested		
Accepted	328	3153
Rejected	44	171
Elements bonded (including recycle)	419	3985
Elements bond tested		
Accepted	41	2625
Rejected	3	247
Elements to surveillance	270	2634
Number of subassemblies	9	66

Waste Shipments

Cans to burial ground	4	63
Oxide and glass scrap to ICPP	2	28

[a]Structural materials; no fuel.

TABLE I.E.17. Production Summary for FCF Cold Line

	November 1968	Total This Year
Alloy-preparation runs		
New fuel	0	6
Remelts	2	52
Total	2	58
Injection-casting runs	9	104
Pins processed		
Accepted	781	8192
Rejected	173	759
Elements welded	175	6430
Elements rewelded	0	15
Elements leak tested		
Accepted	172	6526
Rejected	3	73
Elements bond tested		
Accepted	240	6251
Rejected	33	404
Elements available for subassembly fabrication	243	-
Subassemblies fabricated (cold-line fuel)	6	72
Elements received from vendor	930	2931
Inspected and accepted	82	82
Inspected and rejected	10[a]	10
Subassemblies fabricated (vendor fuel)	0	1

[a]Rejected by ANL inspection; acceptance criteria are being discussed with the vendor.

The vendor is using a centrifugal-bonding technique whereas ANL uses an impact-bonding technique. The two bonding techniques produce sodium voids of different configurations; this has made it necessary to re-evaluate eddy-current signals. A series of standards is being produced for comparison by AGC and ANL and for the rectification of testing differences.

Rebonding of some of the initial shipments of vendor elements by the impact-bonding technique resulted in indications of voids in the bonding sodium. Very small bubbles of gas remaining in the centrifugally bonded sodium were postulated to be agglomerating when subjected to the

more energetic action of impact bonding. The action of impact bonding will not be duplicated by any of the reactor operating conditions; therefore, tests are being made under conditions more closely simulating those anticipated in the reactor core. In these tests, the elements are vibrated horizontally while they are in a vertical position and at a temperature of 500°C. The amplitude of vibration is 1 to 2 mils and the frequency is 5 cps. The elements are rebond tested at 6-hr intervals. Impact-bonded elements produced in the cold line have been included in the tests for comparative purposes.

After 123 hr of testing, rejectable voids had formed in 30 of 42 vendor elements (representing six batches); the maximum voids detected measured about 0.100 in. in either direction (radial or axial). A small, nonrejectable void was indicated in two of five cold-line elements tested under the same conditions. The results of these tests are being evaluated as to their significance in reactor operation.

The acceptance criteria or standards for void size are also being re-evaluated. The present standards were formulated in 1959, prior to any operating experience with the reactor. These standards set the maximum void size as 0.062 in. in a radial direction and 0.093 in. in an axial direction. In re-evaluating the maximum acceptable void size, two changes in conditions or requirements have been taken into account: (1) the specific linear power rating for the fuel is lower with the present larger core (8.7 kW/ft) than was used for the reference core design (10.5 kW/ft); and (2) the maximum fuel-surface temperature that is now assumed to be critical is the melting temperature of the fuel alloy (1002°C). This temperature is considered realistic because the lower eutectic temperature is valid only for fuel-clad contact, and at contact the effect of the void has disappeared.

(iii) Surveillance or Failure Analysis of Product
(M. J. Feldman, J. P. Bacca, and E. R. Ebersole)

(a) Chemical Analyses (E. R. Ebersole)

The number of fuel-product analyses of hot-line, cold-line, and vendor fuel samples conducted in November, together with the average values and ranges, are as follows:

Analyzed for	Number	Average Value	Range
Total U	19	94.55 w/o	94.18-95.37
^{235}U (% of total U)	19	52.10 w/o	52.03-52.18
Mo	29	2.49 w/o	2.35-2.61
Ru	29	1.89 w/o	1.79-2.10
Rh	19	0.270 w/o	0.248-0.284
Pd	28	0.188 w/o	0.170-0.216
Zr	56	0.078 w/o	0.026-0.140
Nb	25	0.010 w/o	0.006-0.014
Si	75	360 ppm	220-580
Al	25	110 ppm	60-200
C	18	300 ppm	190-440
Cr	19	53 ppm	25-200
Fe	33	200 ppm	50-740
Ni	21	170 ppm	98-200
Th	1	18 ppm	
Total Analyses	416		

November analyses for surveillance of irradiated pins from the reactor are tabulated below:

Analyzed for	Number	Average Value	Range
Si	24	490 ppm	75-1070
Fe	10	398 ppm	300-640
Al	9	205 ppm	110-280
C	12	360 ppm	155-585
Burnup	4	0.97 a/o	0.86-1.09
Total Analyses	59		

(b) Postirradiation Analysis of EBR-II Fuel (J. P. Bacca)

(1) Mark-IB Fuel Surveillance. Postirradiation examination of elements from Mark-IB Subassembly C-2135 (maximum burnup 1.0 a/o) indicated an average fuel swelling of 4.0 v/o; maximum swelling of individual elements was 4.4 v/o. Silicon content in the eight fuel batches represented in the subassembly ranged from 150 to 570 ppm.

The fuel-swelling values observed are in close agreement with swelling exhibited by similar fuel in Mark-IA elements following comparable burnup. The fifth Mark-IB subassembly of the program (C-2136) is currently undergoing irradiation. The target burnup of 1.20 a/o will be attained during Run 32.

(2) Cold-line Fuel Surveillance. Elements from cold-line surveillance Subassembly C-2129 (maximum burnup 1.0 a/o) were

examined to assess irradiation swelling of the fuel. An average swelling of 3.5 v/o was indicated for all elements in the subassembly; swelling of individual elements ranged from 2.4 to 4.4%. These values indicate that fuel produced in the FCF cold line is performing satisfactorily in the EBR-II core, at least to 1 a/o burnup. The next subassembly of this qualification program is C-2130, which attained a burnup of 1.18 a/o at the completion of Run 31. Postirradiation examination of elements from this subassembly is underway.

(3) Irradiation Program for 70%-enriched Fuel. Subassemblies C-2174 and C-2175, each containing 91 elements having 70% ^{235}U enrichment, are being irradiated in EBR-II. After the target burnup of 1.0 a/o has been attained, one subassembly will be examined while the other will be held in the reactor storage basket for possible additional irradiation, depending on the results of the examination of the first subassembly.

(4) Encapsulated Mark-IA Fuel. A precise diametral survey was conducted of the Mark-IA element enclosed in Capsule BF05 of experimental Subassembly XO17. Diametral increases of the element, irradiated to 2.5-a/o maximum burnup, ranged from approximately 0.3 to 0.8%. These values include increases caused by swelling of the cladding as well as of the fuel. The diametral increases are in close agreement with those observed earlier for the Mark-IA element enclosed in Capsule BF09 of the same subassembly.

The three remaining capsules from Subassembly XO17 that contain Mark-IA elements having maximum burnups of 2.5 a/o (Capsules BF04, BF08, and BF11) are being subjected to sodium rebonding and sodium-bond testing before being returned to EBR-II. Irradiation of these elements for an additional burnup increment of 0.3 a/o (total burnup of 2.8 a/o) is planned to begin at the start of Run 32.

(5) Encapsulated Mark-II Fuel. All capsules from Subassembly XO29 (Type B-37) were neutron radiographed at TREAT. This subassembly contained 37 encapsulated Mark-II fuel elements that had achieved a burnup of approximately 2.1 a/o. Evaluation of the radiographs indicates that all fuel elements are in satisfactory condition. Tentatively, destructive examinations are planned for three of the capsules (No. 201, 212, and 251). The remaining 34 capsules, along with three nonirradiated replacements, were reloaded into an experimental subassembly and transferred to EBR-II for an additional burnup of 1 a/o. Irradiation is currently planned to begin at the start of Run 32.

(6) Controlled-flow Subassemblies. Three driver subassemblies, C-2185, C-2186, and C-2187, having special flow orifices that allow irradiation of the fuel at temperatures typical of those experienced

during higher-power operation of EBR-II are currently in the core. Target burnup of the subassemblies is 0.85 a/o, after which C-2185 will be subjected to surveillance examinations. Subassemblies C-2186 and C-2187 will be held in the basket for additional irradiation pending the results of the examinations. The target burnup of 0.85 a/o will be attained during Run 33.

(c) Compatibility Studies (J. P. Bacca and R. V. Strain)

Results of metallographic examination of fuel-element jackets from Subassembly C-278 were reported in ANL-7513, pp. 88-89. An investigation of the preferential sensitization of the jacket tubing near the inner and outer surfaces has shown that "as received" tubing exhibits the same characteristics after heat treatment at 1100°F for 1 hr as does the jacket tubing from C-278.

Chemical analysis of the outer 2 mils of the "as received" tubing shows that the carbon content is much higher near the surfaces than it is near the center of the tubing wall. The carbon content of samples from the outer 2 mils of the tubing was analyzed as 575 ppm as compared to 283 ppm in samples from the center of the tubing wall. (The carbon content of the whole-tube sample was analyzed as 370 ppm.) The sensitization (carbon precipitates at the grain boundaries) extended 1.5 mils into the tubing from the outer surface and 0.8 mil from the inner surface after heat treatment for 1 hr at 1100°F. These values are nearly the same as those measured for the sensitization exhibited by the samples from the top of elements from C-278.

These results indicate that the more heavily etched grain-boundary regions near the surface of samples of cladding irradiated in EBR-II result from nonuniform carbon concentrations in the "as received" tubing rather than from the effect of reactor sodium or subsequent sodium-removal operations. The metallographic examination did not indicate that the grain boundaries near the surface of the tubing are sensitive to the sodium environment. The sensitization becomes apparent only after the samples have been electro-etched in 10% oxalic acid. Other etchants do not reveal any change in the microstructure of the cladding near the surfaces after irradiation.

(1) Metallographic Examination of Stainless Steel Rods from Blanket Subassembly A-809. Two stainless steel rods from stainless steel-blanket Subassembly A-809 have been examined metallographically. This subassembly was in service in EBR-II from February 17, 1967 to July 7, 1968, in grid position 7D3. No corrosion or erosion was observed on the surfaces of the rods, nor was sensitization of the stainless steel noted. Inclusions, presumably carbides, were observed in the material microstructure, and these were more dense near the surface of the rods

than at the central regions. Control (reference) samples of the rods are not available, so the microstructural observations cannot be correlated with irradiation service of the material.

(2) Examination of Bushings from Control Rod L-498. Aluminum-bronze bushings from Control Rod L-498 were subjected to postirradiation examinations. This rod experienced service in grid position 5E3 from May 8 to September 29, 1968. Preliminary results of the examinations of the upper and lower bushings indicate no observable wear, corrosion, or microstructural changes.

Examination of two ring assemblies (a stainless steel retainer and an Al-Cu bushing ring) from the upper and lower bushing sets of the control rod also failed to indicate wear, corrosion, or microstructural changes. Examination of the center set of bushings from the control rod and dimensional surveys of all the bushings are underway.

(iv) Fuel Management and Handling (N. R. Grant and P. Fineman)

A summary of fuel-handling operations is included in Tables I.E.16 and I.E.17.

(v) Experiment Handling and Interim Examination (V. G. Eschen and N. R. Grant)

Subassembly X900 was dismantled. This subassembly was part of a demonstration program on the returnability of stressed tubing, and contained capsules that had been pressurized before insertion into the reactor. The subassembly had been cycled between the storage basket and the FCF four times, using the standard wash cycle in the interbuilding coffin. Some capsules were removed and replaced with new capsules after each wash cycle. The last cycle included an irradiation in the inner blanket of the reactor. Six of the capsules will be punctured to measure the remaining capsule pressure (used to stress the tubing), and specimens will be cut from the tubing for metallurgical examination. The rest of the capsules will be stored for other tests.

(vi) Reactor Support (N. R. Grant)

Five experimental subassemblies containing dosimetry or flux-monitoring samples were received from the reactor. The first (XO45), received after low-power irradiation, was dismantled in the Air Cell, and the capsules in it were removed for evaluating the experiments and procedures. The remaining four subassemblies (XO46, XO47, XO48, and XO49) were irradiated at 50 MW for eight days. The first of these subassemblies

was transferred to the FCF 4 hr after reactor shutdown and the remainder as soon as scheduling permitted. Expeditious handling was required to reduce the decay of some of the short-lived isotopes produced during the irradiation. The four subassemblies were washed and dismantled, and the capsules were removed, packaged, and made available to the experimenter (PNL) on the site within 27 hr of total elapsed time after reactor shutdown (48 hr was the maximum time allowed by the experimenter). The capsules were then transferred by the experimenter in a chartered plane to PNL for analysis.

Examination of Irradiated Safety-rod Thimble. Preparations were begun for examination of the highly irradiated stainless steel safety-rod thimble removed from grid position 3D1 of the EBR-II core. Special sodium-removal techniques were used in the FCF to ensure preservation of the material in its "as irradiated" condition. The thimble will be subjected to dimensional surveys, gamma scanning, and segmenting. Component parts of the thimble will be supplied to several laboratories for studies of irradiation damage. This stainless steel material has been irradiated in a fast flux to the highest fluence (close to 10^{23} n/cm^2 max) available to date in the U.S. for examination.

PUBLICATIONS

Precise Cross-section Measurements Using the Manganese Bath
Alexander DeVolpi and K. G. Porges
Bull. Am. Phys. Soc. 13, 1421 (Nov 1968) Abstract

Compton Continuum Measurements for Continuous Gamma-ray Spectroscopy
Raymond Gold
Bull. Am. Phys. Soc. 13, 1405 (Nov 1968) Abstract

Experiments and Calculations for Densely Loaded, Slightly Enriched UO_2-fueled Cores
K. E. Plumlee and E. M. Pennington
The Physics Problems in Thermal Reactor Design, Proc. Intern. Conf., London, June 27-29, 1967. Brit. Nucl. Soc., London, England, 1967, pp. 73-75

Spontaneous-fission Decay Constant of ^{238}U
J. H. Roberts,* Raymond Gold, and R. J. Armani
Phys. Rev. 174, 1482-1484 (Oct. 20, 1968)

Safety Analysis of a Nominal 3700-liter UO_2 Core in the ZPR-6 and -9 Facility
G. K. Rusch and R. A. Karam
ANL-6271 Addendum 2 (July 1968)

*Northwestern University.

The following appeared as Abstracts in Trans. Am. Nucl. Soc. 11(2) (Nov 1968):

Criticality Hazards Control for ZPPR Fuel
P. I. Amundson, R. G. Matlock, R. J. Forrester, J. C. Young, and J. M. Gasidlo
p. 673

Relative ^{238}U Fission Yields by Gamma-ray Analysis
L. S. Beller and D. W. Maddison
p. 607

Computer-aided Calibration of a Fine Autorod
C. E. Cohn, R. A. Karam, J. E. Marshall, and J. M. Van Doorninck
p. 566

Fast Spectrum Doppler Measurements on ^{238}U and Refractory Metals to 2000°K
J. W. Daughtry, E. F. Groh, and C. E. Till
p. 562

Study of Conversion of TREAT Facility for Testing of Fast Reactor Subassemblies
H. P. Iskenderian
p. 643

Fluxes Intrastructure in a Large, Plate-type Heterogeneous UO_2 Fast Core (Assembly-6, ZPR-6)
R. A. Karam, J. E. Marshall, and Tomoo Nakamura
p. 598

A 4000-liter Uranium-oxide Fast Core Assembly-6 of ZPR-6
R. A. Karam, W. Y. Kato, J. E. Marshall, Tomoo Nakamura, and G. K. Rusch
p. 597

Measurement of Reaction Ratios and Neutron Spectra in a Soft-spectrum Fast Reactor
W. Y. Kato, C. A. Preskit,* J. C. Young,* J. M. Neill,* C. D. Swanson, R. J. Armani, and J. H. Roberts**
p. 599

Compatibility of Vanadium Alloys with (U,Pu) Carbides
T. W. Latimer
p. 511

---

*Gulf General Atomic.

**Northwestern University.

Electronic System Developments for Proton Recoil Spectra Measurements in Plutonium Critical Facilities
J. M. Larson and J. E. Powell
p. 635

Verification of Zoned Fast Critical Assemblies
L. G. LeSage
p. 595

Time-optimal Digital Control of Zero Power Nuclear Reactors
T. J. Marciniak
p. 633

Monte Carlo Interpretation of a U-238 Spherical Shell Transmission Experiment at 24 keV
L. B. Miller and W. P. Poenitz
p. 606

Plutonium Fuels Performance--ANL Experience
L. A. Neimark, W. F. Murphy, F. L. Brown, and J. H. Kittel
p. 516

Approach to Critical by Modal Analysis for Plutonium-fueled Systems
A. P. Olson and R. G. Palmer
p. 675

Self-shielding Factors by the Ladder Method
Meir Segev
p. 593

The Investigation of Sodium Penetration into 304 Stainless Steel with the Laser Microspectrophotometer
E. S. Sowa
p. 505

A New Definition of the Microscopic Multigroup Transport Cross Sections
Armando Travelli
p. 532

Use of Group-space-dependent Bucklings to Simulate a 3-D Split-cylindrical Reactor in 2-D
A. J. Ulrich and J. C. Beitel
p. 560

The following appeared in Proc. Intern. Conf. on the Utilization of Research Reactors and Reactor Mathematics and Computation, Mexico City, May 2-4, 1967. Centro Nuclear de Mexico, Mexico, D.F., 1968:

Reactor Physics Measurements in the Argonne Fast Source Reactor
P. I. Amundson, W. G. Davey, R. N. Curran, G. S. Brunson, and R. J. Huber
Vol. 3, pp. 1308-1326

Use of a Research Reactor in the National Nuclear Program
G. S. Brunson
Vol. 1, pp. 94-100

BANDSAW, A Proposal for Remeasuring Delayed Neutron Energies, Yields, and Half-lives in AFSR-type Reactors
G. S. Brunson and R. J. Huber
Vol. 1, pp. 310-318

A New Approach to Calculation of Flux Distribution in a Reactor Based Upon a Few Measured Values
P. F. Gast
Vol. 3, pp. 1407-1427

Management of Low Power Research Reactors
W. Y. Kato
Vol. 3, pp. 1611-1619

Use of the ELMOE-SNARG Programs to Study Details of Neutron Spectra Through Regions of Resonance-scattering Media
David Meneghetti, A. L. Rago, and K. E. Phillips
Vol. 3, pp. 1515-1533

A Generalized Formulation for Fast Reactor Fuel Cycle Studies
D. A. Meneley, G. K. Leaf, P. M. Walker, and S. H. Kyong
Vol. 3, pp. 1349-1367

II. OTHER FAST REACTORS--CIVILIAN--OTHER FAST BREEDER REACTORS

A. Fuel Development

1. Corrosion of Fuel Jacket Alloys (W. E. Ruther)

Last Reported: ANL-7445, p. 6 (April 1968).

The impurity atoms picked up by vanadium alloys during long high-temperature exposure to cold-trapped (~110°C) sodium are concentrated in a thin, hardened, subsurface zone in titanium-bearing alloys. In vanadium* and in vanadium-chromium binary alloys, the acquired impurities are more uniformly distributed throughout the metal. These differences in distribution are expected to influence the high-temperature mechanical properties. Conversely, the distribution (and perhaps even the amount) of impurity atoms acquired might be influenced by the applied mechanical stress.

A new dynamic-test facility designed to permit the evaluation of the interrelationship between applied stress and corrosion is now completing its operational-test period. The schematic diagram of the test loop is shown in Fig. II.A.1. The hot section contains five entry ports for the determination of mechanical properties and one sample port for corrosion studies. Two additional ports, one of each type, are located in the cooler section. The entire sodium flow (about 1300 kg/hr) is pumped through each port. Depending upon the insert chosen, sodium velocities of up to 9 m/sec past the corrosion specimens and stressed samples are possible. The combination of significant mass flow and high velocity should accentuate mass-transfer problems, if they exist. Design specifications are given in Table II.A.1.

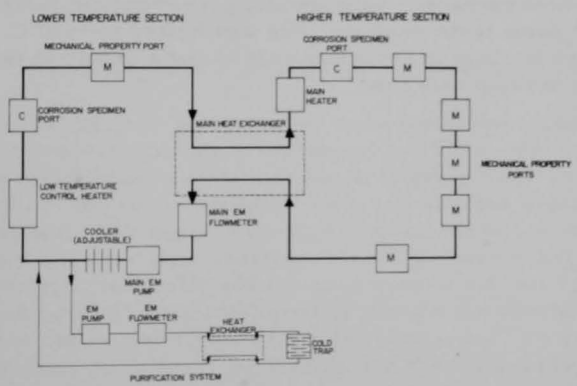

Fig. II.A.1. Schematic Diagram of the Dynamic Test Facility

*The original impurity content in the vanadium metal was ~1500 ppm.

TABLE II.A.1. Design Specifications of the Dynamic Test Facility

Maximum Temperature (°C)	750
Maximum ΔT (°C)	200
Mass Flow (kg/hr)	1300
Maximum Velocity Past Specimen (m/sec)	9
Material of Construction (Except for Emp and Emf)	347 SS
Purification Flow	1 w/o of main flow
Dwell Time in Cold Trap at Above Flow (min)	5

The individual test ports were designed to permit continued operation of the loop at temperature (but at reduced flow) while inserting or removing a mechanical pulling train or corrosion-specimen holder. This procedure, coupled with minimum temperature cycling, will provide a stable environment for creeptesting. A sodium freeze seal is established around each mechanical-property insert to prevent the displacement of sodium into the gas-phase portions of the facility by the pressure of the sodium pump.

The stringent requirement of sodium purity is being met by a separately pumped and metered cold-trap system. A single oxygen analysis (by distillation) gave a value of 1.5 ppm prior to recent repair work.

Although the operation of the loop successfully meets the design specifications, the operational-test period has been prolonged because leaks developed in the main heat exchanger. Welds in the relatively thin-walled tubing of the heat exchanger successfully passed helium leaktests when cold, but failed the same tests when the joint was heated to ~650°C. Repairs have been made and the loop is currently undergoing a prooftest to determine if further leaks develop with time.

III. GENERAL REACTOR TECHNOLOGY

A. Applied and Reactor Physics Development

1. Theoretical Reactor Physics--Research and Development

a. Cross Section Data Evaluation (C. N. Kelber)

Last Reported: ANL-7513, p. 94 (Oct 1968).

A set of unresolved resonance parameters was previously produced for ^{235}U for use in combination with the ENDF/B ^{235}U data and has been distributed to members of the CSEWG. Two new sets have been derived. One set is the same as the first except that the smooth cross sections in the unresolved region on the corresponding ENDF/B tape have been changed so that the smooth capture and fission cross sections are set equal to zero. The reduced neutron widths are then altered in processing through ETØE so that the original cross sections, calculated as the sum of smooth and infinite-dilution resonance contributions, are produced. The second new set is based on unresolved data provided by Pitterle.* Doppler-coefficient calculations are being performed for a typical assembly using all three sets of parameters for comparative purposes.

2. Nuclear Data--Research and Development

a. Burnup Analysis and Fission Yields for Fast Reactors (R. P. Larsen)

(i) Determination of the Absolute Fast Fission Yields of Burnup Monitors and Nonfission Nuclear Transformations in a Fast Reactor

Last Reported: ANL-7513, pp. 94-95 (Oct 1968).

Preparations are being made for an experiment to measure the effective capture-to-fission ratio (alpha) for ^{239}Pu. This will be accomplished by an irradiation in a critical facility having a soft neutron spectrum, which emphasizes the 10-keV neighborhood in which the greatest uncertainty in the alpha exists. The basic concept is to perform an irradiation of sufficient length to produce (1) a change in the ^{240}Pu content that can be measured mass spectrometrically and (2) an amount of a fission product isotope (^{140}Ba) that can be adequately measured by gamma spectrometry. The number of captures can be determined from the change in ^{240}Pu content; the number of fissions, from the ^{140}Ba content and the ^{140}Ba fission yield.

*Pitterle, T., Atomic Power Development Associates, Detroit, Michigan, private communication.

The planned 5-day irradiation (see Progress Report for July 1968, ANL-7478, pp. 26-27, 91-93) will produce a change of only 100 ppb in ^{240}Pu content; this requires that the starting material have a ^{240}Pu content of ~10 ppb or less. Five hundred micrograms of ^{239}Pu of this purity has been produced in the isotope separator of the Chemistry Division. The difficulty of determining the change in ^{240}Pu content and the danger of cross contamination make it necessary to limit the use of the high-purity material to capture measurements. Therefore, the irradiation capsules will contain separate specimens (foils) for capture and fission measurements. The capture foils will consist of 50 μg of pure ^{239}Pu mounted on stainless steel; the fission foils will be ~15-mg disks of normal plutonium metal. The preparation and encapsulation of these capture and fission foils has been completed (see ANL-7478, pp. 91-93).

To measure the number of fissions that occur during the irradiation, the fission foils will be assayed for ^{140}Ba activity (half-life of 13 days) by counting the 1.59-MeV gamma emitted by the 40-hr ^{140}La daughter. The relationship between ^{140}Ba counts and the number of fissions will be determined in a short irradiation (~2 hr) prior to the 5-day irradiation. Included in the short irradiation will be (1) fission foils of the type to be used in the long irradiation and (2) fission track counters. The fission track counters will consist of mica disks alternately stacked with platinum disks on which are mounted nanogram amounts of plutonium. The fission foils will be assayed for ^{140}Ba and plutonium; the number of fission tracks on the mica disks will be counted under a microscope. From the ^{140}Ba counts, the number of fission tracks, and the weights of plutonium in the fission foils and fission counters, a fission/count factor can be calculated. This factor will be used to determine the number of fissions that occur in the fission foils in the long irradiation.

Data obtained in preliminary short irradiations indicated that a possible increase in precision of the ^{140}Ba count-to-fission ratio could be obtained by improved precision in counting of the fission tracks. It was believed that this could be accomplished by dispersing the plutonium over a wider area on the platinum plates of the fission track counters. The technique of stippling from nitric acid solution, which was previously reported to show promise (see Progress Report for September 1968, ANL-7500, p. 93), still resulted in significant pileup of fission tracks. Improved precision was obtained, however, by stippling a hexone solution of plutonium onto the platinum plates in about 50 small droplets, followed by evaporation to dryness. The preparation of the ^{239}Pu plates for fission-track counting by this technique has been completed.

The objectives of the ^{239}Pu alpha experiment have now been expanded to include the measurement of alpha for ^{233}U and ^{235}U. These materials will be irradiated at the same time as the ^{239}Pu, and the same basic concepts will be used for the measurements. Preparation and encapsulation

of capture foils of isotopically pure ^{233}U and ^{235}U have been completed. Preparation of fission foils and fission track counters will begin shortly.

(ii) Development of Analytical Procedures for Fission Product Monitors

Last Reported: ANL-7500, pp. 93-94 (Sept 1968).

(a) X-ray Spectrometric Determination of Rare Earth Fission Products. Development of a method for determining rare earth fission products by X-ray spectrometry is continuing. Attention is being given to devising a simple separation procedure which will isolate the rare earths in a form suitable for X-ray spectrometry. A successful separation must meet at least two criteria: (1) the separated rare earths must be free of other elements that emit X rays in the region of the L-spectra of the rare earths, and (2) the separated rare earths must be free of such bulk constituents as uranium, plutonium, and cladding. The latter criterion is necessary because the L-spectra of the rare earths consist of very soft X rays that are easily absorbed by other solids.

Anion exchange is being considered as a means of separating the rare earths from the bulk constituent of the fuel and cladding. The proposed procedure involves (1) passing a 6N HCl solution of the fuel through an anion-exchange column, (2) evaporating the effluent to dryness several times with HNO_3, (3) redissolving the residue in a minimum volume of 2N HNO_3, (4) transferring to an aluminum plate, and (5) evaporating to dryness. The X-ray intensities of the separated rare earths would then be compared with the intensities of standards prepared by plating a 2N HNO_3 solution of rare earths directly on aluminum. The above procedure was tested with a solution containing only a fission product mixture of rare earths and the terbium internal standard. Results of initial tests showed no difference in rare earth-to-terbium ratio of the standard and the "separated" rare earths (see ANL-7500). However, subsequent separations produced plates with significant decreases (~2-5%) in rare earth-to-terbium ratios and even larger decreases (25-50%) in X-ray intensities.

It has been concluded that both the change in ratios and the decreased intensities were the result of an increased attack of the aluminum by residual chloride. The resultant increase in solids on the plate accounts for the overall decrease in intensity of the rare earth X rays; it also accounts for the change in ratio because the presence of solids can be expected to have a more pronounced effect on the less energetic X rays.

Because complete removal of chloride from nitric acid solutions is very difficult and irreproducible, other methods of plating that tolerate chloride are being considered. Two courses of action are open: (1) changing the plating technique to reduce the amount of attack on aluminum

or (2) using a different plate material. The former course is preferable because aluminum has many desirable characteristics as a plating material for X-ray spectrometric measurements.

b. Reactor Code Center (M. Butler)

Last Reported: ANL-7513, p. 99 (Oct 1968).

Six new packages were added to the Code Center Library and are now being readied for distribution. These are No. 341, GANDY, a GGA UNIVAC-1108 code for evaluation of effective cross sections in the unresolved resonance region; Nos. 342 and 343, MO648 and MO756 (LETO), Bettis CDC-6600 programs solving the one-dimensional-slab, many-region transport problem with energy degradation; No. 344 GEM, a KAPL CDC-6600 general matrix-manipulation program intended to solve the eigenvalue problem for discrete vibrating systems; No. 347, CODILLI/CURVEPLOT/SIGMA, University of Illinois IBM-360 programs written to analyze the low-energy cross sections of fissile elements with multilevel formalism; and No. 348, TOPS (MO543), the Bettis CDC-6600 digital simulation of pressurizer dynamics.

In addition, an IBM-360 version of the WAPD LEOPARD program, our number 279, has been received and incorporated as a replacement for the original IBM-7090 version, and a CDC-1604 version of No. 294 MO899/HOH has been added as received from the Idaho Division of ANL.

B. Reactor Fuels and Materials Development

1. Fuels and Cladding

a. Research and Development

(i) Behavior of Reactor Materials

(a) Thermal Properties of LMFBR Fuels (O. L. Kruger)

Last Reported: ANL-7513, pp. 99-102 (Oct 1968).

(1) Structures and Properties of Advanced Fuel Materials. Thermal-diffusivity data of UO_2 and PuO_2 as a function of temperature (reported in ANL-7513) were combined with known heat capacities to calculate thermal conductivities of the compounds. The thermal-conductivity curves have been compared with the results obtained by other investigators.

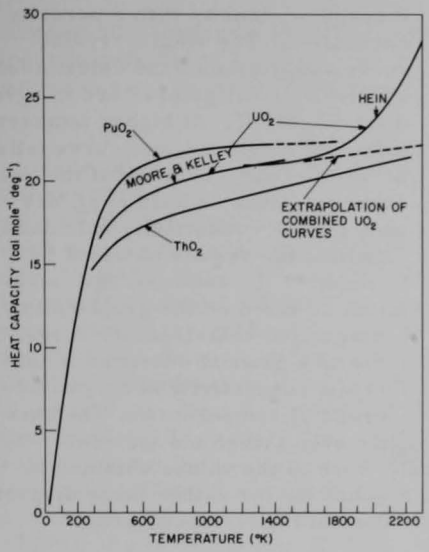

Fig. III.B.1. Heat Capacities of Some Actinide Dioxides

The heat-capacity curves of UO_2 and PuO_2, shown in Fig. III.B.1, were examined closely because these values have a direct influence on the thermal conductivity calculation. The ThO_2 curve, which was determined by a computer evaluation* of high- and low-temperature data, is shown for comparison. In the temperature region from about 200 to 1500°K, the heat capacity of the three compounds increased gradually with increasing temperature. The low-temperature curve for UO_2 by Moore and Kelley,** however, does not meet smoothly or coincide with the high-temperature curve obtained by Hein et al.† Godfrey et al.* used a computer-fit technique on the enthalpy data to determine the heat-capacity curve for UO_2 from 298 to 3000°K. These data dip unrealistically at about 1300°K and, therefore, were unsuitable for thermal-conductivity calculations. To circumvent the problems of computer-fit techniques and yet arrive at a realistic treatment of the data, a graphical solution was employed. The high- and low-temperature data were plotted on enlarged graph paper, and a smooth curve was drawn between the plotted points. The extrapolation of the smoothed heat-capacity curve is shown in Fig. III.B.1 along with the high-temperature curve of Hein et al. Both curves were used to evaluate the high-temperature thermal conductivity of UO_2.

The heat-capacity curve for PuO_2 was determined from the high-temperature measurements of Kruger and Savage†† and the low-temperature data of Sandenaw.‡ The curve has been extrapolated beyond the highest measurement of 1400°K.

Thermal-conductivity data for single-crystal and polycrystalline UO_2 determined in this study have been corrected for the volumetric expansion of the specimen with temperature, and the curves are compared with the results of other investigators (see Fig. III.B.2). All of the thermal-conductivity data shown in the figure have been adjusted to

*Godfrey, T. G., Woolley, J. A., and Leitnaker, J. M., ORNL-TM-1596 (Oct 1966).

**Moore, G. E., and Kelley, K. K., J. Am. Chem. Soc. 69, 2105 (1947).

† Hein, R. A., Sjodahl, L. H., and Szwarc, R., J. Nucl. Mater. 25, 99 (1968).

†† Kruger, O. L., and Savage, H., J. Chem. Phys. (in press).

‡ Sandenaw, Th. A., J. Nucl. Mater. 10, 165 (1963).

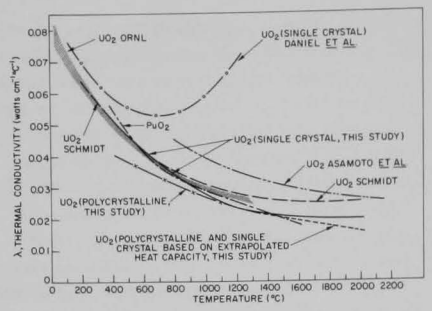

Fig. III.B.2. Calculated Thermal Conductivities of UO_2 and PuO_2 Compared with Results of Other Investigators

theoretical density with a porosity correction. The single-crystal curve and the data band determined by ORNL investigators* are in agreement to ~850°C. At higher temperatures the single-crystal curve falls below the ORNL data and if the heat-capacity values of Hein et al. are used for the conductivity calculation, parallels the results obtained by Schmidt.** If, however, the calculation is based on the graphically extrapolated heat-capacity curve, there is a gradual decrease in the thermal conductivity of UO_2 with increasing temperature. The data of Schmidt appear to be considerably higher even though his thermal-diffusivity measurements were relatively close to the values obtained in this work. There is no obvious way to account for the rather large disparity between the calculated thermal conductivities at high temperatures.

The slope of the curve for polycrystalline UO_2 at 400°C indicates that the room-temperature thermal conductivity of this material would be near 0.05 W cm^{-1} $°C^{-1}$. The thermal conductivity of the polycrystalline UO_2 specimen (93.7% of theoretical density) agreed exactly with the single-crystal curve above 1200°C, if the Loeb equation was used for the conductivity data:

$$\lambda_T = \frac{\lambda_M}{1 - P}, \tag{1}$$

where λ is the thermal conductivity, P is the fractional pore volume, and the subscripts T and M refer to the theoretical and measured conductivities. Recent investigators have favored a modification of the Loeb equation with conductivity data or a modified Maxwell-Eucken equation of the type

$$\lambda_T = \frac{1 + \beta P}{1 - P} \lambda_M, \tag{2}$$

where β is a proportionality factor. Various values have been proposed for β, depending on the type and amount of porosity present in UO_2. A value of 0.5 has been suggested for β when the density is greater than 90% of

*Godfrey, T. G., Fulkerson, W., Kollie, T. G., Moore, J. P., and McElroy, D. L., J. Am. Ceram. Soc. 48, 297 (1965).

**Schmidt, H., Kernforschungszentrum Karlsruhe, Germany (private communication).

theoretical. However, use of Eq. (2) to evaluate the thermal conductivity of theoretically dense UO_2 from the data for the 93.7% dense UO_2 specimen gave a curve above that observed for the single crystal.

Unfortunately, most of the previous work on porosity corrections was at either ambient temperature or below 1000°C. In this temperature region there is considerable evidence of the scattering of phonons by grain boundaries and porosity. Calculations based on the ORNL work give a phonon mean-free-path of 0.0015 μ at 700°C. The UO_2 specimens used by ORNL were annealed for 4 hr at 1850°C prior to measurement. This treatment produced grains of a mean diameter of from 10 to 20 μ and coalesced the pores. The polycrystalline UO_2 specimen heated in this study to 1600°C had a mean grain diameter of from 4 to 8 μ, and the porosity was finely distributed throughout the grains. Also, many of the grains were close to 1 μ in diameter. The combination of fine grains and pore distribution could easily account for a minimum mean-free-path of the order of that calculated for the phonons at 700°C. Heating of the polycrystalline UO_2 specimen to 2000°C produced a microstructure similar to that of the ORNL specimens. Unfortunately, no diffusivity data were taken on cooling below 1200°C. An investigation of the thermal-conductivity curve for annealed polycrystalline UO_2 is in progress, and the data are expected to fall on the curve obtained for the single-crystal specimen.

Measurements of single-crystal UO_2 by Daniel et al.* showed a rapid increase in the thermal conductivity with increasing temperature above 700°C. This type of behavior was not observed in our work. Asamoto et al.** have suggested the curve shown in Fig. III.B.2 for theoretically dense UO_2. Even the most optimistic combination of heat-capacity and diffusivity data will not yield thermal conductivities for UO_2 of this magnitude at high temperatures. In fact, our most optimistic calculations, which use the highest heat-capacity values for UO_2, show no evidence of a significant rise of λ at high temperatures. The rather rapid increase in the heat capacity of UO_2 at high temperatures, as observed by Hein et al., has been attributed to a vacancy-propagation mechanism. However, this mechanism does not appear to be consistent with the thermal-diffusivity results. Any unusual increase in the vacancy concentration should produce a corresponding decrease in thermal diffusivity, but no such change has been observed. Further study of UO_2 at high temperatures is needed to resolve this disparity.

Some investigators have suggested the use of porosity corrections that incorporate a radiation contribution to the conductivity at high temperatures. Thus far we have found no evidence that would substantiate this type of interpretation of the thermal-conductivity data.

---

*Daniel, J. L., Matolich, J., Jr., and Deem, H. W., HW-69945 (1962).

**Asamoto, R. R., Anselin, F. L., and Conti, H. E., GEAP-5493 (1968).

The thermal conductivity of PuO_2 is somewhat higher than that of UO_2 at lower temperatures. In the temperature range from 500 to 1400°C the conductivities of the two compounds are similar, and the slope of the conductivity curve for PuO_2 at high temperatures suggests a decrease in λ with increasing temperature. High-temperature heat-capacity data for PuO_2 are needed, however, to evaluate properly the thermal conductivity of this compound at high temperatures.

(b) Irradiation Behavior of Uranium-Plutonium Base Alloys (D. R. O'Boyle)

Last Reported: ANL-7513, pp. 105-106 (Oct 1968).

Two of the U-Pu-Zr alloys that were prepared to study the effects of temperature and pressure on the swelling behavior of U, Pu-base fuels have high concentrations of oxygen and silicon (see Progress Report for August 1968, ANL-7487, p. 1). The original assumption was that these impurities were picked up from the silica molds used in the injection-casting process. The analysis of subsequent melts, however, has indicated that part of the oxygen came from the zirconia crucibles used to melt the charges. Consequently, a study was conducted to determine whether oxygen pickup could be reduced by using a more stable crucible material. Prototype crucibles were fabricated from each of the following materials: dysprosia, yttria, and gadolinia. A 20-g charge of U-15 w/o Pu-12 w/o Zr was melted in each crucible and held at approximately 1500°C for 30 min. After the melts were allowed to freeze in the crucibles, samples were taken from the center of each ingot for chemical analyses of the oxygen contents and for spectrographic analyses to determine the amount of metal pickup from the crucibles. The results were 4200 ppm dysprosium and 57 ppm oxygen, 500 ppm yttrium and 91 ppm oxygen, and 150 ppm gadolinium and 77 ppm oxygen for the alloys melted in dysprosia, yttria, and gadolinia crucibles, respectively.

Based on these chemical analyses gadolinia appears to be the best crucible material. However, the metal ingot did not adhere to the yttria crucible but did adhere to the other two materials. Because of the additional advantages of a lower fast-neutron-capture cross section, and lower cost, yttria crucibles will be used for the remaining U-Pu-Zr melts of this series.

(c) Swelling and Gas Release in Metal Fuels (P. G. Shewmon)

(1) Studies of Fuel Swelling and Gas Release (S. R. Pati)

Last Reported: ANL-7457, pp. 104-105 (May 1968).

In-reactor Swelling Studies. An instrumented capsule has been assembled to study the effect of external restraints on the

in-reactor swelling behavior of metallic fuels. The capsule was designed to permit continuous measurement of unrestrained as well as restrained swelling rates of metal fuels under different external restraints and burnup conditions.

The specimen will be encapsulated in a chamber completely filled with NaK. The chamber incorporates bellows that actuate a pushrod, the motion of which is detected by a linear variable differential transformer. A volume change in the specimen will displace NaK in the chamber. This displacement, which will compress the bellows, will be detected from the motion of the pushrod. Thus, the system allows continuous monitoring of the unrestrained swelling as a function of burnup. The application of pressure to the other side (away from the NaK-filled chamber) of the bellows will pressurize the NaK surrounding the specimen and allow measurements of the swelling rates of fuel pellets irradiated under different hydrostatic pressures. In addition, the unrestrained swelling of a fuel pellet could be monitored to a desired percent burnup, at which point measurements of the response of the pellet to an applied hydrostatic pressure could be made. From this type of measurement, information might be gained about the flowrates of materials into the microcracks and cavities formed within the fuel under different burnup conditions. Provision has also been made to place heater windings around the specimen chamber to control the temperature during irradiation.

The NaK-filled chamber is made of V-5 w/o Ti-15 w/o Cr alloy, which is capable of safely withstanding 10,000 psi internal pressure at 650°C. The criteria for determining the thickness of the specimen chamber were obtained from the ASME Boiler and Pressure Code.* The measurement of swelling of the specimen depends on constancy of the external dimensions of the specimen chamber. The ternary V-Ti-Cr alloy, chosen for constructing the specimen chamber, has a yield strength (0.2% elongation) of 48,000 psi at 650°C and a creeprate of less than 1/100 percent per 1000 hr at the design stress. Thus the alloy will not undergo detectable dimensional changes during the experiment, and will be suitable for the intended measurement. The pressure is applied to the chamber by compressing helium through a diaphragm-type compressor, which has a maximum discharge capacity of 30,000 psi. A U-8.75 w/o Fs (9.85% enriched) fuel rod, 0.144 in. in diameter by 7/16-in. long, will be placed in the capsule and irradiated in CP-5 to test the feasibility of the design.

*Section III, Nuclear Vessels.

(ii) Chemistry of Irradiated Fuel Materials (C. E. Crouthamel)

(a) Development of Analytical Facilities, Microstructure Sampling Techniques and Analytical Procedures for Analysis of Irradiated Fuels

Last Reported: ANL-7478, p. 100 (July 1968).

Construction work on the shielded fuel-evaluation facility has been completed. Tests of the inert-atmosphere enclosure showed a leakrate for air of less than 0.05 cfm, the minimum that can be detected by a pressure change within the cell. Further evaluation of the leakrate will be made after the enclosure is filled with helium.

Installation of in-cell equipment and the remote metallograph has begun. Steel shielding for the metallograph has been delivered, and the metallograph has been moved to the cave area.

A wet-chemistry box has been constructed adjacent to an exit port of the helium cell to provide for sample dissolution or other chemical work associated with the operation of the facility. The box is made of plastic, and is equipped with two manipulators and the necessary ports for transferring samples in and out of the helium cell and into the Air Cell.

Excavation work has begun for the pneumatic sample-transfer tube which will connect the shielded fuel-evaluation facility and the analytical facility. The terminal facilities for the tube inside the helium cell have been completed.

2. Coolants, Moderators, and Control Materials--Fundamentals of Corrosion in Liquid Metals

a. Corrosion Mechanisms (D. L. Smith)

Last Reported: ANL-7460, pp. 93-95 (June 1968).

The equilibrium distribution coefficients for oxygen between the Group-V refractory metals (vanadium, niobium, and tantalum) and liquid sodium are being measured experimentally. Refractory-metal wires are exposed to liquid sodium for periods sufficient to equilibrate the oxygen in the wires with the oxygen in the sodium. The distribution coefficients are being measured as functions of both temperature and oxygen concentration. The oxygen concentration in the sodium is determined by vacuum distillation and from solubility data. The oxygen in the solid wires is determined by vacuum fusion or by internal-friction techniques.

The internal-friction technique is a sensitive indicator of low interstitial concentrations in the body-centered-cubic refractory metals. In order to speed up the internal-friction measurements, a new system has been designed, constructed, and tested. This inverted pendulum-type apparatus is equipped with an automatic readout of the oscillation amplitude, the cycle number, and the specimen temperature. The oscillation amplitude is measured with a solar cell whose light beam is cut by a vane on the oscillating pendulum. The machine is capable of operating automatically through a temperature cycle. The operation has been checked with wires previously measured with a manual internal-friction apparatus. Only a few adjustments are required before the new apparatus is ready for continuous operation.

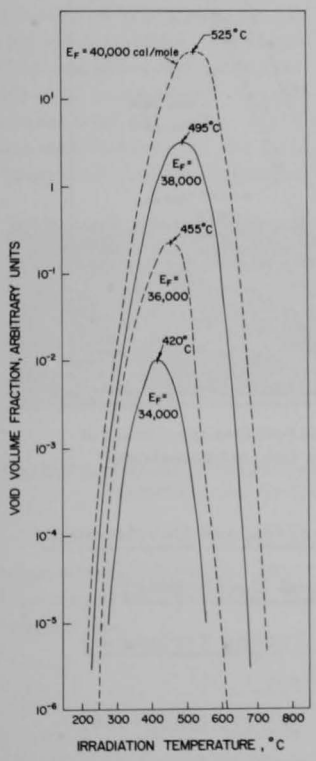

Fig. III.B.3. Void Formation as a Function of the Vacancy Energy of Formation

3. Radiation Damage on Structural Materials--Research and Development--In-Reactor Creep Studies

a. Void Formation and Growth (S. D. Harkness)

Last Reported: ANL-7513, pp. 107-110 (Oct 1968).

A model was developed that describes quantitatively the effects of temperature and fast-neutron flux on void formation in austenitic stainless steel. This model was able to duplicate the experimental temperature dependence of void formation and growth. A time-dependent growth rate has since been incorporated into the model, and several interesting implications can now be stated:

(1) Void formation is sensitive to small changes in the energy of vacancy formation (see Fig. III.B.3). Decreases in this parameter will shift void formation to lower temperatures and reduce the magnitudes.

(2) An increase in the surface energy of the material also results in a shift of void formation to lower temperatures and a reduction in magnitude (see Fig. III.B.4).

(3) For samples irradiated to a constant integrated neutron exposure, those exposed to a lower flux for a longer time should show more void formation (see Fig. III.B.5).

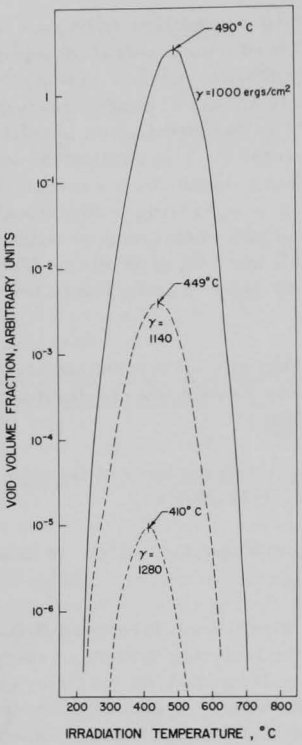

Fig. III.B.4. Void Formation as a Function of the Surface Energy

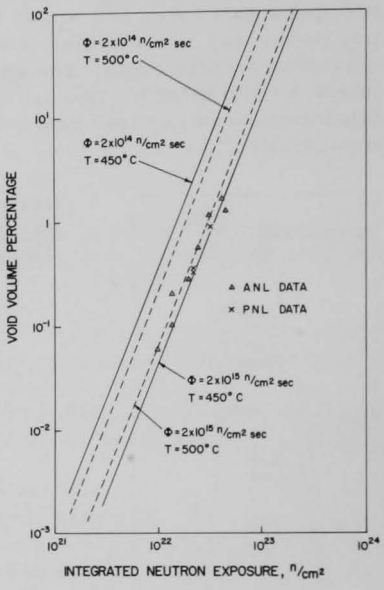

Fig. III.B.5. Void Formation as a Function of Flux Level and Temperature

4. Techniques of Fabrication and Testing--Research and Development

a. Nondestructive Testing--Research and Development

(i) Development of Nondestructive Testing Techniques (C. J. Renken)

Last Reported: ANL-7500, pp. 100-101 (Sept 1968).

(a) Feasibility Study of Ultrasonic Inspection of the Sodium Bond in Irradiation Capsules. The study of the feasibility of applying ultrasonics to the detection of nonwetted areas (outer jacket ID) in irradiation capsules is in progress. Initial tests were conducted in the high-temperature (110°C) facility at frequencies of 10 and 20 MHz. At these frequencies various response patterns were obtained from different areas

of dummy capsules. Some areas produced a pattern similar to that obtained with the transducer positioned above the sodium level (in the plenum), which indicates that the ultrasonic test is detecting nonwet areas. The minimum area and thickness of nonwetted sections that can be detected are not yet known. Because the tests in the hot facility were slow and tedious, subsequent tests to determine the optimum ultrasonic technique were conducted at room temperature with cold capsules.

The capsules were inspected at room temperature by X radiography to locate shrinkage voids for the ultrasonic study. Collimated and focused transducer probes were evaluated at both normal and angled incidence (1-30° in 1° steps) at frequencies of 5, 10, and 20 MHz. Several ultrasonic instruments were also evaluated. Void areas could be discerned from bonded areas by all of the applied techniques, but with varying sensitivities. Perhaps the best technique is illustrated in Fig. III.B.6. The oscilloscope presentations in the figure were obtained with a Magnaflux PS-902 instrument, a 5-MHz focused transducer probe, and an angle of incidence of 19°. The first pulse in both pictures is a reflection from the outside surface of the capsule. An unbonded area is characterized by the "ringing" pattern following the surface reflection.

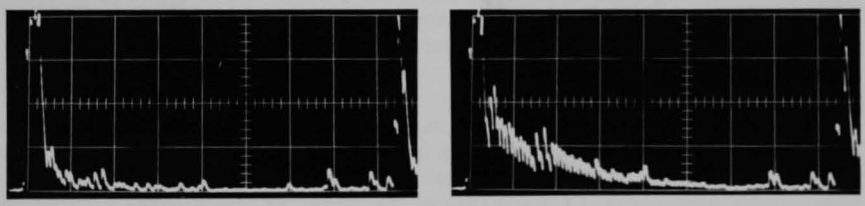

Bonded Unbonded

Fig. III.B.6. Oscilloscope Presentations of Bonded and Unbonded (Shrinkage void) Areas in a Dummy EBR-II Mark-II Capsule. (Sensitivity--0.1 V/major division; time scale--2 μsec/major division.)

Several techniques will be evaluated further in the high-temperature facility. Nonwet areas detected by these techniques will be compared with those detected by X radiography and eddy-current inspection.

(b) Passive Ultrasonic Test Techniques. Experiments are continuing to improve joining techniques for high-temperature acoustic sensors. Lithium niobate crystals, gold-platinum-palladium electrodes, and an Au-18 w/o Ni brazing alloy were used in the experiments because of encouraging, although inconsistent, prior results with these materials.

In the first experiment, a Harshaw Z-cut crystal was brazed to a Type 304 stainless steel plate. Figure III.B.7 shows the

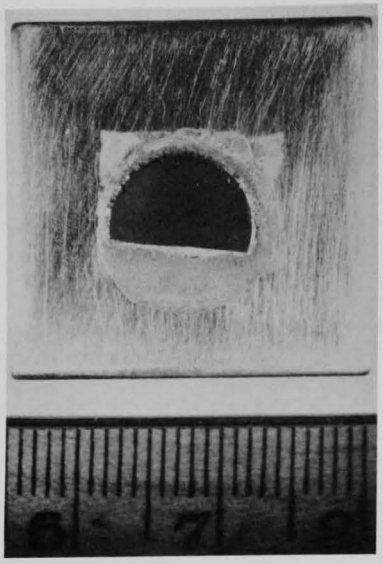

Fig. III.B.7. Lithium Niobate Crystal Bonded to a Type 304 Stainless Steel Plate (Scale is in millimeters)

crystal firmly attached to the plate, and no evidence of electrode deterioration during the brazing process is evident.

In the next experiment, a Type 304 stainless steel cylindrical container was substituted for the plate, and a Type 304 stainless steel cylindrical backing was added. This unit was subjected to the same brazing process employed in the previous experiment. Again, the components appeared to be firmly attached. Operation of the unit was ascertained by acoustic tests, which included reception of signals generated by finger tapping the container and also signals generated by a 5-MHz transducer. Unfortunately, this unit was broken during the welding of a positive signal lead to the backing. Consequently, the manufacturing sequence has been modified; the wire is now welded to the backing prior to brazing.

Four subsequent attempts to manufacture acoustic sensors have been unsuccessful. All attempts resulted in electrode removal from the crystals during brazing. An investigation of the electrode-attaching procedure is being conducted to determine if this is the cause of the failures.

(c) Development of an Electrodynamic Ultrasonic Transducer. An electrodynamic ultrasonic transducer is a device for the generation and detection of ultrasound by means of the interaction of a magnetic field and a current. Recent developmental efforts have been directed to increasing the sensitivity of the transducer, generating and detecting various modes of propagation of ultrasound, and determining the effectiveness of the transducer for flaw detection in metals.

Increased sensitivity can be achieved in two ways: increasing the magnetic field, and increasing the current in the coil. The magnet is already operating at its maximum ($\sim 20 \times 10^3$ G). Since sources with sufficient power to pulse the coil are not commercially available, a pulse generator was built (an identical generator is used in the nondestructive eddy-current tests). This generator increased the amplitude of the output pulse from the coil and from all the detected signals by a factor of approximately 2-3 when compared with the response of an Arenberg oscillator operating at 5.0 MHz, and made the sensitivity of the electromagnetic

transducer competitive with piezoelectric transducers. Output pulses as small as 0.1 μsec are possible without loss of pulse amplitude. In comparison, maximum amplitude is obtained with the Arenberg oscillator when the pulse length is about 10 μsec (minimum pulse length is about 1.5 μsec).

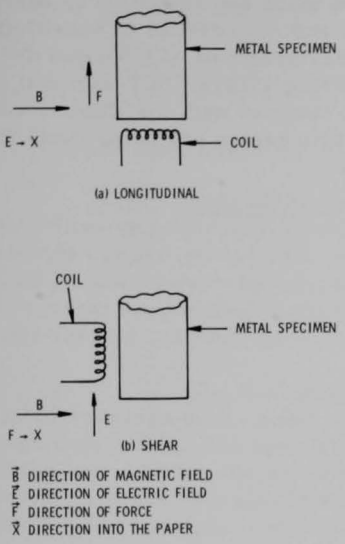

Fig. III.B.8. Generation and Detection of (a) Longitudinal- and (b) Shear-wave Motion with the Electromagnetic Transducer (Pulse-echo technique)

The initial configuration of coils, specimen, and magnet produced longitudinal wave motion in the specimen. Another orientation was tried, and shear waves were generated and detected in an aluminum bar (verified by measuring the time between reflections). The two geometries used to generate and detect longitudinal and shear wave motion are shown in Fig. III.B.8.

A hole, 1.27 mm in diameter and 8.53 mm long, was drilled into a 12.7-mm-long aluminum bar to simulate a defect. Two pancake coils of 12.7-mm diameter were orientated to produce and detect shear waves in the specimen, and were located about 0.8 mm from the specimen surface. This defect was readily located by a through-transmission method and by a pulse-echo (one coil) method. Figure III.B.9 shows the decrease in amplitude of the transmitted pulses when the coils were placed over the flaw area. No amplification of the received pulse was made other than that provided by the oscilloscope.

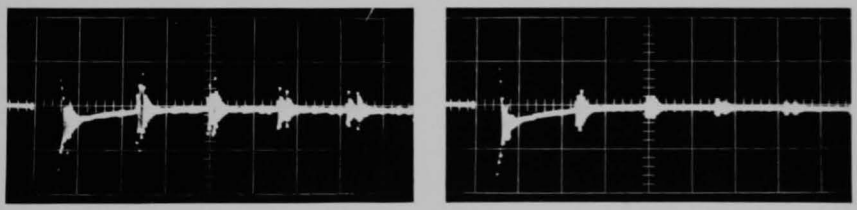

(a) No Flaw (b) Flaw area

Fig. III.B.9. Detection of a Defect in a 12.7-mm Aluminum Bar by Means of the Electromagnetic Transducer. Through-transmission technique; receiver coil is connected directly to the oscilloscope (sensitivity--0.02 V/major division; time scale--5.0 μsec/major division; coil diameter--12.7 mm).

The possibility that a decrease in the diameter of the coils might produce greater sensitivity to the defect was investigated. Coils with 6.55- and 3.28-mm diameters were made and tested. The energy output from the smaller coils was much less, and no increase in sensitivity was observed. However, a bank-wound, double-layer coil of 6.55-mm diameter showed sensitivity equal to that of the single-layer 12.7-mm coil. This indicates that greater sensitivity can be obtained with the smaller coils provided they contain many layers. Coils of this design are being made for an evaluation of their ability to detect defects.

C. Engineering Development

1. Heat Transfer and Fluid Flow

a. Heat Transfer in Liquid Metal Cooled Reactor Channel (R. P. Stein and J. V. Tokar)

Last Reported: ANL-7513, p. 114 (Oct 1968).

(i) LMFBR High-flux Operation and Its Consequences. High-heat-flux operation will be explored in a stainless steel-sodium loop that provides pressure and flow characteristics resembling those of typical LMFBR configurations. Hopefully, the tests also will determine the accuracy of current engineering methods for predicting the steady-state and transient heat-transfer performance of fast reactors.

The heat exchanger for the loop has been ordered, and detailed drawings of the dump tank, hot trap, top plenum and preheater have been completed. The loop framework is being constructed. The complex of the test section, the pressure transducers, the electron-bombardment heater, and the vacuum chamber have been planned in sufficient detail to initiate final design. Detailed analysis of piping flexibility has begun.

To predict the occurrence of "flow instability" (i.e., the uncontrollable loss of coolant flow) during experiments with slowly increasing power or decreasing flow, it is necessary to know the pressure-drop versus flowrate characteristics of the simulated fuel or blanket regions. Computations of these pressure-flow characteristics require determination of the pressure distribution along the length of the duct simulating the fuel or blanket region, and must include, of course, the influence of coolant vaporization. The present bases for these computations are the usual one-dimensional flow models applied to liquid sodium with outlet plenum pressures between 1 and 2 atm. These are conditions at which the occurrence of a "choked" flow (critical mass velocity) are very likely, and may well be the controlling mechanism determining both "flow instability" and the distribution of voids within the fuel or blanket region. Several aspects of these computations are being studied and deserve mention, especially since they seem to have received little or no attention in the literature.

The first aspect derives from the assertion that consistency within the framework of a one-dimensional flow representation requires that the pressure gradient along the length of the duct becomes infinite at the duct outlet when the flow is "choked." For the familiar case of thermodynamic equilibrium between liquid and vapor, and where vapor-volume fraction (or slip ratio) is an independent function of physical properties and weight-fraction vapor, this assertion leads to the generalized expression for the critical mass velocity, G_c:

$$G_c^{-2} = -[\alpha_K v_K + \beta_M + (\alpha_K \beta_M - \alpha_M \beta_K)\, G^2 v_K], \tag{1}$$

where

$$\alpha_j = \left(\frac{\partial v_j}{\partial h}\right)_P, \quad j = K \text{ or } M;$$

$$\beta_j = \left(\frac{\partial v_j}{\partial P}\right)_h, \quad j = K \text{ or } M;$$

$$v_M = \tilde{v}[1 + (s - 1)\, x];$$

$$v_K = \tilde{v}[1 + (s^2 - 1)\, x]^{1/2};$$

$$\tilde{v} = x\frac{v_g}{s} + (1 - x)\, v_f;$$

s = slip ratio (ratio of vapor velocity to liquid velocity);

G = mass velocity;

h = enthalpy of vapor-liquid mixture;

P = pressure;

v_g, v_f = specific volume of saturated vapor and liquid

(the usual conversion factors g_c and J are omitted here). For the homogeneous-flow model with $s = 1$, Eq. (1) reduces to the usual expression for a single-phase compressible fluid. If a value of G_c as computed by some other expression is larger than the value computed from Eq. (1), it will not be possible to use the particular one-dimensional flow model consistent with the relationship used for s for computing the pressure distribution within the duct. This difficulty arises because a value of G_c larger than that given by Eq. (1) corresponds to the physical impossibility of a positive pressure gradient at the duct outlet.

The second aspect being studied relates to the methods used to numerically integrate the pressure gradient ($dP/d\ell$) to obtain the pressure distribution along the duct. With coolant vaporization, $dP/d\ell$ is very large at the duct outlet (at the choked-flow condition it may be infinite). As a result, the accuracy of the numerical integration could be extremely poor, especially at the choked-flow condition. This difficulty is avoided by simply considering duct length ℓ as the dependent variable rather than the pressure P, i.e., $d\ell/dP$ is integrated rather than $dP/d\ell$. Computer programs based on this simple interchange of independent and dependent variables are being developed.

The third aspect being studied concerns the existence of a set of differential equations that are consistent with one-dimensional flow representations and that can always be derived if enough details of the flow patterns are specified. In principle, the solution of this set of equations will give both the pressure and vapor-volume-fraction distributions along the length of the duct without, as is the current practice, the necessity to assume an independent relationship for the vapor volume fraction.

b. Electron Bombardment Heater Test Facility (R. D. Carlson and R. E. Holtz)

Last Reported: ANL-7513, p. 116 (Oct 1968).

The central pin of the 7-pin EBH cluster has been operating at low powers. Cathodes for all seven pins in the cluster are being assembled. Future tests will involve the operation of the entire cluster rather than a single pin.

2. Engineering Mechanics

a. Anisotropic Thermoelasticity Studies (R. A. Valentin)

(i) Specific Design Problem

Last Reported: ANL-7487, p. 93 (Aug 1968).

The stress-function formulation associated with the solution of specific design problems has been modified to generalize Youngdahl's isotropic-cylinder stress functions* to the case of transversely isotropic materials. In this formulation it will be possible to treat nonaxisymmetrical problems for general cylindrical regions provided the preferred material direction coincides with the direction of the cylinder generators. The solution of the displacement equations of equilibrium for a transversely isotropic solid having its principal direction along the z axis and occupying a cylindrical region whose generators are in this same direction can be represented in terms of three stress functions Σ, Λ, and ψ, with the displacement field (u_x, u_y, u_z) defined by

$$u_x = \frac{\partial \Sigma}{\partial x} - \frac{\partial \Lambda}{\partial y}, \quad u_y = \frac{\partial \Sigma}{\partial y} - \frac{\partial \Lambda}{\partial x}, \quad u_z = k_2 \frac{\partial \Sigma}{\partial z} + \frac{\partial \psi}{\partial z}.$$

The stress functions satisfy the Poisson-like equations

$$\nabla_3^2 \Lambda = g_2; \quad \nabla_2^2 \Sigma = \frac{A_2}{1 + A_2} \left\{ -A_3 \frac{\partial^2 \psi}{\partial z^2} + B_1 T + A_2^{-1} g_1 \right\};$$

*Youngdahl, C. K., On the Completeness of a Set of Stress Functions Appropriate to the Solution of Elasticity Problems in General Cylindrical Coordinates, to be published in Int. J. Eng. Sci.

$$\nabla_1^2\psi = A_1^{-1}\{A_2(B_2 - \nu_1 k_2 B_1)\, T - \nu_1 k_2 g_1 + g_3\},$$

where

$$\nabla_i^2 = \frac{\partial^2}{\partial x^2} + \frac{\partial^2}{\partial y^2} + \nu_i \frac{\partial^2}{\partial z^2},$$

and the constants ν_i and k_2 are roots of certain quadratic equations involving the five elastic constants of the material. The constants A_i are various ratios of the elastic constants, B_i are related to the two linear-thermal-expansion coefficients, and g_i refer to certain integrals of the body-force field. Specialization of this representation to rotational symmetry for circular cylindrical regions results in a representation closely related to the previously employed Singh functions.

(ii) Fuel Growth Models

Not previously reported.

For burnup of the order of a few atom percent, it is reasonable to compute the internal stresses caused by spacially nonuniform fuel swelling by means of the usual thermal-stress equations of classical elasticity with the "αT" terms replaced by $\frac{1}{3}(\Delta V/V)$, where $(\Delta V/V)$ is a position-dependent volume swelling rate computed from some applicable model. In the case of a thermal reactor, the spatial variation of the swelling can be attributed to a variable fission rate caused by self-shielding within a fuel pin, and the computation can be performed in an elementary manner (e.g., Yu. I. Likhachev et al., Atomn. Ener. 18, 483 (1965). In a LMFBR oxide-fuel pin, the position dependence of the swelling is controlled by the complex of phenomena associated with growth and migration of fission-gas bubbles; construction of a suitable expression for the spatial dependence of $(\Delta V/V)$ then becomes closely associated with the growth model describing an individual gas bubble because the spatial diffusion of such bubbles is a function of their radius. It seems reasonable to describe the fission-gas bubbles in a fuel material by a suitable distribution function, $f(\underline{r}, \underline{v}, \rho, v_\rho, t)$, which is assumed to depend on position $\underline{r}$, spatial bubble velocity $\underline{v}$, bubble radius ρ, bubble surface velocity v_ρ, and time t. It is then possible to derive a Boltzmann-like equation governing bubble transport, from this to derive various approximate continuity equations, and, from solutions of these continuity equations coupled with the equation describing fission-gas production, to derive a spatial distribution of expected bubble radius $\langle\rho\rangle$ and local bubble density. This information should furnish the spatial variation of $(\Delta V/V)$ to use in the thermoelastic analogy or in a finite-deformation model applicable to higher burnup. In conjunction with an initial study of this problem, the bubble-growth model postulated to yield an expected value of bubble surface velocity $\langle v_\rho\rangle$ is of the form

$$\langle v_\rho\rangle = A\ \mathrm{sgn}(g)\ g^n \rho\,; \qquad g = [p_0 + 3kTDt\rho^{-2}c(t) - p - 2\gamma\rho^{-1}],$$

where A and n are known constants, p_0 is an initial gas pressure in the bubble, D is a surface diffusion coefficient, c(t) is a gas concentration in the fuel matrix, γ is the surface energy, and p is external hydrostatic pressure. This model will be studied in conjunction with the continuity equation

$$\frac{\partial f}{\partial t} + \frac{\partial}{\partial \rho}(\langle v_\rho \rangle f) = 0$$

and the gas balance equation

$$\frac{dc}{dt} = a - 4\pi DN\langle \rho \rangle c(t),$$

where a is a constant gas-production rate, to obtain a position-independent value of $(\Delta V/V)$. If this result is physically reasonable, a modified continuity equation containing a spatial gradient of the distribution will be included to obtain the final model for $(\Delta V/V)$.

b. Structural Dynamics Studies--Parallel-flow-induced Vibrations (P. L. Zaleski and M. W. Wambsganss, Jr.)

(i) Transducer Development

Last Reported: ANL-7500, p. 109 (Sept 1968).

Initial calibration of the 1/8-in.-dia pressure-transducer pairs showed them to be excessively strain sensitive. Minor vibration-induced deformations of the 1/2-in. tube on which the transducers are mounted produced a signal large enough partially to mask the pressure-induced signal. We believe that these transducers as they are now installed will be usable if the resonant frequency of the tube is increased beyond the range for which the pressure measurements are desired. A rigid mounting fixture is being built to hold the rod in tension. It is expected that sufficient axial tension can be applied to double the first-mode vibration frequency.

The most recent test series of the miniature pressure transducers have produced a more durable, uniformly responsive device. Seven of these units are being installed on a test rod.

(ii) Flowtest Single Cylinders

Last Reported: ANL-7513, pp. 117-118 (Oct 1968).

Displacement-time histories, obtained from tests employing a 1-in.-ID test section, were processed with the spectrum analyzer; spectral-density curves were plotted from which rms displacements were computed.

The smaller-diameter test section was used to achieve higher flow velocities, with no consideration given to possible wall or entrance effects that might result from the smaller cross-sectional flow area. Results are presented in Fig. III.C.1. The important piece of information to be derived from these results is that the approximate power-function relationship between rms displacement and mean axial flow velocity is followed over the extended range of flow velocities; previous results were obtained for flow velocities to 20 ft/sec.

c. Structural Dynamics Studies--Crossflow-induced Vibrations (M. W. Wambsganss, Jr.)

Last Reported: ANL-7478, pp. 94-95 (Aug 1968).

(i) Experiment Design. The importance of baffle-tube clearance as it affects the vibrational characteristics and response of heat-exchanger tubes was identified under the EBR-II superheater vibration study (see Progress Report for July 1968, ANL-7487, pp. 67-68). It also was reaffirmed in a recent meeting with representatives of Oak Ridge National Laboratory; the purpose of the meeting was to discuss the flow-induced vibration of heat-exchanger tubes, emphasizing the areas requiring research and experimental study. A preliminary analytical study of the effect is being carried out (see Progress Report for August 1968, ANL-7487, pp. 61-62; September 1968, ANL-7500, p. 71; and this Progress Report Sect. III.C.2.b.(ii)). The analysis involves several assumptions related to mode shapes and response. To evaluate these assumptions and to gain further insight into the phenomena involved in the impact of a tube with a stop, an experiment is being designed. The initial experiment will involve vibrating a beam on a shaker with adjustable stops of variable geometry. For various amplitudes and frequencies of a sinusoidal input, displacements and impact forces will be measured.

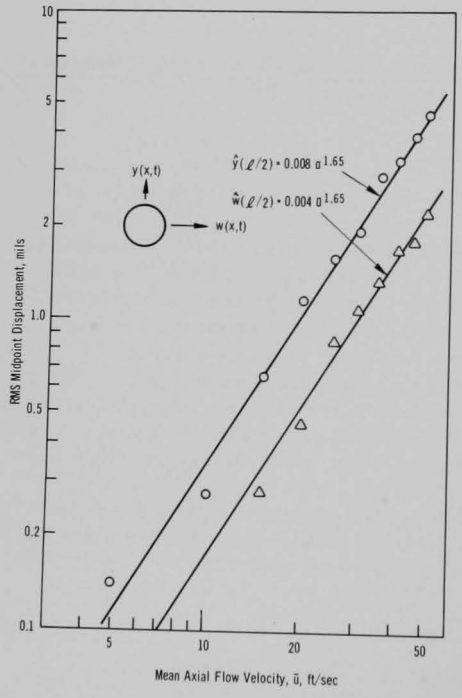

Fig. III.C.1. Relationship between rms Displacement and Mean Axial Flow Velocity as Determined by Flowtesting a Single Cylinder

D. Chemistry and Chemical Separations

1. Aqueous and Volatility Processes--Research and Development--Fluoride Volatility Process

a. Development of Head-end Steps (M. J. Steindler)

Last Reported: ANL-7487, p. 95 (Aug 1968).

(i) Chemistry of Stainless Steel. Our current concept for the reprocessing of LMFBR fuels calls for the decladding of stainless steel-clad fuel by a sequence of mechanical steps that result in the separation of the cladding from the oxide fuel.

An alternative to the partially untried mechanical-decladding step is the reaction of clad fuel with HF-O_2 mixtures to yield powdered Fe_2O_3, Cr_2O_3, NiO, etc., and partially fluorinated and exposed fuel. Exploratory experiments have been carried out to compare the rates of reaction of samples of unirradiated Type 304 stainless steel with similar samples that have been irradiated to 15,540 MWd in EBR-II, thus allowing a conclusion to be made about the effect of irradiation on the rate of reaction of the chemical-decladding step.

The procedure was to etch each stainless steel sample with aqua regia, then to react it with ~50 v/o HF-O_2 in a thermobalance at ~600°C. In general, the reaction rate of the irradiated samples was lower by a factor of two to four than the reaction rate of the unirradiated samples. It is tentatively concluded that fast-neutron irradiation decreases the reactivity of Type 304 stainless steel. No further work in this area is planned for the near future.

b. Fluorination Chemistry and Procedures (M. J. Steindler)

Last Reported: ANL-7487, pp. 95-96 (Aug 1968).

Initial scoping experiments to develop fluorination procedures for fast breeder reactor fuel consisted of a statistically designed series of five experiments, FF-A1 to FF-A5. The first step in each experiment was a 4-hr oxidation with ~20 v/o oxygen in nitrogen at 450°C, which pulverized the fuel and mixed it with the inert fluid-bed material. In the next step, uranium was removed by 3-hr fluorination with 10-15 v/o fluorine in nitrogen to form uranium hexafluoride, which was collected in one NaF trap during the first hour of the run and in a second NaF trap during the last two hours of the run. The final step consisted of fluorination with recycled 90 v/o fluorine in nitrogen to volatilize plutonium, which was collected in a separate NaF trap.

The fluidized bed was sampled for uranium and plutonium analysis at intervals during the run, and the dumped bed was sampled for determination of the uranium and plutonium retained in the final bed (which will be disposed of as waste). After dumping of a bed, fines removed from filters and the upper walls of the reactor were sampled and similarly analyzed.

The series was designed to determine the effects on plutonium retention in the final fluidized bed for two levels of fuel-to-alumina ratio (0.3 and 0.6), two uranium-fluorination temperatures (350 and 450°C), and two plutonium-fluorination sequences (10 and 20 hr). The 20-hr plutonium-fluorination sequence consisted of 4 hr at 300°C, 3 hr each at 350, 400, 450, and 500°C, and 4 hr at 550°C; the 10-hr sequence consisted of 3 hr at 450°C, 3 hr at 500°C, and 4 hr at 550°C. The latter sequence was chosen in an effort to obtain high fluorination rates for plutonium. In each run, the feed consisted of ~650 g solid-solution UO_2-20 w/o PuO_2 to which was added ~69 g of nonradioactive oxides of the elements formed by fission in a fast breeder reactor core. The inert-bed material consisted of 1100 g of 48-100 mesh alumina.

Experimental results for Run FF-A4 have been obtained, completing the accumulation of data for these experiments. In Runs FF-A1 to FF-A5, the percentage of the plutonium charge in the final bed ranged from 0.51 to 3.19%. Only one experiment, Run FF-A2, gave results significantly above the acceptance criterion of 1%. Conclusions drawn from the statistical analysis showed that increasing the fuel-to-alumina ratio from 0.3 to 0.6 and increasing the temperature of the initial fluorination step from 350 to 450°C increases the fraction of the plutonium charge retained in the final bed; using the 20-hr rather than the 10-hr sequence reduces the fraction of the plutonium charge retained by the final bed. The results indicate that optimization of fluorination conditions should result in plutonium losses in the bed waste material that are considerably below 1%.

An average of 21.2 g of fines per run was recovered from the reactor filters after the experimental runs. These fines contained about 0.5% of the uranium charge and about 3% of the plutonium charge. Recovery of plutonium from these fines has been demonstrated previously.* The variables studied in these experiments had no effect upon the quantity of fines recovered or upon the fraction of the uranium and plutonium charge in the fines.

In general, the highest rates of plutonium fluorination were obtained during the initial part of the plutonium-fluorination sequence, when the plutonium concentration in the fluid bed was highest. Excluding

*Chemical Engineering Division Semiannual Report, July-December 1966, ANL-7325, p. 61 (April 1967).

Run FF-A4, for which production rates were low during the initial plutonium-fluorination period, the production rate for PuF_6 averaged 1.2 to 3.0 lb/(hr)(ft^2), and the reactor operated at 17.2 to 55.4% of equilibrium for the reaction $PuF_4(s) + F_2(g) \rightleftharpoons PuF_6(g)$. Rate constants of 0.7×10^{-3} min^{-1} at 300°C and 4.4×10^{-3} min^{-1} at 450°C correspond to an apparent activation energy of 10.2 kcal/mol.

To achieve adequate material balances, the actinide input to a fuel-processing plant must be obtained by taking a representative sample of the fuel before fluorination. For the series of five experiments, samples were taken after the oxidation step (i.e., when the pulverized fuel was intimately mixed in the fluidized bed). The average U/Pu ratio was 3.84 ± 0.50 (95% confidence level), compared with a ratio of 3.96 in the charge. At the same confidence level, the uranium material balance calculated from all solids collected in the run was 92.0 ± 13.8% of the uranium charged. Similarly, the calculated plutonium material balance was 92.0 ± 11.8% of the plutonium charged. The U/Pu ratio in the samples, the uranium balance, and the plutonium balance are within the expected precision of the experimental results, based on analytical and sampling uncertainties. However, sampling of the fuel prior to charging to the fluid-bed reactor may be necessary for accurate material balances.

One of the objectives of a fluorination step with dilute fluorine would be to fluorinate most of the uranium so that the subsequent fluorination of plutonium with concentrated fluorine is not hampered by reactor temperature-control problems. In these runs, total uranium fluorinated during this step ranged from 69.7 to 96.5% of the charge. Total plutonium fluorinated was 0.6 to 9.0% of the charged plutonium except in Run FF-A4, in which 27.7% of the charged plutonium was fluorinated. It was observed that most of the plutonium volatilization occurred after the bulk of the uranium had reacted. The two NaF traps that had been used in turn in each run to collect the product from the uranium-fluorination step were analyzed for uranium and plutonium. Decontamination factors as high as 10^3 were obtained for the separation of plutonium from uranium during the first hour of fluorination with dilute fluorine. The best decontamination factor for the entire uranium-fluorination period was about 1.5×10^2. These results show that an initial separation of uranium from plutonium may be possible by fluorination with dilute fluorine.

c. Purification Procedures and Fission Product Chemistry
(M. J. Steindler)

Last Reported: ANL-7513, pp. 118-119 (Oct 1968).

(i) Fission Product Chemistry. The conceptual fluoride volatility process for irradiated UO_2-PuO_2 reactor fuel includes the volatilization of uranium as UF_6 by reaction of powdered fuel oxide with

dilute fluorine in oxygen at 350°C. An earlier examination of the literature (see ANL-7513) suggested that the volatile compounds NbF_5, RuF_5, SbF_5, TeF_6, $MoOF_4$, $TcOF_4$, and IOF_5 may form in this step.

An exploratory investigation has been performed to determine qualitatively the products formed when Nb, Mo, Ru, Sb, Te, I_2, Xe, Nb_2O_5, MoO_3, RuO_2, Sb_2O_5, and TeO_2 are individually reacted with O_2-10% F_2 mixture at 350°C. Samples were reacted for ~1 hr in a vertical 1-in. dia, 9-in.-long furnace, and the reaction gases were discharged through a series of traps including cold traps, activated alumina, and soda lime. The reaction products were tentatively identified by their volatilities (condensation temperatures), vapor pressures, and hydrolysis or reduction behavior. The major products of the reactions with Nb, Ru, Sb and Sb_2O_5, and Te and TeO_2 were NbF_5, RuF_5, SbF_5, and TeF_6. Molybdenum and xenon form low-volatility fluorides, probably $MoOF_4$ and XeF_4. The volatility of the product of I_2-F_2 reaction was higher than the volatilities of IF_5 or IF_7, suggesting the formation of IOF_5. Nb_2O_5 showed no significant reaction; the reaction of MoO_3 apparently formed an oxyfluoride richer in oxygen than $MoOF_4$; the product of RuO_2 reaction was a volatile compound, apparently RuO_4.

d. Engineering-scale Development for Fast Breeder Reactor Fuels (N. M. Levitz)

Last Reported: ANL-7513, pp. 119-120 (Oct 1968).

(i) Pulsed-gas Fluidization Studies. Pulsed flow of gas (see Progress Report for April 1968, ANL-7445, pp. 117-118) for fluid-bed fluoride volatility processes is being studied for possible use in the oxidation and fluorination steps as an alternative to conventional steady-gas-flow fluidization. Preliminary data have been obtained using a 4-in.-dia pulsed-bed column with an annular heater of 1.25-in. diameter.

Information on the maximum pressure drop in a system is necessary to design equipment, and data on bed expansion is needed in determining the process conditions that give maximum gas-solids contacting. Preliminary data on pressure drops and bed expansions have been obtained for glass beads having average diameters of 580 and 138 μm. Pulse frequency ranged from 0.67 to 4.0 Hz, on-period (gas flow) and off-period (no gas flow) each from 0.125 to 1.0 sec, static bed height from 8 to 12 in., and gas velocity (ft/sec) as follows:

	Glass-bead Diameter	
	580 μm	138 μm
Mean gas velocity during on-period	0.26-3.4	0.066-1.48
Mean gas velocity during entire cycle	0.14-1.8	0.028-0.586

Typical data for maximum pressure drops for a pulsed bed consisting of 580-μm-dia glass beads (minimum fluidization velocity of 0.7 ft/sec) are compared with the pressure drops for fluidized and packed beds over a range of gas velocities in Fig. III.D.1. The ordinate is a dimensionless maximum pressure drop $[\Delta P/(W/A)]$, and the abscissa is a dimensionless instantaneous gas velocity (v/v_{mf}), where ΔP is the maximum pressure drop, W is the bed weight, A is the cross-sectional area of the column, v is the superficial gas velocity during the on-period, and v_{mf} is the minimum fluidization velocity. For gas velocities greater than the minimum fluidization velocity (0.7 ft/sec), the maximum pressure drop for pulsed beds was higher than that for fluidized beds and lower than that for packed beds. The maximum pressure drop increased linearly with the gas flowrate during the on-period and was independent of the other pulsing conditions.

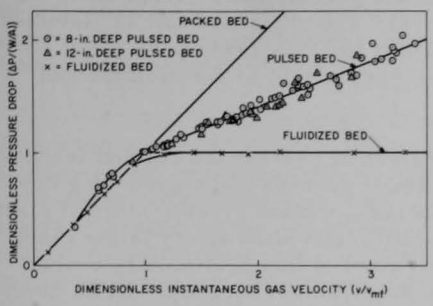

Fig. III.D.1. Maximum Pressure Drops in Pulsed, Fluidized, and Packed Beds (avg diameter of glass beads: 580 μm; v_{mf} = 0.7 ft/sec)

The relationships between bed expansion and gas-flowrate were examined. The bed-expansion ratio (maximum bed height/static bed height) appears to increase with increasing gas velocity, to decrease with increasing pulse frequency, and to decrease as the on-period fraction of the cycle is increased. The bed expansions were greater for pulsed beds than for fluidized beds at the same gas throughputs.

e. Small-scale Studies with Irradiated Fuels (A. A. Chilenskas)

Last Reported: ANL-7487, p. 97 (Aug 1968).

Two PaR electromechanical manipulators along with their bridges, carriages, and electrical cables have been installed in the senior cave facility of the Chemical Engineering Division. Three Model J manipulators also were installed. The modification work is completed, and the cave is ready for operation. Planning of experiments with irradiated fuel to be conducted in this facility is underway.

f. Engineering Design, Analysis, and Evaluation (N. M. Levitz)

Last Reported: ANL-7513, p. 120 (Oct 1968).

Conceptual design studies of fluoride-volatility-processing plants for fast breeder reactor fuels are in progress. Process and engineering flowsheets have been prepared, including basic layouts of the

process cell and the overall plant and design of some major equipment items. A tentative process flowsheet has been selected for a central plant with a capacity of 1 metric ton of actinides per day (the average daily discharge rate from a 15,000-MWe network). The reference fuel is stainless steel-clad UO_2-PuO_2 (see Progress Report for May 1968, ANL-7457, pp. 121-122). An overall minimum recovery of 99% of the uranium and plutonium is specified.

The objectives of this study are to present the current technological basis for such a plant in the form of process and engineering flowsheets, and to define process uncertainties (problem areas). Overall plant problems such as criticality, accountability, and plant safety in the event of hexafluoride release have been considered in this preliminary evaluation. From this study, a research and development program will be developed and executed to demonstrate the flowsheet and to develop engineering information to establish the technical feasibility of the process.

In the proposed process, the fuel element is disassembled and mechanically treated in the head-end step to provide powdered fuel and separated stainless steel hulls (ANL-7457, pp. 121-122). Next, uranium oxide and plutonium oxide are converted to fluoride gases in separate vessels (see Fig. III.D.2) with fluorine as the fluorinating agent. Bulk separation of the uranium from plutonium, as well as separation of the uranium and plutonium from contaminants that remain solid under the reaction conditions, is achieved by continuous fluorination in two fluid-bed reactors in series.

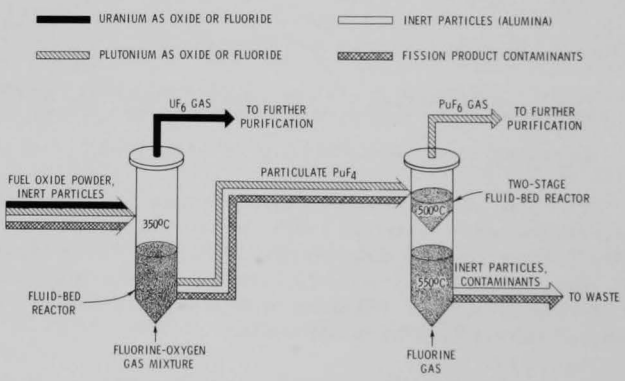

Fig. III.D.2. Two In-series Fluid-bed Reactors for Continuous Fluorination of FBR Fuel

Basically, the continuous-fluorination scheme involves feeding powdered oxides and fresh alumina to the first fluid-bed reactor where, at 350°C, the bulk of the uranium is converted to UF_6 with oxygen-20 v/o fluorine while less than 5% of the plutonium is converted to PuF_6. The volatile

actinide fluorides and fission product fluorides pass from the uranium fluorination reactor to other vessels for further purification. Solids, rich in plutonium (now present as PuF_4), continuously overflow from the uranium fluorinator and are fed to a two-stage fluid-bed reactor where the conditions favor fluorination of PuF_4 to PuF_6.

The fluorinating gas in the two-stage reactor is ~90 v/o fluorine with a velocity of ~1 ft/sec. The upper stage, where most of the plutonium is fluorinated, is maintained at 500°C and has a steady-state concentration of plutonium in the solids of 3 w/o. It is assumed that under these conditions the PuF_6 content of the off-gas will be at least 90% of the equilibrium ratio of 0.01. The solids flow into the lower stage, where fluorination at 550°C reduces the plutonium concentration in the solids to 0.05 w/o. The major contaminants in the PuF_6 off-gas stream from the two-stage reactor are UF_6, NbF_5, and RuF_5. The UF_6 and PuF_6 off-gas streams are each passed through two cold traps (fission product trap and product-collection trap) where further separation from fission products occurs.

A continuous fluorination scheme was selected for the fluoride volatility process instead of a batch fluorination scheme after consideration of the heat loads (chemical and fission product) as well as nuclear criticality safety. Heat loads are most severe in the main fluorination vessels, which have large inventories of fission products, and particularly in the uranium fluorinator, which also has a large chemical heat load. With maximum heat fluxes in the continuous process of the order of 11,000 Btu/(hr)(ft^2), calculations show that satisfactory heat removal can be achieved with air cooling of a finned reactor surface. A slab design for the fluorination vessels (see Progress Report for September 1968, ANL-7500, pp. 111-112) appears to be advantageous for handling the heat problem. It provides a greater surface for heat transfer than would a cylindrical vessel of comparable volume and in addition presents a small dimension (4-in.-thick vessels in the present design) across which the heat must be transferred. Also, a slab design provides nuclear criticality safety for large inventories of plutonium.

The UF_6 product stream may contain sufficient PuF_6 to warrant its recovery. This is accomplished in the present flowsheet by combining the UF_6 and PuF_6 product streams and carrying out a nearly quantitative separation in a fluid-bed thermal decomposer in which PuF_6 is converted to solid PuF_4. This step also further purifies the plutonium from remaining volatile fission products. The overhead stream from the thermal decomposer carries the UF_6. Small amounts of PuF_6 in this stream are recovered in lithium fluoride traps by formation of a $LiF-PuF_4$ complex; the plutonium can be volatilized from the traps by fluorinating the complex with fluorine.

Separation of volatile fission product fluorides from the uranium hexafluoride stream from the decomposer necessitates the use of

several techniques. For example, by passing the stream through a trap at 15°C, RuF_5 is removed by desublimation; collection of UF_6 in cold traps at -78°C allows xenon and krypton to pass through for final gas treatment or storage; distillation is proposed for separating UF_6 from higher- and lower-boiling components of the gas stream; the gas stream from the distillation step is passed through MgF_2 and NaF to remove TcF_6 and NpF_6.

Purification of the plutonium in the thermal-decomposition step is followed by refluorination of the PuF_4 to PuF_6 with fluorine, recombination of the purified hexafluorides, and simultaneous reaction with steam and hydrogen to form dense, homogeneous UO_2-PuO_2 particulate suitable for refabrication. If a separate uranium oxide form is desired, the UF_6 not used to prepare UO_2-PuO_2 can be converted to UO_2 by reaction with steam and hydrogen.* Or, if PuO_2 is the desired final form, the PuF_4 formed in the thermal decomposer can be pyrohydrolyzed to the oxide in a fluid-bed operation.

The alumina stream, which cascades through the fluorination reactors and finally to waste receivers, represents the main solid waste stream, providing a vehicle for the disposal of those fission products in the feed that do not form volatile fluorides. Recycling of the gaseous reagents conserves reagents and also minimizes the quantity of effluent gas that must be treated.

To eliminate the release of noxious materials to the environment, the main process off-gas is treated. For the disposal of (1) excess fluorine, (2) HF (from conversion), and (3) volatile fission product fluorides, the off-gas is passed through solid reactants. Oxygen is converted to water, which may be stored or disposed of, depending on the activity level. The rare gases xenon and krypton are compressed and can be stored, allowing xenon to decay. Possibly, clathrates can be used for ultimate krypton disposal. Since fluorine is extensively recycled and the wastes are primarily solids, discharge of the off-gas stream through a stack is eliminated.

A preliminary draft of the report (see ANL-7513, p. 120) on the conceptual design studies of a large fluoride volatility plant for processing fast breeder reactor fuels is nearly complete. The main body of the report includes sections on process description, material and heat balances, and the engineering flowsheet, which are complete. Near completion is the critique section, which incorporates the bases for design, indicates uncertainties and alternatives, and evaluates the status of technology.

---

*Knudsen, I. E., Levitz, N. M., and Jonke, A. A., Engineering Development of Fluid-bed Fluoride Volatility Processes, Part 6. Preparation of Dense Uranium Dioxide Particles from Uranium Hexafluoride in a Fluidized Bed, ANL-6902 (Dec 1964).

2. Closed Cycle Processes--Research and Development--Compact Pyrochemical Processes

a. Supporting Chemical Studies (I. Johnson)

Last Reported: ANL-7513, pp. 121-122 (Oct 1968).

Experiments were performed to determine the effect of magnesium content in the Mg-Cu/$MgCl_2$ reduction system on the reduction of UO_2. Individual UO_2 pellets were suspended in molten $MgCl_2$ salt phases which were in contact with Mg-Cu alloys of varying magnesium content. The rate of reduction proved to be directly proportional to the thermodynamic activity of magnesium in the Mg-Cu alloy. The concentration of magnesium in the $MgCl_2$ salt had been shown previously to be proportional to the activity of magnesium in the alloy (see Progress Reports for February 1967, ANL-7308, pp. 37-38, and December 1966, ANL-7286, p. 32). Therefore, the rate of UO_2 reduction is directly proportional to the concentration of magnesium dissolved in the salt, i.e., the reaction is first order with respect to the magnesium concentration in the salt.

b. Process Engineering Studies (R. D. Pierce)

Last Reported: ANL-7513, pp. 122-123 (Oct 1968).

A graphite crucible coated with tungsten by vapor deposition (see Progress Report for June 1968, ANL-7460, p. 115) has been tested for containment of molten salt. The crucible was filled with a $MgCl_2$-30 m/o KCl-20 m/o NaCl salt mixture and cycled three times between 650 and 800°C over a period of 55 hr in an inert atmosphere. The crucible remained intact and contained the salt, although some wetting by the salt was observed. The weight of the crucible increased about 0.4%, and slight scaling of the outside surface was noted. Further tests will be conducted with combinations of liquid metal and molten salt phases.

c. Experimental Flowsheet Investigations (R. D. Pierce)

Last Reported: ANL-7513, p. 123 (Oct 1968).

Work is continuing on the design and construction of the Plutonium Salt Transport Facility (see Progress Report for September 1968, ANL-7500, p. 115). The design and drafting work for a condenser to be used in box 3 has been completed, and the job has been submitted to the shops for fabrication. This condenser will collect residual zinc from the decladder prior to the reduction step. Design work on the process vessels for box 3 is complete. Plans are being drawn for the process piping and instrumentation to control the atmospheres in the six processing vessels in box 3. Control valves have been selected and are on order. Wiring

diagrams and panel layouts for pressure control are essentially complete. The heated transfer lines for box 3 are being designed, and drawings for a lifting mechanism to raise and lower the transfer lines are complete. Parts for movable agitator drives for the process vessels in box 3 have been ordered.

Two helium-atmosphere-purification systems are being installed in the facility, one for box 3 and the other for box 2 and pass-through tunnel 6. All of the major components of the two systems are on hand, and the associated piping is being installed.

Filter housings have been fabricated and installed in boxes 3 and 4. New end plates were made and welded into these two boxes to accommodate the filter housings and transfer lock 7. Installation of hoist rails is complete in box 4 and is in progress in box 2. The fume hood is installed except for the window panel, which is on order.

d. Liquid Metal-Molten Salt Contactors (R. D. Pierce)

Last Reported: ANL-7513, pp. 123-124 (Oct 1968).

A solid-rotor agitator pump designed for use in mixer-settlers for pyrochemical processing was tested with a Mg-42 a/o Cu alloy at 670°C. The objectives of these experiments were: (1) to determine the performance of the agitator-pump with liquid metals and molten salts, (2) to compare the pumping rate as a function of submergence and rpm in the alloy with that determined previously with water (see Progress Report for September 1968, ANL-7500, p. 100), and (3) to observe the dynamic effects (splashing and flow) at the pump discharge.

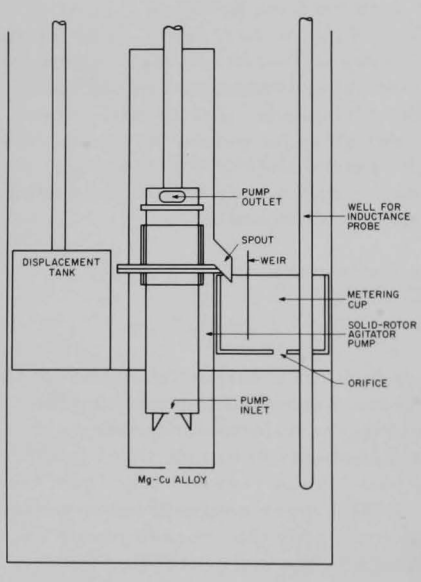

Fig. III.D.3. Schematic Diagram of Mixer-Pump Test Assembly

The pump and associated equipment (see Fig. III.D.3) were fabricated from Type 304 stainless steel. A glass viewing window in the top of the test vessel allows visual observation of the pump operation. A displacement tank can be lowered into the molten alloy to provide control over the submergence depth of the pump. The Mg-Cu alloy is discharged from the top of the pump into a shroud surrounding the outlet and flows through a spout into a metering cup. The metering cup has an orifice, a weir to prevent turbulence in the cup, and a mutual-inductance

liquid-level probe (see Progress Report for February 1968, ANL-7427, p. 123). The alloy flows through the orifice and returns to the inlet of the pump in the bottom of the test vessel. The level of Mg-Cu alloy in the metering cup is related to the pump output and is measured with the liquid-level probe.

The pump has operated successfully in shakedown experiments. The signal from the probe varied almost linearly with changes in the liquid level. The metering cup and induction probe have proved to be a highly successful system for monitoring flowrate.

When the tests with the Mg-Cu alloy have been completed, the system will be tested with metal and salt together, and measurements of stage efficiency will be made.

A 5-hr run was completed successfully in a facility for testing continuous liquid metal-molten salt contacting equipment (see Progress Report for August 1967, ANL-7371, pp. 98-99). Uranium was transferred between two mixer-settlers at 600°C by the salt-transport method. The first mixer-settler contained a liquid metal phase of the nominal composition Cd-2.5 a/o Mg-10 a/o U. Since the solubility of uranium in cadmium at 600°C is only 1.1 a/o, most of the uranium in this unit was present as a solid. The second mixer-settler contained a Cd-48 a/o Mg alloy. The composition of the salt circulating through the mixer-settlers was $MgCl_2$-30 m/o NaCl-20 m/o KCl. The salt flowrate was 0.6 gpm.

Preliminary chemical analyses indicate that the rate of uranium transfer from the first to the second mixer-settler was 72 g/min at the initial alloy compositions. This value is close to the maximum rate predicted.

3. General Chemistry and Chemical Engineering--Research and Development

a. Phase Diagram Study of the Ternary System U-Pu-O (P. E. Blackburn and A. E. Martin)

Last Reported: ANL-7487, p. 102 (Aug 1968).

In our earlier study of the U-UO_2 system, the existence of a wide liquid miscibility gap at high temperatures was established.* At the monotectic temperature, 2470°C, the gap extended over an O/U ratio composition range from about 0.05 to 1.3. It seemed likely that this liquid miscibility gap would extend well into the U-Pu-O system, possibly completely

*Edwards, R. K., and Martin, A. E., Thermodynamics, Vol. 2, Proc. Symp. Vienna, 1965, IAEA, Vienna (1966), p. 423.

across the system to the Pu-PuO_2 binary side. Our initial experiments in the recently completed plutonium facility were aimed at investigating these possibilities.

Arc-melt preparations were made from physical mixtures of plutonium and plutonium dioxide with overall O/Pu ratios of 0.29, 0.38, 0.57, 0.85 and 0.99. The products of the first four mixtures consisted of both metallic- and oxidic-appearing portions, whereas the product of the fifth contained only an oxidic material. Metallographic examinations of the two-portion products showed that each metallic portion had a similar structure, namely, plutonium with some oxide inclusions, and that each oxidic portion also had a similar structure, namely, that of a monotectic with plutonium as a dispersed phase in a matrix of oxide. Some of the larger oxide inclusions in the metallic portions were globular with monotectic structures, whereas some of the larger inclusions in the oxidic portions were globules of plutonium.

The metallographic appearance of the 0.99 O/Pu preparation, which experienced the relatively large weight loss of 22.7% to yield a product with an O/Pu ratio of 1.11, was essentially the same as that of the oxidic portions of the two-portion arc-melt products. The obvious conclusion from these tests is that a wide liquid miscibility gap does exist in the Pu-PuO_2 system at the arc-melting temperature, estimated at about 2500°C.

Measurements of the relative amounts of the metallic and oxidic portions of the preparations with 0.29 and 0.85 O/Pu, with some corrections for minor selective losses of plutonium during melting, have indicated the liquid miscibility gap extends between O/Pu compositions of about 0.1 and 1.0 at the arc-melt preparation temperature. In view of the relatively small amount of metallic inclusions of appreciable size in the oxidic portions, it is likely that the monotectic composition is also about 1.0 in O/Pu ratio.

An X-ray diffraction examination* of a sample of the monotectic portion of the 0.38 O/Pu preparation showed that the dominant phase was hexagonal Pu_2O_3 with alpha plutonium as a "possible, very minor" constituent. Thus, Pu_2O_3 was shown to be the oxide phase in the monotectic structure and also the most plutonium-rich oxide phase in the Pu-PuO_2 system at high temperatures.

To establish the monotectic temperature, a Pu_2O_3 crucible was formed. Metallic plutonium was melted in this crucible for short periods at successively higher temperatures until a temperature above the monotectic was reached; this was apparent when the reaction of the plutonium with the crucible caused the charge to melt the crucible. In this way the

*The X-ray diffraction examination was carried out by R. Schablaske, Chemical Engineering Division.

monotectic temperature was indicated as between 1778 and 1863°C. The monotectic temperature will be more accurately defined by similar experiments utilizing smaller temperature increments. (Melting tests of 50-mg portions of the oxidic portion of the 0.38 O/Pu preparation in tungsten crucibles confirmed the approximate value of the monotectic temperature. A sample heated to 1850°C melted, whereas one heated to 1800°C did not.)

Since the liquid miscibility gap was observed in both the U-UO_2 and the Pu-PuO_2 systems and since the gap was in about the same O/M composition range in both systems, it seemed likely that a liquid miscibility gap extends as a two-phase field across the ternary U-Pu-O system at about the same O/M values. One check for the existence of this two-phase field in the ternary system was made at the Pu/U section of 0.25. An alloy of 20% Pu-80% U, which was made by arc melting, was in turn arc melted with 20% PuO_2- 80% UO_2 oxide in proportions so that the overall O/M composition was 0.5, which was well within the expected two-phase field. The metallographic examination of the product showed that there was a miscibility gap in the ternary U-Pu-O system at this Pu/U section.

b. Total Vapor Pressure and Oxygen Potentials in the Ternary U-Pu-O System (P. E. Blackburn and A. J. Becker)

Last Reported: ANL-7478, pp. 120-121 (July 1968).

Some modifications have been incorporated into the gas-handling manifold of the transpiration apparatus designed for studying the total pressure and oxygen potentials over known compositions of the plutonium-oxygen system. Other modifications of the apparatus will be made (1) to obtain oxygen potentials from either a hygrometer when water-hydrogen mixtures are employed as the carrier gas, or an oxygen meter when oxygen-inert gas mixtures are used as dynamic atmospheres, (2) to provide options for diverting either entering or exiting furnace gases into one or both of the two analytical devices, and (3) to give additional protection to the apparatus, including the glovebox and helium recirculator, by changing the coolant for the O-ring and joint from water to L-45 silicone oil and placing the cooling lines, as far as is possible, in parallel rather than in series with the cooling apparatus' heat exchangers.

The study of the U_3O_8-U_4O_9 system will begin soon. As stated in ANL-7478, a transpiration study of this system will serve as a test of the apparatus before work on the Pu-O system is initiated.

The literature, including two recent publications,* yields no report of experimentally obtained total pressures under conditions of

*Riley, F. B., Techniques for the Study of Oxide Systems at High Temperature: The Plutonium-Oxygen System, Ph.D. thesis submitted to University of London (1967); C. A. Alexander, Lecture delivered to the Libby-Cockcroft Exchange Meeting on Phase Diagrams and Thermodynamics of Fuel Materials, Harwell (May 20-22, 1968).

controlled solid-phase composition, nor is there agreement on oxygen pressures and thermodynamic values.

The projected work with the Pu-O system is needed to resolve the discrepancies in the literature, and to add new information not presently available.

c. Total Effusion of Pu-O and U-Pu-O (P. E. Blackburn and R. K. Edwards)

Last Reported: ANL-7487, pp. 102-103 (Aug 1968).

The effusion apparatus, previously used to determine the congruently vaporizing composition of urania as a function of temperature, is being coupled to a glovebox so that effusion studies of plutonium-bearing materials may be carried out. Design work for internal components of the effusion apparatus (Knudsen cell mounting device, etc.) has been completed and construction is underway. Modification of the apparatus to allow installation of a quadrupole mass spectrometer and the coupling to the glovebox to the apparatus are nearing completion. The spectrometer, which was received during the previous report period, is currently being checked out in preparation for its installation in the effusion apparatus.

A vacuum microbalance will also be installed in the effusion apparatus. The microbalance has been temporarily installed in an existing vacuum system for testing and subsequent calibration.

PUBLICATIONS

A Mass Spectrometric Study of the Rhenium-Oxygen System
J. E. Battles, G. E. Gundersen, and R. K. Edwards
J. Phys. Chem. 72(12), 3963-3969 (Nov 1968)

Thorium-Uranium-Plutonium Alloys as Potential Fast Power-reactor Fuels. Part 1. Thorium-Uranium-Plutonium Phase Diagram
Bernhard Blumenthal, J. E. Sanecki, and D. E. Busch
ANL-7258 (Sept 1968)

Polarization of Neutrons Elastically Scattered from Medium- and Heavy-weight Elements
S. A. Cox and E. E. D. Whiting
Bull. Am. Phys. Soc. 13, 1420 (Nov 1968) Abstract

Compact Centerless Grinds "Hot" Materials
D. E. Grosvenor
Tool Mfg. Engr. 61(5), 22-24 (Nov 1968)

Electrical Connectors That Resist High Temperature
D. E. Grosvenor, D. J. Raue, and R. V. Kinzler
Chem. Eng. 75, 172 (Oct. 21, 1968)

Corrosion-resistant Heated Transfer Tubes for Molten Metals and Salts
D. E. Grosvenor, I. O. Winsch, W. E. Miller, G. J. Bernstein, and R. D. Pierce
Nucl. Appl. 5(5), 329-332 (Nov 1968)

CHEMLOC-II. A Computer Program Describing the Core Heating and Cladding-Steam Reaction for a Water-cooled Power Reactor Following a Loss of Coolant
J. C. Hesson, J. L. Anderson, and R. O. Ivins
ANL-7361 (April 1968)

Fragment Angular Distribution for Monoenergetic Neutron-induced Fission of Pu^{239}
J. R. Huizenga, A. N. Behkami, J. W. Meadows, and E. D. Klema*
Neutron Cross Sections and Technology Conf., Washington, D.C., March 4-7, 1968. Natl. Bur. Stds., Spec. Publ. 299. U.S. Govt. Prtg. Office, Washington, D.C., 1968, p. 603

Nuclear Pairing Energy of Transition Nucleus Pu^{240}
J. R. Huizenga, A. N. Behkami, J. W. Meadows, and E. D. Klema*
Phys. Rev. 174, 1539-1544 (Oct. 20, 1968)

Plutonium Fuel Development for Fast Reactors in the United States
J. H. Kittel, L. R. Kelman, J. H. Handwerk, E. L. Zebroski,** W. E. Bailey,** and A. Strasser†
High Temperature Nuclear Fuels, Proc. Symp., Delavan, Wis., October 1966. Met. Soc. Conf. Vol. 42, Gordon and Breach, New York, 1968, pp. 311-327

Knight Shifts of ^{31}P in the Paramagnetic State of the UP-US Solid Solutions
Moshe Kuznietz, G. A. Matzkanin, and Yehuda Baskin
Phys. Letters 28A(2), 122-123 (1968)

Multilevel Analysis of the ^{239}Pu Fission Cross Section from 40 to 150 eV
P. P. Lambropoulos, T. R. Hill, and C. N. Kelber
Bull. Am. Phys. Soc. 13, 1409 (Nov 1968) Abstract

Low-level-occupation Probability Ratios in the (n,γ) Process
W. P. Poenitz
Bull. Am. Phys. Soc. 13, 1389 (Nov 1968) Abstract

Vanadium and Fast Neutrons
A. B. Smith and J. F. Whalen
Bull. Am. Phys. Soc. 13, 1420 (Nov 1968) Abstract

---

*Northwestern University.
**General Electric Co., San Jose.
†United Nuclear Corp.

The Fluorination of Neptunium(IV) Fluoride and Neptunium(IV) Oxide
L. E. Trevorrow, T. J. Gerding, and M. J. Steindler
J. Inorg. Nucl. Chem. 30(10), 2671-2677 (Oct 1968)

The Reaction of Neptunium Hexafluoride with Sodium Fluoride
L. E. Trevorrow, T. J. Gerding, and M. J. Steindler
Inorg. Chem. 7(11), 2226-2229 (Nov 1968)

The following appeared as Abstracts in Trans. Am. Nucl. Soc. 11(2) (Nov 1968):

Fluidized-bed Fluoride Volatility Processing of UO_2-PuO_2 Fuels with Simulated Burnups of 10,000 and 30,000 MWD/T
L. J. Anastasia, P. G. Alfredson, and M. J. Steindler
p. 447

Comparison of the Propagation Characteristics of Compression and Rarefaction Pressure Pulses in Two-phase, One-component Bubble Flow
M. A. Grolmes and H. K. Fauske
p. 683

The Effects of High Fast Fluences on the Microstructure and Mechanical Properties of Type-304 Stainless Steel
S. D. Harkness, Richard Carlander, and F. L. Yaggee
p. 480

Salt Transport Process for Fast Breeder Reactor Fuels
R. K. Steunenberg, Irving Johnson, and R. D. Pierce
p. 447

Pre-layup Inspection of EBWR Reactor Vessel
C. R. Sutton and Nicholas Balai
p. 648

The following appeared in Proc. Intern. Conf. on the Utilization of Research Reactors and Reactor Mathematics and Computation, Mexico City, May 2-4, 1967. Centro Nuclear de Mexico, Mexico, D. F., 1968, Vol. 3:

The Argonne Reactor Computation System, ARC
C. N. Kelber, G. C. Jensen, L. C. Just, and B. J. Toppel
pp. 1428-1445

A Method of Computing Resonance Integrals in Multiregion Reactor Cells
P. H. Kier
pp. 1495-1514

Generation of Multigroup Cross Sections Using a Coupled MC^2-THERMØS Code
D. A. Sargis, B. J. Toppel, and A. L. Rago
pp. 1446-1459

IV. NUCLEAR SAFETY

A. Reactor Kinetics--Other Reactor Kinetics--Research and Development

1. Reactor Control and Stability

a. Transfer Function Techniques to Measure Large Fast Reactor Stability (L. Habegger)

Last Reported: ANL-7478, p. 124 (July 1968).

(i) Spatial Effect. The analysis of space-dependent transfer functions in large fast reactors is being extended to more realistic reactor systems by using the Galerkin method.

The mathematical model of the reactor system that is being used in the study includes equations for the temperature distributions of the fuel and coolant.* These temperature equations, for a given point in a reactor, are based on a nodal analysis of the temperature distribution in a unit fuel cell located at that point.

A study has been made of the effect of the number of nodes used in this temperature analysis. The large temperature gradients in a unit cell indicated that the analysis used in the past with a single node in the fuel and another node in the coolant might be inadequate for some applications.

For this study, a typical LMFBR unit cell was used with oxide fuel, gas bond, stainless-steel cladding, sodium coolant, and uniform heat input to the fuel as the forcing function. A constant heat-removal rate from the coolant was assumed.

The results indicated that the transfer function of the power input to the average fuel temperature is largely independent of the number of nodes in the frequency range of interest. However, at frequencies above approximately 40 rad/sec, the gains of the transfer functions of the power input to the coolant and cladding temperatures are overestimated when too few nodes are used. Only minor changes in transfer functions resulted from increasing the number of nodes beyond three fuel nodes, two cladding nodes, and one coolant node.

*Hsu, C., Control and Stability Analysis of Spatially Dependent Nuclear Reactor Systems, ANL-7322 (July 1967).

2. Coolant Dynamics

a. Critical Flow (H. K. Fauske and M. A. Grolmes)

Last Reported: ANL-7513, pp. 131-132 (Oct 1968).

(i) Sodium Tests. The installation of a voidmeter in the sodium loop has been completed; flow and temperature calibrations are in progress.

(ii) Sonic Velocity and Pressure-wave Propagation. A new test section has been installed, and the system has been satisfactorily checked out in operation. In addition to measurements of the propagation velocity in a two-phase, one-component system, it is planned that information concerning the attenuation characteristics of the total pressure pulse will be obtained. To this end, the piezoelectric transducers are being calibrated in place. Data will be acquired soon.

(iii) Voiding Models. Analytical study of expulsion processes in fast-reactor coolant channels continues. The coupling of the continuity, momentum, and energy equations has led to solutions for the slug-type voiding model. The effects of considering incipient superheats and a liquid film remaining on the wall have been studied. Without liquid film, the calculations indicate an expulsion rate limited primarily by heat conduction, but with film, the rate is essentially inertia limited. In addition, high-speed movies of the expulsion of a superheated fluid (Freon-11) have been obtained. Slug-type expulsion events clearly show a film remaining on the wall. These movies also illustrate a two-phase flashing mode of expulsion that might be important in later stages of a slug-type expulsion or, in certain cases, that might influence a slug-type expulsion itself. These movies will be analyzed quantitatively.

b. Coolant Dynamics (R. M. Singer and R. E. Holtz)

Last Reported: ANL-7513, pp. 132-133 (Oct 1968).

(i) Sodium Superheat Experiments. Sodium superheat data are still being gleaned from both the out-of-pile and Juggernaut tests. The out-of-pile tests are continuing so as to determine the effect of impurities (such as of oxide content) upon incipient boiling superheats; the Juggernaut tests are being conducted to determine the effect of a reactor environment on superheat.

(ii) Coolant-expulsion Experiments. The assembly of the sodium-expulsion experiment is complete; the dump tank has been charged with sodium. Upon completion of a minor instrumentation change, the test section will be filled with sodium and testing will begin.

(iii) Transient Experiments. The electromagnetic pump has been received; assembly of the transient loop is continuing. Tests with the flowmeter calibration system continue.

c. Convective Instability (R. M. Singer)

Last Reported: ANL-7513, p. 133 (Oct 1968).

(i) Flow-coastdown Experiment. Design of the coastdown loop is essentially complete. The electromagnetic pump, radiant heaters, and several other components are on hand; the rectangular test section and heat exchanger are being constructed.

3. Fuel Meltdown Studies with TREAT (C. E. Dickerman)

a. Meltdown Studies with Ceramic Fuels

Last Reported: ANL-7500, pp. 126-129 (Sept 1968).

(i) Sodium-logged/Defected Oxide Pins. Safety experimentation is to be performed with UO_2 fuel pins logged with sodium in order to study the behavior of oxide fuel in contact with sodium, under transient heating conditions, and to guide the development of analytical models for accident analyses. The fuel has been delivered. Although the oxygen-to-uranium ratio from this batch was measured to be 1.98, higher than the value of 1.96 from a trial run (see ANL-7500, p. 127), this ratio is within the limits set for the experiments, and the batch has been accepted without further furnace treatment.

The sample-pin design for the experiments is as follows: Each pin is to consist of a stack of 93% dense, 13% enriched UO_2, with length in the range 11.5-12.1 cm, contained inside a Type 304L stainless steel jacket. Oxide outer diameter is 0.384 cm, and the cladding has a 0.442-cm OD with a 0.023-cm-thick wall. Contained sodium weight is 0.34 g maximum. Bottom and top fittings are standard stainless steel EBR-II Mark-IA end pieces. Two fast-response, Chromel-Alumel thermocouples are to be welded directly to the cladding surface of the first three pins at ±1.0 cm from the axial center of the fuel stack. These three pins are to be run in TREAT, in photographic experiments, using the standard slot-liner transparent facility apparatus.*

*Golden, G. H., Dickerman, C. E., and Robinson, L. E., Facility for Photographing In-pile Meltdown Experiments in TREAT, ANL-6457 (1962).

b. Development of Experimental Methods

Last Reported: ANL-7513, p. 137 (Oct 1968).

(i) Boron-loaded Thermal-neutron Shield. For future loop TREAT experiments with high enrichment, plutonium-bearing fuel pins, thermal-neutron shielding is needed to produce a relatively uniform radial power profile in the samples. The shield should have high-temperature capabilities to match those of the Mark-II integral TREAT loop. The compound B_6Si was selected as the shielding material because of its combination of high density (2.47 g/cc; 69.7 w/o boron) and good stability in flame spraying. Attempts to flame spray the hexaboron silicide on a stainless steel backing were quite successful for thicknesses of ~0.025 cm, but difficulties were encountered in building up thicker layers, even with the use of metal-bonding techniques. The method finally adopted consists of "loading" the high-temperature silicone base paint (used to coat the inside of transparent meltdown capsule) with approximately 50 w/o hexaboron silicide, thinning with solvent to the consistency required for application, applying, and then vitrifying the mixture by air drying followed by baking (in air) at 190°C. Uniformity of coatings of ~0.150-cm thickness has been verified by thermal-neutron-transmission tests at the Argonaut reactor. The vitrified paint is rated up to 1000°C. Samples of the B_6Si-silicone coating, vitrified on a Type 304 stainless steel backing sheet, were cycled from room temperature to 500°C ten times without producing visible degradation. Following the cycling treatment, one sample was then heated in air at 750°C for 30 min. Slight discoloration of the dark grey surface resulted. The vitreous coating was found to remain bonded to the steel substrate even when the steel was bent 30° from straight, but cracks were produced in the region of the bend. For use with the Mark-II loop, the vitrified coating is applied to the outside surface of a Type 304 stainless steel can formed to fit closely inside the loop-containment can. In this arrangement, the vitreous material forms the inside of a sandwich, designed to hold the material in place even if it should crack during loop shipment and handling.

(ii) Holddown Device for Use in Mark-II Integral Sodium TREAT Loop Experiments. The loop holddown device, whose design was reported in the Progress Report for August 1968 (ANL-7487, pp. 107-108), has been furnished by the shops, and delivered for testing prior to shipment to TREAT. The device is designed to permit slow expansion and contraction of the loop as it is heated and allowed to cool, but it is to transmit any impulse load to the 22,700-kg load of the reactor rotating plug and cover shield blocks, in order to prevent an accident from ejecting the loop from the reactor core.

(iii) Status of Glovebox for Handling Low-activity Plutonium-bearing Samples. A plutonium glovebox complex is being installed in Building D-301 for operations with TREAT loops and capsules involving

mixed-oxide samples which contain only the relatively low activation resulting from TREAT exposure. The gas-supply system has been leak checked. Repairs were made where necessary to produce a "tight" system, and the gas-supply system has been accepted. Minor work was found necessary to make the large exhaust valve in the emergency (high-capacity) branch of the gas exhaust work smoothly. The valve is installed inverted, so that it will "fail safe" opening the high-capacity branch of the exhaust system. Both the auxiliary loading table and the auxiliary loading hood are in the shops for fabrication. The special Mark-II loop-loading flange for coupling a Mark-II loop to the box is being built. The loading flange assembly is designed for loading and unloading loops without introducing the entire loop into the glovebox.

4. Materials Behavior and Energy Transfer (R. O. Ivins)

Last Reported: ANL-7487, pp. 108-109 (Aug 1968).

a. Pressure Generation due to Violent Meltdown. To provide a better understanding of the mechanics of fuel-rod breakup during a nuclear excursion, the nature of pressures generated during the meltdown of stainless steel-clad UO_2-core fuel rods contained within a sodium-filled piston autoclave is being studied. The autoclave used in the TREAT meltdown experiments has been described (see Progress Report for May 1968, ANL-7457, pp. 135-136).

The fuel loading for the first experiment consisted of an array of five rods containing 10%-enriched UO_2 pellets and four dummy rods filled with helium. The fueled rods (0.29 in. in diameter, 12 in. long, with 15-mil wall thickness) were divided into two sections: a fueled section and an unfueled "blanket" section. The lower half of the rod contained helium-bonded, 41-g, sintered UO_2 pellets. The upper or "blanket" section, which contained helium, was designed to collapse under external pressures somewhat less than 6000 psi. The dummy rods were of the same overall dimensions and were filled with helium at 15 psi.

The first experiment (CEN-S2) in the piston-autoclave assembly involved a series of three transients at energies of 312, 481, and 495 MW-sec, corresponding to average fission energies of 214, 330, and 340 cal/g UO_2. Results from the three transients are presented in Table IV.A.1. All transients produced movement of the motion transducer and an indication of pressure increase. The output of the pressure transducer shifted during the transients because of both an increase in autoclave pressure and heating of the transducer. Separation of these two effects has not yet been possible, but further investigation of the thermal behavior of the transducer should allow accurate estimation of the pressures produced during the transients.

TABLE IV.A.1. Results from TREAT Meltdown Experiment CEN-S2 with Stainless Steel-clad UO_2-core Fuel Rods Submerged in Sodium

	Transient No.		
	1	2	3
Reactor Characteristics			
Integrated power (MW-sec)	312	481	495
Peak power (MW)	1048	1790	2310
Period (msec)	90	70	63
Results			
Peak temperature[a] (°C)	470	710	-
Maximum indicated motion (cm)	2.3	3.8	7.4
Maximum piston velocity (cm/sec)	1.6	8.5	27
Appearance of fuel rod	Intact[b]	Intact[b]	Split
Energy Calculations			
Fission energy input (cal/g UO_2)	214	330	340

[a]Measured by the thermocouple located in the sodium 3 in. above the bottom autoclave head.
[b]Determined from neutron radiographs of the autoclave assembly.

The motion transducer indicated a maximum displacement of 2.9 in. at a maximum rate of 10 in./sec during the third transient. Oscillations in the trace of the motion transducer indicated development of sodium boiling upon completion of the transient. The sodium temperature was between 600 and 700°C at the time this was observed.

The center rod of the array failed during the third transient, and 24.3 g of UO_2 dispersed into the sodium coolant. Figure IV.A.1 shows the rupture in the cladding that occurred at the top of the fueled section, 3/8 in. below the connection between the fueled and "blanket" sections. The rupture appears as a ragged tear in the wall of the tubing, and there is no sign of the cladding having melted. All the rods were warped, including the dummy elements, but none except the central rod showed signs of rupture or crushing. Although the cause of rod warpage is not known, it may have been due to restraint of the rods during assembly of the autoclave.

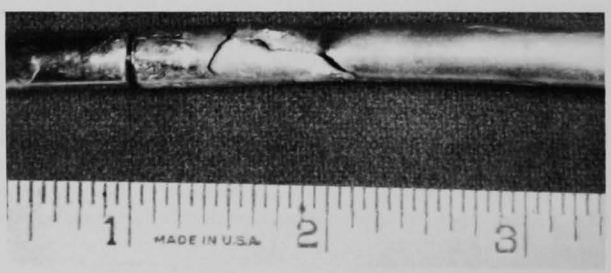

Fig. IV.A.1. Portion of Ruptured Fuel Rod Showing Cladding Failure

Several sharp pressure pulses were observed during the third transient. The largest of these pulses (above an unknown autoclave pressure) had a band width of 2 msec and an amplitude of 180 psi.

The second experiment (CEN-S3) involved two transients at 344 and 669 MW-sec; results will be reported.

5. Fast Reactor Safety Test Facility Study (C. N. Kelber)

Not reported previously.

This project* was organized and work undertaken at the request of RDT to attain these specific objectives:

1. evaluate the type and number of in-reactor experiments which should be performed in the LMFBR Safety Program;
2. develop facility requirements for the performance of such experiments;
3. estimate the optimum scheduling of the various test series;
4. determine the practicality of performing the tests in existing or firmly planned facilities;
5. provide recommendations to AEC for the performance and conceptual design studies of any new facilities for safety work which cannot be practically performed in existing or modified facilities.

These objectives will be attained by a work program organized in three tasks: A. Preparation of Work Plan; B. Programmatic Justification and Definition; C. Facility Definition and Utilization.

Task A, Preparation of Work Plan

The proposed work plan in the form of a revised form 189a has been submitted for Laboratory review.

Task B, Programmatic Justification and Definition

The first report under this task is due no later than the third quarter of FY 1969. The introduction, table of contents and detailed chapter outlines have been prepared. Most of the writing assignments have been made.

*This is essentially Task 10-5.1 of the LMFBR Program Plan.

B. TREAT Operations

1. Reactor Operations (J. F. Boland)

Last Reported: ANL-7513, p. 142 (Oct 1968).

Neutron radiographs were made of seven groups of capsules from EBR-II Subassembly XO29, one group of EBR-II driver fuel elements, and a group of BNL heaters containing boron carbide insulation.

Experiment CEN-S3 was subjected to two transient irradiations, neutron radiographed, and disassembled. All five oxide-fuel elements had failed, with all the fuel dispersed as fine particles. The clad adjacent to the fuel was destroyed, with some damage to the clad of the hollow dummy section above the fuel. Analysis of the pressure-transducer, linear-motion-transducer, and thermocouple data is in progress.

The reactor has been reloaded for additional transients for determining reactor characteristics when the fuel temperature is above 400°C. These transients will be performed in accordance with the recently revised reactor operating limits.

2. Development of Automatic Power Level Control System (J. F. Boland)

Last Reported: ANL-7513, p. 142 (Oct 1968).

Only one vendor bid on the hydraulic control-rod-drive system. Negotiations are being conducted to optimize the bid. Additional preliminary discussions have been held with digital control vendors.

C. Chemical Reaction--Research and Development--Chemical and Associated Energy Problems (Thermal) (R. O. Ivins)

Last Reported: ANL-7487, pp. 110-112 (Aug 1968).

1. Analysis of Excursion Accidents (K. A. Varteressian and J. J. Barghusen)

As part of the in-pile study of the characteristics of fuel failure, a program has been established to develop a computational procedure that, with a minimum of experimental data, will define and predict fuel-pin failure thresholds reasonably consistently with factual observations. For this purpose, the effects of chemical interactions and many details needed for a more sophisticated treatment have been excluded. As a basis of reference, average values of heat distribution and accompanying changes in phase, temperature, volume, and pressure inside the cladding enclosure have been considered. The threshold of failure has been taken to be that combination

of cladding temperature and hydrostatic pressure within the fuel rod that corresponds to the initiation of inelastic strains within the cladding. Preliminary results from the experimental program (see Progress Report for May 1968, ANL-7457, pp. 144-146) suggest the existence of two modes of fuel failure: a prompt failure manifest by rapid pressurization within the fuel specimen, followed by rupture of the cladding; and a delayed failure primarily due to degradation of the cladding (loss of cladding strength) by hot fuel-cladding interaction. In both cases, the fission energy associated with failure is between 240 and 290 cal/g UO_2.

For purposes of illustration, the test system treated consists of 5%-enriched vibrapacked UO_2 fuel between two end pellets of depleted uranium dioxide, enclosed under a helium atmosphere in tubular Zircaloy-2 cladding. The dimensions and weights of the component parts of this standard test assembly are given in Fig. IV.C.1.

The reference calculational procedure is based on mass, energy, and volume balances, coupled with the conventional gas laws and tangential stress expressions. For test specimens of fresh or low-burnup fuel, the only experimental data needed are fission-energy input to the active fuel section, and average temperatures of cladding and coolant at various times during the test. The essential thermal and mechanical properties required are specific volume and enthalpy of the fuel, cladding, and coolant, and the yield strength of the cladding, at various temperatures.

This simplified calculational procedure has been applied, for example, to a hypothetical test in which two fuel pins, one initially with 0% and the other with 1% burnup, are exposed to similar power transients under identical conditions. The results of the calculations are plotted in Fig. IV.C.2. The computed values indicate that the two specimens follow different gas-pressure:cladding-temperature paths to arrive at different failure thresholds. At the time of the initiation of inelastic strains in the cladding, the system with the 0%-burnup fuel has absorbed 344 cal/g UO_2, the fuel is at 2842°C with 46% of it melted, the cladding is at 825°C, and the gas pressure is 261 lb/in.^{2}. On the other hand, the system with the 1%-burnup fuel has absorbed 266 cal/g UO_2, the fuel is at 2600°C with none of it melted, the cladding is at 665°C, and the gas pressure is 1142 lb/in.^{2}.

In the example considered, both specimens are expected to undergo "prompt" failure because in both cases the fuel and therefore the gas temperatures are still on the rise as the cladding-yield pressure-temperature curve is reached. Power transients that involve less total energy absorbed per unit mass of fuel, and perhaps higher rates of energy generation, would be more conducive to the detection of the occurrence of "delayed" failure thresholds. In such cases, measurements of cladding and coolant temperatures will have to be extended beyond the period of the power transient.

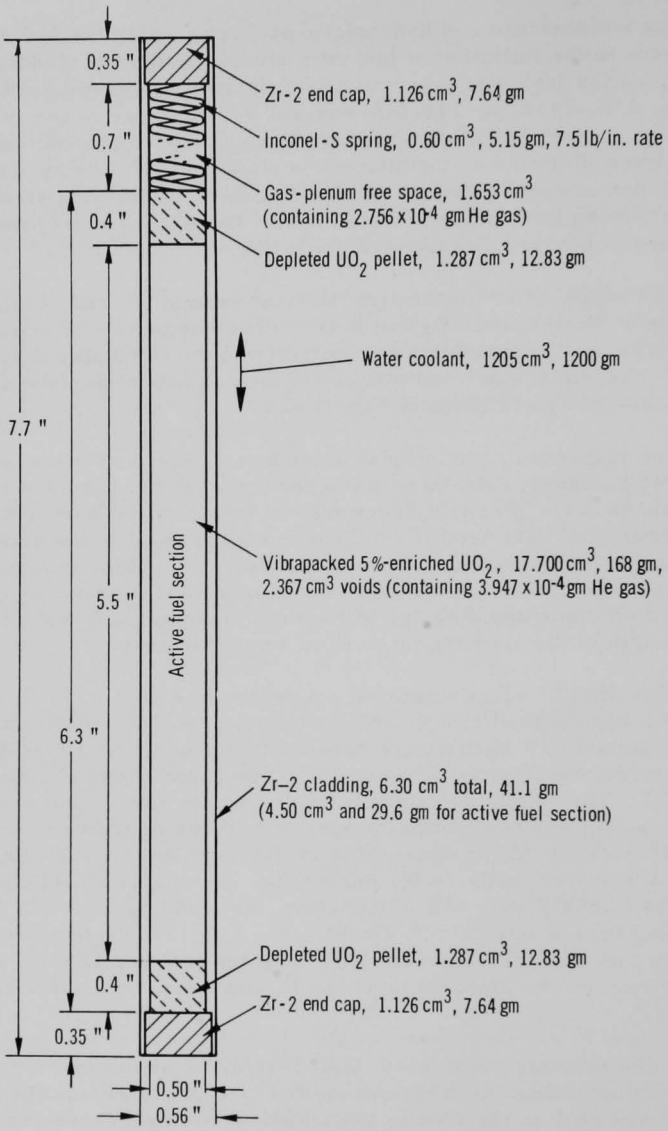

Fig. IV.C.1. Test Fuel Element for Reference in Calculational-model Development

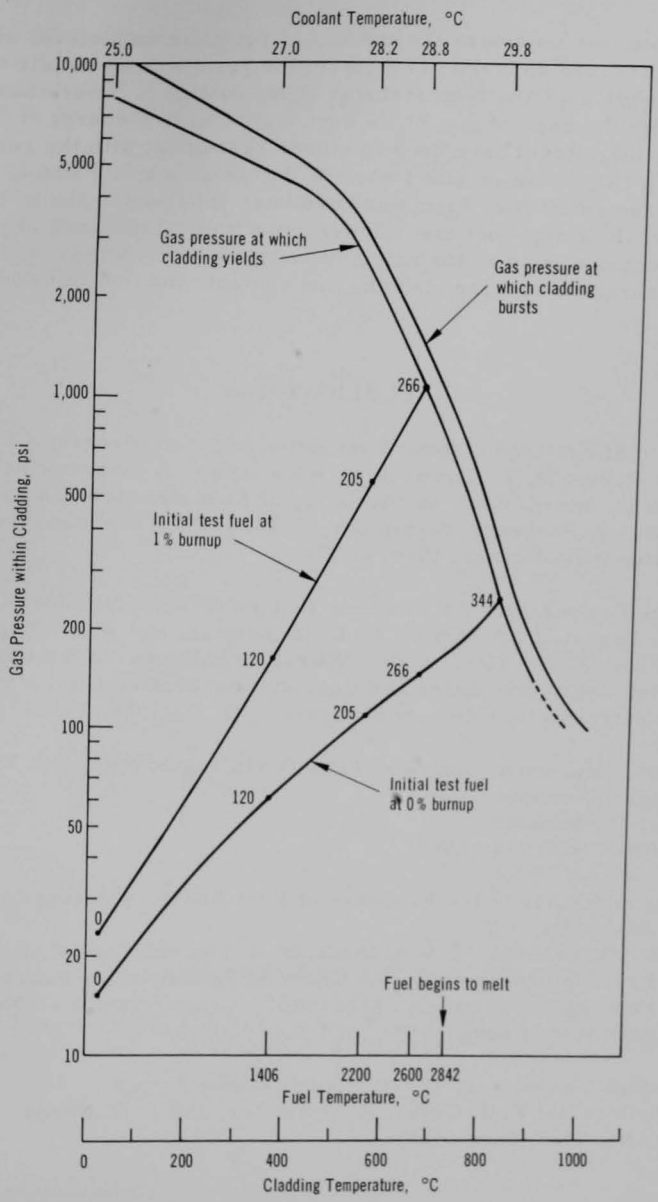

Fig. IV.C.2. Variation of Gas Pressure with Simultaneous Temperatures of Fuel, Cladding, and Coolant during a Hypothetical Transient Test. Numbers at points on curves indicate calories absorbed by system per g UO_2 initial fuel.

When one considers the number of yet unknown factors, the calculational procedure does tend to confirm the results from in-pile tests. If slightly higher cladding temperatures at the instant of failure had been assumed for the case of fuel of 0% burnup, the fission energy at failure (344 cal/g UO_2) would have been in closer agreement with the results (~290 cal/g UO_2) from in-pile tests. Wide variations in cladding temperature over the entire fuel specimen have been observed in the in-pile experiments. It is apparent that further experimental data are required to provide accurate input to the calculational program, namely, additional time-temperature data for cladding and coolant, and fuel internal-pressure data.

PUBLICATIONS

The United States Liquid Metal Fast Breeder Safety Program
Louis Baker, D. T. Eggen, R. O. Ivins, and S. A. Szawlewicz*
Proc. Intern. Conf. on the Safety of Fast Breeder Reactors, Aix-en-Provence, September 19-22, 1967. Commissariat a l'Energie Atomique, France, 1968, p. VI-1

Transient Temperature Calculations Using a Hybrid Computer
L. T. Bryant, L. W. Amiot, C. E. Dickerman, and W. P. Stephany
Proc. Intern. Conf. of the Utilization of Research Reactors and Reactor Mathematics and Computation, Mexico City, May 2-4, 1967. Centro Nuclear de Mexico, Mexico, D. F., 1968, Vol. 2, pp. 682-708

Transient Free-convection Heat Transfer in Liquid Metals in Vertical Rectangular Channels
Roger P. Heinisch
ANL-7452 (May 1968)

Theoretical Studies of the Response of Fast Reactors during Sodium Boiling Accidents
D. R. MacFarlane, N. A. McNeal, D. A. Meneley, and C. K. Sanathanan
Proc. Intern. Conf. on the Safety of Fast Breeder Reactors, Aix-en-Provence, September 19-22, 1967. Commissariat a l'Energie Atomique, France, 1968, p. I-5

A Heat-pipe Cooled Fast-reactor Space Power Supply
J. J. Roberts, E. J. Croke, R. P. Carter, and J. E. Norco
ANL-7422 (June 1968)

*U.S. Atomic Energy Commission, Washington.

A Hydrodynamical Analysis for Reactor Primary Containment by Energy Absorption
H. C. Sorensen* and S. H. Fistedis
Nucl. Eng. Design 7, 547-577 (June 1968)

Heat Transfer from Spheres into Subcooled Liquid Sodium during Forced Convection
L. G. Witte, Louis Baker, and D. R. Haworth**
ASME J. Heat Transfer 90C, 394-398 (Nov 1968)

The following appeared as Abstracts in Trans. Am. Nucl. Soc. 11(2) (Nov 1968):

Analysis of Transient Behavior of Unbonded EBR-II Fuel Pin Incident
C. E. Dickerman, R. R. Smith, F. L. Willis, A. B. Cohen, and J. P. Regis
p. 698

Development of a Family of Annular Linear Induction Pumps for Use in Fast Reactor Safety Integral-loop Experiments
L. E. Robinson and R. D. Carlson
p. 639

Asymptotic Stability with Positive Moderator Reactivity Coefficients
W. T. Sha and Chun Hsu
p. 572

Maximum Accident of Zoned Fast Reactors
W. T. Sha and R. B. Nicholson
p. 696

The Rate of Bubble Growth in Superheated Liquid Sodium
T. Theofanous,† L. Biasi,† H. S. Isbin,† and H. K. Fauske
p. 692

TREAT Experimental Study of Survival of EBR-II Fuel Pin in a Loss-of-bond Incident
F. L. Willis, C. E. Dickerman, P. B. Henault, R. T. Purviance, J. F. Boland, and R. A. Noland
p. 698

---

*Washington State University.
**University of Houston.
†University of Minnesota.

ARGONNE NATIONAL LAB WEST
3 4444 00008210 7